Technische Universität München

Fakultät für Medizin

Igf2^{+} and *Asc-1*$^{+}$ preadipocytes regulate healthy white adipose tissue function and expansion in mice

Irem Altun

Vollständiger Abdruck der von der Fakultät für Medizin der Technischen Universität München zur Erlangung des akademischen Grades einer

Doktorin der Naturwissenschaften

genehmigten Dissertation.

Vorsitz: Prof. Dr. Heiko Lickert

Prüfer*innen der Dissertation:

1. TUM Junior Fellow Dr. Siegfried Ussar
2. apl. Prof. Dr. Johannes Beckers

Die Dissertation wurde am 06.12.2022 bei der Technischen Universität München eingereicht und durch die Fakultät der Medizin am 21.03.2023 angenommen.

Eidesstattliche Erklärung

Ich erkläre an Eides statt, dass ich die bei der Fakultät für Medizin der TUM zur Promotionsprüfung vorgelegte Arbeit mit dem Titel:

"*Igf2*$^{+}$ and *Asc-1*$^{+}$ preadipocytes regulate healthy white adipose tissue function and expansion in mice"

am Institut für Diabetes and Adipositas (Helmholtz Zentrum München) unter der Anleitung und Betreuung durch Dr. Siegfried Ussar ohne sonstige Hilfe erstellt und bei der Abfassung nur die gemäß § 7 Abs. 6 und 7 angegebenen Hilfsmittel benutzt habe.

Ich habe keine Organisation eingeschaltet, die gegen Entgelt Betreuerinnen für die Anfertigung von Dissertationen sucht, oder die mir obliegenden Pflichten hinsichtlich der Prüfungsleistungen für mich ganz oder teilweise erledigt.

Ich habe die Dissertation in dieser oder ähnlicher Form in keinem anderen Prüfungsverfahren als Prüfungsleistung vorgelegt.

Teile der Dissertation wurden noch nicht veröffentlicht.

Ich habe den angestrebten Doktorgrad noch nicht erworben und bin nicht in einem früheren Promotionsverfahren für den angestrebten Doktorgrad endgültig gescheitert.

Die öffentlich zugängliche Promotionsordnung sowie die Richtlinien zur Sicherung guter wissenschaftlicher Praxis und für den Umgang mit wissenschaftlichem Fehlverhalten der TUM sind mir bekannt, insbesondere habe ich die Bedeutung von § 27 PromO (Nichtigkeit der Promotion) und § 28 PromO (Entzug des Doktorgrades) zur Kenntnis genommen. Ich bin mir der Konsequenzen einer falschen Eidesstattlichen Erklärung bewusst.

Mit der Aufnahme meiner personenbezogenen Daten in die Alumni-Datei bei der TUM bin ich einverstanden.

München, den Irem Altun

I. Abstract

Newborns display a rapid and massive expansion of adipose tissue, which is essential for healthy development and their adaptation to temperature changes. However, if this expansion continues to adulthood, this would result in obesity, insulin resistance and the metabolic syndrome. The aim of this PhD project is to identify factors or subpopulations of cells that regulate tissue function without causing metabolic disorder. For this purpose, we compare the composition of white and brown adipose tissues of pre-weaned (2 weeks old) and adult (8 weeks old) C57BL/6 wild-type mice by single cell RNA sequencing analysis. We focused on the stromal vascular fraction, which contains preadipocytes, endothelial, neuronal and immune cells. Projection of age revealed a distinct separation between pre-weaned and adult adipose depots specifically in *Pdgfra* expressing cells, which is a commonly used preadipocyte marker. Re-clustering and differential gene expression analysis revealed two genes significantly highly expressed in pre-weaned subcutaneous preadipocytes: *Igf2* and *Asc-1*. In the first part of this project, we focused on the role of *Igf2*, which is a well-known secreted protein promoting fetal growth. Supplementation and neutralizing experiments showed no effect of IGF2 on adipogenesis of primary murine preadipocytes. However, IGF2 supplementation induced significantly higher proliferation rates of preadipocytes from adult mice, where *Igf2* was rarely expressed. Fluorescent *in situ* hybridization showed that some of *Igf2*$^{+}$ cells are located in close proximity to blood vessels, where some of the adipocyte progenitor cells are predominantly localized. These findings indicated a potential role of IGF2 in hyperplastic expansion of the tissue most likely via regulating preadipocyte pool size. In the second part of this PhD project, we investigated the role of *Asc-1* expressing cells. ASC-1 is an amino acid transporter that was previously identified by our group as a surface marker for white adipocytes. We have shown that both the sorted ASC-1 low-expressed and stable *Asc-1* knockdown cells (shAsc-1) differentiated toward beige adipocytes. This was partly due to high quantities of D-serine accumulation in the cell, which was reversed by transient knockdown of the enzyme that converts L-serine to D-serine: serine racemase. Thus, we were able to identify a subpopulation of preadipocytes expressing *Asc-1* regulating white vs beige lineage fate decision. Altogether, our findings highlight the complexity in function and heterogeneity in the white adipose tissue. We also propose here previously unrecognized subsets of preadipocytes playing a role in healthy tissue modeling that can be implemented in the adult state.

II. Zusammenfasslung

Bei Neugeborenen kommt es zu einer raschen und massiven Vermehrung des Fettgewebes, die für eine gesunde Entwicklung und die Anpassung an Temperaturschwankungen unerlässlich ist. Setzt sich diese Expansion jedoch bis ins Erwachsenenalter fort, führt dies zu Fettleibigkeit, Insulinresistenz und dem metabolischen Syndrom. Ziel dieses Promotionsprojekts ist es, Faktoren oder Subpopulationen von Zellen zu identifizieren, die die Gewebefunktion regulieren, ohne Stoffwechselstörungen zu verursachen. Zu diesem Zweck vergleichen wir die Zusammensetzung von weißem und braunem Fettgewebe von jungen (2 Wochen alten) und erwachsenen (8 Wochen alten) C57BL/6-Wildtyp-Mäusen mittels Einzelzell-RNA-Sequenzierungsanalyse. Wir konzentrierten uns auf die stromale vaskuläre Fraktion, die nicht nur Präadipozyten, sondern auch endotheliale, neuronale und Immunzellen enthält. Die Projektion des Alters zeigte eine deutliche Trennung zwischen den Fettdepots vor dem Absetzen und den Fettdepots von Erwachsenen, insbesondere bei Zellen, die Pdgfra exprimieren, einen häufig verwendeten Präadipozytenmarker. Eine erneute Clusterbildung und differenzielle Genexpressionsanalyse ergab zwei Gene, die in subkutanen Präadipozyten vor dem Absetzen signifikant stark exprimiert werden: Igf2 und Asc-1. Im ersten Teil dieses Projekts konzentrierten wir uns auf die Rolle von Igf2, einem bekannten sekretierten Protein, das das fötale Wachstum fördert. Supplementierungs- und Neutralisierungsexperimente zeigten keine Wirkung von IGF2 auf die Adipogenese von primären murinen Präadipozyten. Eine IGF2-Supplementierung induzierte jedoch signifikant höhere Proliferationsraten von Präadipozyten aus erwachsenen Mäusen, in denen Igf2 nur selten exprimiert wurde. Die Fluoreszenz-In-situ-Hybridisierung zeigte, dass sich einige der Igf2+-Zellen in unmittelbarer Nähe der Blutgefäße befanden, wo einige der Vorläuferzellen der Adipozyten vorwiegend lokalisiert sind. Diese Ergebnisse deuten auf eine mögliche Rolle von IGF2 bei der hyperplastischen Ausdehnung des Gewebes hin, höchstwahrscheinlich durch Regulierung der Größe des Präadipozyten-Pools. Im zweiten Teil dieses Promotionsprojekts untersuchten wir die Rolle von Zellen, die Asc-1 exprimieren. ASC-1 ist ein Aminosäuretransporter, der zuvor von unserer Gruppe als Oberflächenmarker für weiße Adipozyten identifiziert worden war. Wir konnten zeigen, dass sich sowohl die sortierten ASC-1-low als auch die stabilen Asc-1-Knockdown-Zellen (shAsc-1) zu beigen Adipozyten differenzieren. Dies war zum Teil auf eine hohe D-Serin-Akkumulation in der Zelle zurückzuführen, die durch vorübergehendes Ausschalten des Enzyms, das L-Serin in D-Serin umwandelt (Serin-Racemase), aufgehoben wurde. Auf diese Weise konnten wir eine Subpopulation von Präadipozyten identifizieren, die Asc-1 exprimieren und damit die Entscheidung über das Schicksal der weißen bzw. beigen Linie steuern. Insgesamt unterstreichen unsere Ergebnisse die

Komplexität der Funktion und Heterogenität des weißen Fettgewebes. Wir schlagen hier auch bisher unerkannte Untergruppen von Präadipozyten vor, die eine Rolle bei der Modellierung von gesundem Gewebe spielen, das im erwachsenen Zustand implementiert werden kann.

Table of Content

1 Introduction

1.1 Adipose tissue development and expansion

White adipose tissue (WAT) is an endocrine organ that is critical for energy homeostasis (Friedman, 2019, Scheja and Heeren, 2019, Funcke and Scherer, 2019, Kershaw and Flier, 2004). Therefore, its proper development and expansion is crucial for a functional metabolism. In humans, mesenchymal fat lobules start to appear around 14 weeks of gestation that later differentiate into primitive fat lobules. This is initiated by mesenchymal cell condensation resulting in capillary network development and vascularization. The number of fat lobules is determined by week 23, whereas the size increases until week 29 (Desoye and Herrera, 2021, Poissonnet et al., 1983). In contrast to humans, the AdipoChaser mouse model, capable of tracing the fate of adipocyte progenitor cells, revealed that subcutaneous adipose tissue (SCF) starts to develop between E14 and E18, whereas perigonadal fat (PGF) depot emerges at P1 (Wang et al., 2013). In humans, adipocyte numbers increase until, and reach a constant, around 20 years of age in both lean and obese individuals, suggesting that the differences in adipocyte number are defined at early ages (Spalding et al., 2008). In contrast to this, a recent study showed that weight gain during adulthood increases both adipocyte size and number. Interestingly, bariatric surgery decreased only the adipocyte size, while the cell number was not altered (Petrus et al., 2018). This indicates that regulation of adipocyte cell number during both childhood and adulthood can be used as one of the preventive tools for the development of metabolic syndrome.

Adipose tissue expansion consists of two processes: increase in the number of newly formed (hyperplasia) and/or the size of adipocytes (hypertrophy) (Wang et al., 2013, Spalding et al., 2008). The commitment of preadipocytes to adipocyte differentiation starts with growth arrest followed by several rounds of cell cycle (Fajas, 2003). Given that adipocytes are post-mitotic and grow in size, there are many other factors regulating adipose tissue expansion, including proliferative progenitor cells maintaining the adipose progenitor cell (APC) niche, committed preadipocytes that contribute to hyperplasia to minimize the exhaustion of lipid accumulation in adipocytes and immune cells supporting adipocyte turnover (Altun et al., 2022). In mice, around 4.8-5% of preadipocytes and 1-5% of adipocytes are replaced per day (Rigamonti et al., 2011), whereas humans' annual adipocyte turnover is around 10% (Spalding et al., 2008). Thus, tight regulation of *de novo* lipogenesis, APC expansion and adipocyte death is crucial to maintain the adipocyte number throughout life. Furthermore, differences between human and mouse fat cell turnover should be taken into consideration when interpreting murine research for therapeutic approaches

applicable to humans, especially in terms of inducing beiging or hyperplastic expansion over hypertrophy (Altun et al., 2022).

The accumulation site of the fat is one of the main determinants of metabolic risk. The development of insulin resistance is associated with lipid accumulation in visceral white adipose tissue (vWAT), while the expansion of SCF is considered more protective (Vishvanath and Gupta, 2019, Booth et al., 2018, Hardy et al., 2012). The balance between lipogenesis and lipolysis regulates the amount of triglycerides stored and subsequently tissue remodeling in WAT. Insulin is one of the main mediators of glucose metabolism and lipogenesis. Thus, plays a key role in WAT homeostasis (Cignarelli et al., 2019).

1.2 Insulin and insulin like growth factors

Insulin and insulin-like growth factors (IGF) are peptide hormones belonging to the insulin superfamily and sharing similar structural homology (**Fig. 1**) (Andersen et al., 2017). Rinderknecht and Humbel isolated IGFs for the first time based on their (i) similar behavior to insulin, (ii) mitogenic activity and (iii) downstream players of growth hormone (GH) in mediating skeletal muscle growth (Van Wyk and Smith, 1999, Rinderknecht and Humbel, 1976). Despite being 62% identical to the proinsulin sequence, insulin like growth factor 1 (IGF1) and IGF2 do not undergo post-translational proteolysis (Rinderknecht and Humbel, 1978). However, further investigation revealed that they promote growth more prominently compared to the known insulin-like activities (Rinderknecht and Humbel, 1978). IGF2 binds to IGF1R with lower affinity than IGF1 and with different binding affinities to insulin receptor (InsR) isoforms (Selenou et al., 2022). IGF1, on the other hand, binds to IGF1R with 50-100-fold higher affinity than insulin. Additionally, hybrid heterodimers consisting of IGF1R and InsR also exists in the cell (Hakuno and Takahashi, 2018). Expression levels of receptors are regulated depending on the state of the cells, which also affects ligand concentrations. IGF1R is expressed predominantly in preadipocytes. Upon differentiation, InsR levels start to increase and its expression in adipocytes is slightly more than IGF1R (Boucher et al., 2010b, Entingh-Pearsall and Kahn, 2004). Thus, insulin in mature adipocytes is critical for lipid metabolism, while both insulin and IGF1 are regulators of preadipocyte survival and differentiation (Sakaguchi et al., 2017, Boucher et al., 2010a). Among insulin and IGFs, only IGF2 binds with high affinity to the IGF2 receptor (IGF2R). It was reported a long time ago that IGF2R acts as a scavenger receptor and is responsible for the lysosomal trafficking of IGF2, thus regulating its turnover. The receptor can also bind to mannose 6-phosphate (Brown et al., 2009). However, recent findings showed that the IGF2-IGF2R axis regulates angiogenesis in feto-placental endothelial cells through the extracellular signal-regulated kinase (ERK) 1/2 pathway (Sandovici et al., 2022). Interestingly,

IGF1R and IGF2R contain different domain structure. While, IGF1R has a kinase activity, IGF2R does not (Agrogiannis et al., 2014). Thus, insulin, IGF1 and IGF2 can promote both distinctive and mutual signaling cascades in the cell. Their association with obesity and Type 2 diabetes (T2D) is further discussed below.

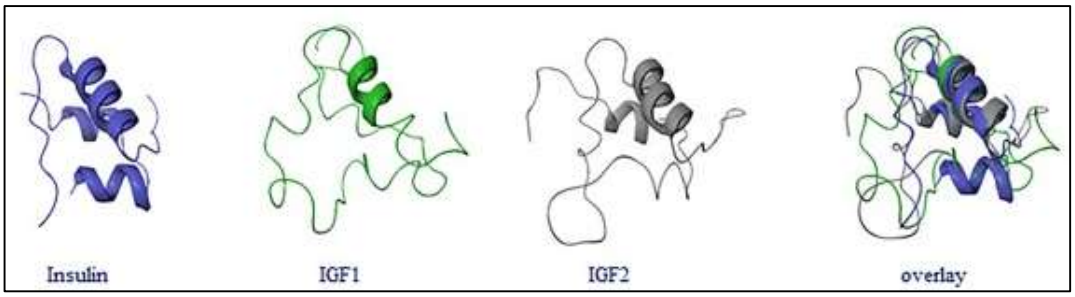

Figure 1: Structural homology of insulin, IGF1 and IGF2. Ribbon structure separately and an overlay of the three peptides are shown. This image is taken from (Andersen et al., 2017).

1.2.1 Insulin action in adipose tissue

Insulin was discovered in 1921 as a component of pancreatic extract that lowers blood glucose levels in diabetic dogs and humans with Type 1 diabetes. It increases glucose uptake in adipocytes and muscle cells and inhibits hepatic glucose production (**Fig. 2**) (Santoro et al., 2021, Rosen and Spiegelman, 2006). Circulating glucose acts as a control mechanism for nutrient storage and mobilization. Glucose taken up into the cell is utilized for ATP production and *de novo* lipogenesis through several processes. Most critically, insulin is responsible for cellular uptake of glucose in adipocytes (Summers et al., 2000, Cushman and Wardzala, 1980).

Insulin is produced and secreted by pancreatic β-cells. It binds to its receptor (InsR) and induces tyrosine kinase activity in β-subunit (Haring, 1991). This action of insulin activates PI3K signaling that results in translocation of glucose transporter-4 to the plasma membrane to increase glucose uptake (Huang et al., 2018). Glucose alone does not affect kinase activity or lipogenesis. However, its presence is required for insulin-activated kinase signaling to stimulate FA synthesis (Krycer et al., 2020). Furthermore, insulin also phosphorylates insulin substrate 1 (IRS-1) and activates mitogen-activated protein kinase (MAPK) signaling pathway. These pathways regulate mitogenic and metabolic signals including cell growth, proliferation and differentiation (Gehart et al., 2010). As a result, lipid storage in adipocytes is activated by stimulating *de novo* lipogenesis, inhibiting lipolysis and inducing glucose uptake (Sakers et al., 2022).

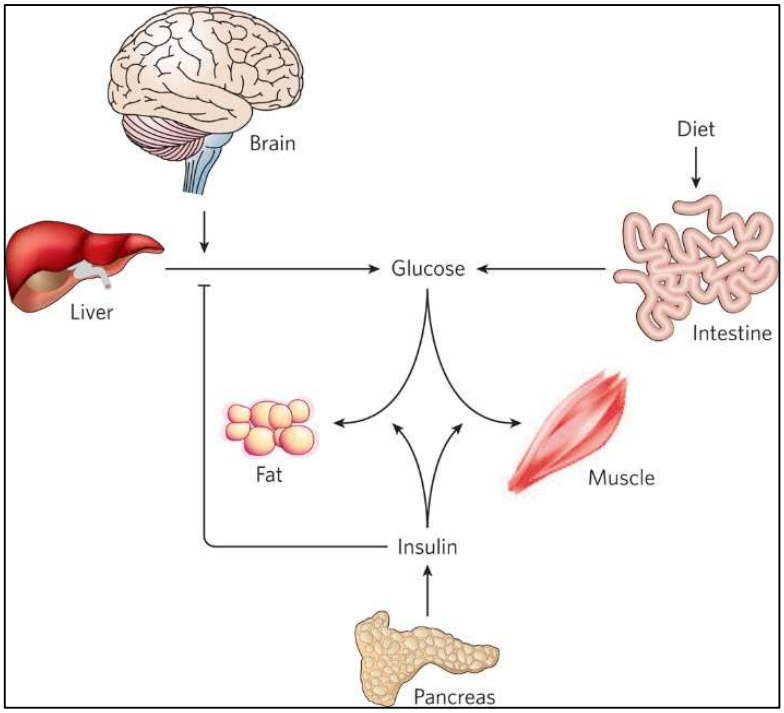

Figure 2: Insulin mediated glucose utilization in the whole body. After a meal consumption, glucose is absorbed in intestine and released into the circulation. This signals pancreas and induces insulin secretion by pancreatic beta cells, which binds to the insulin receptor and translocate glucose transporters to the plasma membrane. This action of insulin induces glucose uptake in muscle and fat cells to be used as energy source later and blocks hepatic glucose production. The figure is take from (Rosen and Spiegelman, 2006).

The majority of the insulin stimulated glucose disposal occurs in skeletal muscle, whereas only 10% occurs in adipose tissue (AT) (Smith and Kahn, 2016). Yet adipose tissue plays an important role in systemic energy metabolism and glucose tolerance (Saltiel and Kahn, 2001). Cross talk between AT, peripheral tissues and the central nervous system regulates lipid metabolism and maintains fat content in AT. However, disruption of this balance due to pathological conditions, such as obesity leads to metabolic complications (Song et al., 2018). The World Health Organization (WHO) identified insulin resistance as one of the components defining the Metabolic Syndrome along with central obesity and high blood pressure (Alberti and Zimmet, 1998). This highlights the importance of insulin signaling in the development of Type 2 Diabetes (T2D). Pancreas tries to compensate for insulin resistance; however, this leads to increased insulin secretion and consequently to hyperinsulinemia (Bunner et al., 2014). This results in beta-cell exhaustion in the pancreas.

Studies also showed that mice lacking insulin were born with growth retardation but died within 2 days after suckling milk due to ketoacidosis and hepatic steatosis (Duvillie et al., 1997). Furthermore, murine offspring with whole body knockout of the insulin receptor (*Insr*$^{-/-}$) did not show differences in intrauterine development but growth retardation was prominent postnatal compared to control littermates. *Insr*$^{-/-}$ mice developed hyperglycemia and died from diabetic

ketoacidosis within a couple of days after birth (Joshi et al., 1996, Accili et al., 1996). There have also been several cases of humans lacking the *INSR* reported. These individuals displayed intrauterine growth retardation, developmental delay and one baby lacked SCF. These patients developed hyperglycemia, which was less severe compared to insulin deficient individuals. In contrast to the findings in rodents, lack of *INSR* in humans is compatible with life. This discrepancy can be explained partly by the insulin action via IGF1R in these patients (Takahashi et al., 1997, Wertheimer et al., 1993, Krook et al., 1993). Moreover, the developmental stage of rodents at birth corresponds to around 26 weeks of gestation in humans. Thus, the embryonic growth phase dependent on INSR is limited in rodents, while this is extended in humans (Kitamura et al., 2003). This also highlights the roles of insulin and InsR in body composition. There are major differences in humans' and mice's lipid content upon birth, being 16% and 2% of whole-body weight, respectively (Kitamura et al., 2003, Widdowson, 1950).

Furthermore, insulin signaling plays an important role in adipocyte differentiation and maintenance. Adipose tissue-specific insulin receptor knockout mice (FIRKO) showed a reduction in fat mass. These mice gained less weight compared to the control group and were protected against insulin resistance induced by aging (Bluher et al., 2002). In addition to this, adipose tissue-specific double knockout of *InsR and Igf1r* (FIGIRKO) mice had disrupted WAT and brown adipose tissue (BAT) development (Boucher et al., 2012). Moreover, mice with inducible fat specific knockout of *InsR* or *InsR*/*Igf1r* developed lipodystrophy and insulin resistance (Sakaguchi et al., 2017). All these findings highlight the importance of insulin signaling in adipose tissue function and the development. Studies on gestational diabetes mellitus (GDM) showed a positive association with offspring adiposity (Tint et al., 2020, Bianco and Josefson, 2019). These findings further indicate the sensitivity of adipose tissue development to insulin. Nonetheless, no medication is approved to treat insulin resistance directly. Medications used in diabetes, such as; metformin, are lowering blood glucose and consequently improve insulin sensitivity. Unfortunately, all of these pharmaceutical treatments have severe side effects including nausea and dizziness (Pu et al., 2020). Thus, new treatment strategies should be found to provide better living standards for diabetic individuals. Understanding the AT composition and interactions within the microenvironment is crucial in curing obesity.

1.2.1 Role of IGF2 in development and growth

IGF2 is a secreted protein that plays an important role in fetal growth and development. Humans and mice show differences in the gene expression patterns. There are 10 exons and 5 promoters in humans, while 8 exons and 4 promoters in mice encoding for *IGF2/Igf2* (Selenou et al., 2022, Baral

and Rotwein, 2019, Monk et al., 2006). The locus includes *INSULIN* and *H19* along with other genes. There is a parent specific expression of *IGF2/Igf2* and *H19* genes leading to genetic regulation by imprinting. The maternal allele expresses *H19* (which is not translated into protein), while the paternal allele expresses *IGF2/Igf2* (Nordin et al., 2014). Studies showed that not the maternal but the paternal inheritance of the *Igf2* gene deletion leads to growth retardation and 40% birth weight loss compared to a normal mouse (DeChiara et al., 1991, DeChiara et al., 1990). There have been growth disorders described to arise from deregulation of imprinted genes on human chromosome 11p15.5, where *IGF2* is located (Chao and D'Amore, 2008). Russel Silver syndrome is characterized by prenatal and postnatal growth retardation (dwarf phenotype), wide forehead, fifth finger clinodactyly and feeding difficulty, which several patients were reported to have hypo-methylation of paternally inherited *IGF2* (Wakeling et al., 2017, Xia et al., 2019, Bartholdi et al., 2009). On the other hand, Beckwith-Wiedemann syndrome was associated with hyper-methylation of maternal allele and biallelic expression of *IGF2* resulting in fetal and neonatal overgrowth (Sparago et al., 2004, Reik and Maher, 1997).

In contrast to humans, where IGF2 is maintained at a certain level it is hardly detectable in adult mice (Holly et al., 2019). Fetal serum levels of IGF2 are higher than IGF1 (Lassarre et al., 1991, Ashton et al., 1985), around 401 vs 113 ng/mL, respectively, between 33-37 gestational weeks (Lassarre et al., 1991). IGF2 could be involved in fetal growth in an organ- and sex-dependent manner, rather than in fetuses' weight and size, which correlate with IGF1 (White et al., 2018, Lassarre et al., 1991). While IGF2 treatment only significantly increased female rat stomach weight, it affected males more and increased their organs' mass significantly except for lungs, heart and kidney (White et al., 2018). Along with this, gene expression analysis of chorionic villi samples taken from 260 pregnancies showed a positive correlation between birth weight and *IGF2* mRNA levels indicating its role in utero growth (Demetriou et al., 2014).

1.2.2 Role of IGF2 in adipogenesis

The postnatal regulation of IGF2 is poorly understood. This is because, firstly, the biological processes stimulated by IGF2 are much more complex than those induced by IGF1R and Insulin. Secondly, post-natal physiology of IGF2 in humans and mice show differences (Holly et al., 2019). Nevertheless, as mentioned in the previous section, many studies indicated a correlation between IGF2 and birth weight, which is partly composed of fat mass. However, there are contradictory data on IGF2 and its postnatal role in adiposity and metabolic function.

A genetic polymorphism study of rs680 SNP of the *IGF2* gene (ApaI) showed significant associations with the metabolic syndrome. People carrying the AA genotype had more circulating IGF2 in their serum than those with GG (Gui et al., 2021a, O'Dell et al., 1997). Females carrying the AA (rare) genotype had significantly higher HbA1c and plasma glucose levels compared with subjects carrying GG (wild-type). On the other hand, males with the AA genotype were positively associated with higher waist-hip ratio and serum triglyceride levels (Gui et al., 2021a). Moreover, healthy Caucasian women and men with the AA genotype showed more fat mass compared to subjects with the GG genotype. However, when other ethnic groups were included, this association disappeared. The same study also did not find differences between circulating IGF2 levels between genotypes (Roth et al., 2002).In contrast to this, a 4.5 year follow-up study on non-obese individuals showed that lower circulating IGF2 levels were associated with weight gain over time compared to individuals with stable weight (Sandhu et al., 2003). Moreover, obese individuals had less circulating IGF2 compared with non-obese (Sandhu et al., 2003, Chang et al., 2002). These discrepancies highlight the importance of ethnic backgrounds and the effect of environmental factors. Nevertheless, these findings point toward an important regulatory function of IGF2 in adipose tissue physiology.

Several transgenic rodent models have studied the *in vivo* function of IGF2 by maintaining persistent circulating levels in adult mice. This was achieved via overexpressing transgene in the liver by the major urinary protein promoter. These mice showed decreased body weight mainly due to reduced fat mass (Rogler et al., 1994). Further characterization of these mice by insulin clamp studies revealed lower plasma glucose and insulin levels with higher glucose disposal rate in the muscle and increased hepatic glycogen synthesis (Rossetti et al., 1996). Moreover, paternal deletion of *Igf2* (*Igf2*$^{+/-}$) in mouse embryos showed increased BAT weight, which was enhanced with double knockout of *Myod* and *Igf2* (*Myod*$^{-/-}$*Igf2*$^{+/-}$) even though *Myod*$^{-/-}$ did not show any difference in BAT mass. This increase in BAT mass of *Myod*$^{-/-}$*Igf2*$^{+/-}$ mice was due to increased hyperplasia. Knockdown of *Igf2* slightly increased lipid accumulation in differentiated brown adipocytes compared to wild-type and this reached significance when there was a double knockdown with *Myod*. These findings show that IGF2 and MYOD act together to repress BAT development (Borensztein et al., 2012). Another study on isolated healthy children's white adipose depots reported that a high dose of IGF2 supplementation (62.5 ng/mL) enhanced the differentiation capacity of subcutaneous preadipocytes, but restricted visceral preadipocytes. This was because the treatment downregulated InsR, FASN and GLUT4 expression levels in visceral adipocytes, which reduced glucose uptake by 34% (Alfares et al., 2018). All these studies highlight that IGF2 has a

depot specific action and the signaling pathways stimulated by the protein in adipose tissue are relatively complex, which still requires further investigation.

1.3 What is Obesity?

Obesity is characterized by excess body fat accumulation resulting in metabolic disorders; such as, hyperglycemia and dyslipidemia. Individuals with a body mass index (BMI) above 30 kg/m^2 are classified as obese, while overweight is defined by the BMI over 25.0 kg/m^2 (Fruh, 2017, Hurt et al., 2010) However, it is still under debate whether BMI is a good indicator in defining obesity. It has been discussed that the BMI reference underestimates body fat in South Asian children, and overestimating in African American children (Hudda et al., 2018). Nevertheless, it provides a good indicator on what is a healthy or unhealthy weight (Gutin, 2018). Over the past decades, the global obesity epidemic has attracted great attention of the public health system. This is not only due to the increased number of cases but also because of the unpredictable medical costs, increased mortality rates and obesity associated comorbidities; such as, cardiovascular diseases, T2D and certain cancers. (Hruby and Hu, 2015, Hurt et al., 2010). It is considered that individuals who display an increase of 20% above the desirable body weight is in great health risk (Capodaglio and Liuzzi, 2013). A European Prospective Investigation into Cancer and Nutrition involving five European countries showed that the prevalence of obesity increased from 13% to 17% at the follow-up between 1998 and 2005 (Hruby and Hu, 2015, von Ruesten et al., 2011). Moreover, it was reported that there were regional differences in terms of the obesity rates, Southern and Eastern Europe have higher rates of obesity compared to Western and Northern Europe (Hruby and Hu, 2015, Berghofer et al., 2008). The numbers were more dramatic in the United States. According to the Centers for Disease Control and Prevention's National Health and Nutrition Examination Survey, 35% of the adult Americans were obese between 2011 and 2012 (Ogden et al., 2013). Moreover, adults living in rural areas had a significantly higher prevalence of obesity than urban adults did between 2005 and 2008 (Befort et al., 2012).

There are familiar traits and genetic factors that play a role in the development of obesity. SCF and vWAT distribution is impacted by family background and is inherited by 44%-57% and 36%, respectively (Fox et al., 2012, Fox et al., 2007). Alternatively, genome-wide association studies (GWAS) showed strong correlations between insulin resistance and adiposity (Chu et al., 2017, Lotta et al., 2017). A population-based genetic analysis revealed 53 genomic regions associated with lower levels of peripheral fat and insulin resistance. Interestingly, individuals with a higher predisposition to insulin resistance had relatively lower ability to expand SCF under caloric challenge. This suggests that the fat accumulation capacity of SCF compared to vWAT is a stronger

indicator of insulin resistance (Vishvanath and Gupta, 2019, Lotta et al., 2017). Additionally, polymorphisms in peroxisome proliferation-activated receptor gamma (PPARγ) and adiponectin (ADIPQ) have been correlated with obesity, T2D and insulin resistance (Howlader et al., 2021, Prakash et al., 2012). Even though genetic components play an important role in the prevalence of obesity, the exponential rise over the past three decades strongly suggests the role of environmental factors. Sedentary lifestyle due to socio-economic status, cultural norms around food and changes in working styles are one of the main components of the environmental influence (Wakefield, 2004). Nevertheless, one of the main drivers in the development of metabolic syndromes is the challenged physiological function and lipid storage capacity of adipose depots.

1.3.1 Metabolically healthy vs. unhealthy obesity

In the 1950s, Jean Vague's described obese individuals with different predispositions to T2D and cardiovascular disease, which could be attributed to their distribution of body fat. The concept of metabolically healthy obesity (MHO) was shaped as a result of these observations and started to attract more attention only a decade ago (Bluher, 2020). Human cohort studies showed MHO as a transient state by nature. Eight years follow-up of healthy obese participants in the English Longitudinal Study of Ageing (ELSA) revealed their transition to an unhealthy state by 44.5%. This change was not connected to physical activity but to increased waist circumference, systemic inflammation and impaired glycemic control, potentially suggesting adverse effects of vWAT (Hamer et al., 2015). Additionally, the North-West Adelaide Health Study reported that only 1/3 of the metabolically healthy obese subjects developed metabolic syndrome. In contrast to the ELSA study, the persistence of healthy metabolism was associated with the younger age (≤40) and more subcutaneous fat accumulation (Appleton et al., 2013). Furthermore, comparison of MHO and metabolically unhealthy obesity (MUO) in response to high calorie diet intervention showed distinct biological responses. Upon moderate weight gain, MHO individuals showed increased lipogenesis compared to MUO subjects, who had worsened effects on plasma adiponectin and triglyceride concentrations (Fabbrini et al., 2015).

On the other hand, although the MHO is defined as obese individuals lacking any metabolic disorder and cardiovascular disease, the classification criteria vary greatly among studies. (Bluher, 2020, Magkos, 2019). In some studies, blood pressure, triglyceride levels, fasting blood glucose, HOMA-IR value, HDL-C and CRP levels were considered. Obese individuals were classified as MH if they have no or 1 of the cardiometabolic abnormalities (Hamer et al., 2015, Wildman et al., 2008). Whereas other studies evaluated, in addition to the mentioned parameters above, waist circumference, drug treatment, glucose tolerance, fasting insulin levels, white blood cell count or

uric acid and plasma fibrinogen levels (Pajunen et al., 2011, Iacobellis et al., 2005). This uncertainty in the classification criteria of MHO can lead to wrong estimations of its prevalence (Liu et al., 2019). For instance, a collaborative analysis of ten large published cohort studies showed that when strict criteria are used based on blood pressure (SBP ≥ 130 mmHg or DBP ≥ 85 mmHg) and blood glucose (fasting ≥ 6.1 mmol/l or non-fasting ≥ 7.0), there are higher numbers of obese individuals with metabolic syndrome reported compared to the analysis based on less strict criteria (blood pressure: SBP ≥ 140 mmHg or DBP ≥ 90 mmHg and blood glucose: fasting ≥ 7.0 mmol/l or non-fasting ≥ 7.8 mmol/l) (van Vliet-Ostaptchouk et al., 2014). Along with this, the classification according to cardiometabolic abnormalities defined in five different studies together with BMI or waist circumference showed 4.2-13.6% or 14-40.2% prevalence to MHO, respectively (Liu et al., 2019).

Nevertheless, there have been some common physiological and phenotypic traits reported among MHO subjects. These individuals have less hepatic and visceral, but more subcutaneous (around the leg) fat content. They are more insulin sensitive with normal blood pressure and lower inflammation (Bluher, 2020, Stefan et al., 2008). One of the primary drivers of healthy adipose tissue expansion is via the recruitment of new adipocytes (Vishvanath and Gupta, 2019). Thus, it is crucial to understand the adipocyte progenitor cell (APC) populations that give rise to adipocytes resident in the AT and how they respond to over-nutrition.

1.3.2 Different adipose tissues and their role in obesity

There are two main types of adipose depots; BAT and WAT. These depots have different developmental origins. Myf5 lineage tracing mouse model showed that except perirenal and peraortic BAT, brown adipocytes are derived from $Myf5^+$ lineage, whereas SCF and PGF are $Myf5^-$ (Sanchez-Gurmaches and Guertin, 2014, Seale et al., 2008). Due to their distinct physiological and pathophysiological roles, these depots respond differently to caloric overflow and consequently to obesity.

1.3.2.1 White adipose tissue

White adipocytes are unilocular and synthesize triglyceride to be stored as lipid droplets. Thus, they are one of the primary sites of long-term energy storage. SCF is located under the skin and is mainly responsible for protection against external forces and serves as an insulator. On the other hand, vWAT is found deep in the abdominal cavity surrounding the organs (Vishvanath and Gupta, 2019, Schoettl et al., 2018). In humans, SCF divided as upper and lower, while in mice it is separated as anterior or posterior. Moreover, mice have PGF and humans have omental fat (Luong et al., 2019, Schoettl et al., 2018). Distribution of these depots is an important determinant for metabolic health

in obesity (Capodaglio and Liuzzi, 2013). Tracking of adipogenesis using AdipoChaser mice revealed that upon high fat diet (HFD) feeding both PGF and SCF expand through cellular hypertrophy. However, prolonged HFD feeding induces adipogenesis (hyperplasia) only in PGF and not in SCF (Wang et al., 2013). WAT undergoes various changes under excess caloric intake to allow nutrient and oxygen flow. This includes remodeling of the extracellular matrix (ECM) because of tissue expansion and upregulation of pro-inflammatory cytokines recruiting immune cells (Pellegrinelli et al., 2016, Schoettl et al., 2018). The degree of these changes varies between different types of WAT and therefore their effect on health as well. Abdominal fat accumulation (apple-shaped obesity), resulting in vWAT expansion, exerts greater metabolic risk; such as, T2D, compared to SCF accumulation in the lower body (pear-shaped obesity) (Vishvanath and Gupta, 2019, Karpe and Pinnick, 2015). One reason for the hazardous effects of vWAT expansion lies within its anatomical location. The secreted adipokines and FFAs by the visceral fat can be facilitated to the liver directly via the portal vein and as a result disrupt hepatic homeostasis (Rytka et al., 2011). The second reason associated with unfavorable effects of fat accumulation in vWAT is due to the restricted area in the intra-abdominal space (Schoettl et al., 2018).

Furthermore, genome-wide association studies showed sexual dimorphism correlated with fat distribution (Randall et al., 2013, Heid et al., 2010). Obese women tend to store fat more in SCF while obese men in vWAT. Estrogen, on the other hand, promotes SCF and limits vWAT expansion (Steiner and Berry, 2022). Therefore, women are more protected against developing the metabolic syndrome compared to men. This effect is lost after menopause. All these findings highlight the metabolic complexity established by the presence of different WAT depots. Therefore, it is important to understand the mechanisms involved in the development and adipogenesis of each WAT depot individually.

1.3.2.2 Brown adipose tissue and beige/brite adipocytes

Brown adipose tissue is present in both rodents and infants. Until recently, it was thought to be absent in human adults. However, PET and CT scans showed that the BAT is present in several parts of human body, including neck (Virtanen et al., 2009, Cypess et al., 2009). Its activity is higher in young and lean people (Townsend and Tseng, 2014). Even though excessive WAT expansion and fat accumulation is considered hazardous during obesity, BAT has been described to have an anti-obesity effect. Its activity was shown to increase energy expenditure and reduce weight gain (Yoneshiro et al., 2013, Stanford et al., 2013).

BAT consists of multilocular adipocytes. The high degree of vascularization and innervation of sympathetic nerves distinguishes it from WAT. Moreover, BAT adipocytes have high mitochondrial content and express uncoupling protein 1 (UCP1) as opposed to white adipocytes (Pellegrinelli et al., 2016, Hocking et al., 2013). UCP1 is a BAT specific protein expressed in the inner membrane of the mitochondria. Studies recently showed heterogeneity in brown adipocytes with different levels of UCP1 expression (Karlina et al., 2021, Song et al., 2020). Activation of this protein via cold exposure or beta-adrenergic signaling enhances glucose and fatty acid oxidation yielding heat rather than ATP. Therefore, BAT is described to be responsible for the non-shivering thermogenesis and is the 'fat burning' organ (Carpentier et al., 2018, Townsend and Tseng, 2014, Argyropoulos and Harper, 2002).

Cousin *et al.* detected for the first time the presence of UCP expression in rat WAT in the early 1990s. The expression was enhanced upon cold or beta-adrenoceptor agonist treatment like in typical BAT (Cousin et al., 1992). This phenomenon was described as the 'browning' of WAT (Bartelt and Heeren, 2014). They are also known as beige adipocytes. Due to their morphology (multilocular lipid droplets), high degree of mitochondrial content and expression of UCP1, were described to be like classical BAT cells (Wu et al., 2012, Cousin et al., 1992). However, unlike brown adipocytes, they are $Myf5^-$ and have a unique gene expression profile. Therefore, beige/brite adipocytes are considered as a different type of thermogenic fat cell than classical brown adipocytes (Wu et al., 2012, Seale et al., 2008). Mapping of quantitative trait *loci* demonstrated differences in the control of UCP1 positive cells in BAT and WAT (Coulter et al., 2003). Additionally, Xue *et al.* showed a peak of *Ucp1* expression and multilocular adipocytes in retroperitoneal fat between P10 and P30. In contrast to this, intrascapular BAT expressed maximal levels of *Ucp1* at P1, indicating developmental differences between brown and beige/brite adipocytes as well (Xue et al., 2007).

1.4 Adipose progenitor cell populations (APCs)

There have been various cell types; such as, mesenchymal stem cells, pericytes and preadipocyte, described to give rise to adipocytes (Schoettl et al., 2018). Genetic lineage tracing and single cell RNA sequencing (scRNA-seq) studies identified distinct adipose progenitor lineages and intermediate states of cells giving rise to adipocytes (Altun et al., 2022, Sakers et al., 2022, Merrick et al., 2019, Lee et al., 2019). However, until recently there was no clear definition of APCs. Sakers *et al.* and we described APCs as cells with stem like properties that are highly proliferative and regulate progenitor niche maintenance. There is a lineage hierarchy, which progenitor cells give rise to committed preadipocytes that later differentiate into adipocytes (Altun et al., 2022, Sakers et al., 2022, Merrick et al., 2019). On the other hand, the term preadipocyte is broadly used in the

literature and referred as cells that have the ability to differentiate into adipocytes (Altun et al., 2022).

Berry and Rodeheffer introduced for the first time the concept of hierarchical difference in the differentiation capacity of progenitor cells. They have shown that Lin^{-}:$CD34^{+}$:$CD29^{+}$:$Sca\text{-}1^{+}$ cells subdivide into two subtypes with having more or less commitment to adipocyte differentiation: $CD24^{-}$ and $CD24^{+}$ cells respectively. This was further confirmed using PDGFRa-cre dependent reporter mice (Berry and Rodeheffer, 2013). Interestingly only a small portion of the stromal vascular cells (SVCs) was composed of $CD24^{+}$ (0.08%), while around 53% of the cells were $CD24^{-}$. Yet transplantation of $CD24^{+}$ but not $CD24^{-}$ APCs formed a functional WAT in A-zip lipodystrophic mice and showed that $CD24^{+}$ produce $CD24^{-}$ cells (Rodeheffer et al., 2008) (**Fig. 3**). In addition to this, Jiang *et al.* described '*developmental*' and '*adult*' APCs (Jiang et al., 2014). PDGFRa-RFP reporter mouse model showed that '*developmental*' $PDGFRa^{+}$ SVCs were necessary for tissue formation and AT expansion, whereas other APC population contributed to '*adult*' adipocytes and

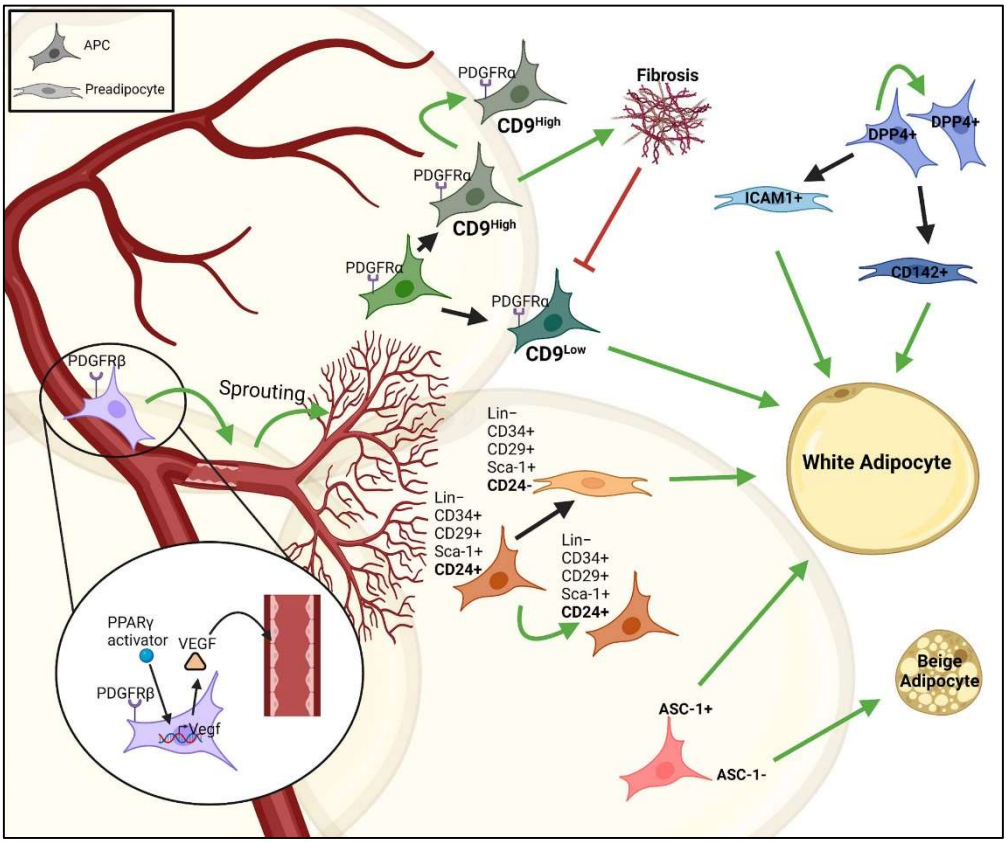

Figure 3: An overview of adipocyte progenitor cells resident in the adipose tissue. There are various subpopulation of APCs with proliferative and self-renewal capacity in the adipose tissue ($CD24^{+}$ and $DPP4^{+}$ cells). This is shown by green arrows, which the cell give rise to the same type of cell. Moreover, there are cell populations giving rise to committed preadipocytes that differentiate into white ($CD24^{-}$, $ICAM1^{+}$ and $ASC\text{-}1^{+}$) or beige ($ASC\text{-}1^{-}$) adipocytes later. There are also progenitor cells regulating vascular-APC interaction ($PDGFR\beta^{+}PPAR\gamma^{+}$ cells) or induce fibrosis in the tissue ($PDGFRA^{+}CD9^{high}$ cells). The image is taken from (Altun et al., 2022)

subsequently to tissue maintenance (Shin et al., 2020). In other studies, PDGFRa signaling was shown to induce tissue fibrosis (Iwayama et al., 2015). In accordance with this, two subpopulations of PDGFRa^{+} have been identified. PDGFRa^{+}CD9^{high} cells were highly proliferative and exhibited a pro-fibrotic phenotype, whereas PDGFRa^{+}CD9^{low} cell were highly adipogenic. However, AT fibrosis, upon HFD feeding, completely abolished the occurrence of PDGFRa^{+}CD9^{low} cells (Marcelin et al., 2017) (**Fig. 3**). Recently Merrick *et al.* identified a highly proliferative dipeptidyl peptidase-4 (DPP4)$^{+}$ progenitor cells that produce CD142^{+} and ICAM1^{+} committed preadipocytes (Merrick et al., 2019). Lineage tracing with DPP4-Cre reporter mouse model was in line with these findings. Additionally, transgenic mice fed with HFD showed fluorescent labelled mature adipocytes indicating that these cells were involved in adipogenesis and a shift from DPP4^{+} to DPP4^{-}ICAM1^{+} committed preadipocytes in SCF (Stefkovich et al., 2021). These cells were sitting in the reticular interstitium surrounding adipose tissue depot (Merrick et al., 2019). It was also shown that subpopulation of APCs display a PPARγ dependent transcriptional activation of PDGFRβ and VEGF axis that regulate APC-vascular niche interaction. This plays a mutual effect meaning that APCs are essential for vascular expansion, while without sprouting APCs cannot maintain their niche and expand (Jiang et al., 2017) (**Fig. 3**).

1.4.1 Subpopulation of cells expressing *Asc-1*

Our group previously identified the alanine/serine/cysteine amino acid transporter 1 (ASC-1) as a surface marker for white adipocytes (Ussar et al., 2014). Its expression is upregulated upon differentiation (Arianti et al., 2021, Jersin et al., 2021, Ussar et al., 2014). ASC-1 is encoded by *Slc7a10* gene and is a sodium independent neutral amino acid transporter (Ussar et al., 2014). It is a selective transporter for L-alanine, L-serine, L-threonine and L-cysteine (Fukasawa et al., 2000). Additionally, ASC-1 has a high affinity for the N-methyl-d-aspartate-type glutamate (NMDA) receptor co-agonists, D-serine and glycine (Rutter et al., 2007, Fukasawa et al., 2000). It is responsible for the synaptic clearance of D-serine and synaptic transport of glycine for the control of glycinergic transmission (Ehmsen et al., 2016, Safory et al., 2015, Rutter et al., 2007, Matsuo et al., 2004). Whole body *Asc-1* knockout *(Asc-1$^{-/-}$)* mice showed seizure, ataxia and tremors causing early lethality (21 days postnatal) limiting long term *in vivo* studies. These behavioral effects were attributed to over-activation of the NMDA receptor, which was reduced by the NMDA antagonist (MK-801) (Xie et al., 2005). Moreover, these behavioral phenotypes reported in *Asc-1$^{-/-}$* mice were rescued by glycine and L-serine administration (Safory et al., 2015). These findings indicate an important physiological role of ASC-1 in the regulation of synaptic activity in the brain. However, our group previously showed that *Asc-1* expression is 5-fold higher in WAT than brain (Ussar et al.,

2014). Yet its role in metabolic regulation is a recently emerging field. *Asc-1* knockout Zebrafish gained more weight and had bigger lipid droplets in PGF compared to the wild-type controls. Moreover, there was a negative correlation between insulin resistance and omental obesity in humans and *Asc-1* expression levels. 3T3-L1 cells and human adipose stromal cells treated with ASC-1 inhibitor (BMS-466442) had increased lipid accumulation compared to DMSO-treated cells (Jersin et al., 2021). Addition to this, we have also shown recently (parts of it is discussed in this thesis later) that loss of *Asc-1* function or sorting of ASC-1$^-$ cells in white preadipocytes induced beiging and overexpression of *Asc-1* in brown adipocytes down regulated browning markers. Thus, we were able to identify a subpopulation of cells expressing ASC-1 that regulates white vs beige cell fate decision partly via D-serine metabolism (**Fig. 3**) (Suwandhi et al., 2021).

These findings highlight the complexity in lineage commitment and heterogeneity in the WAT. Moreover, to treat obesity and metabolic disorders, it is important to understand the core mechanisms regulating tissue homeostasis and expansion, which is regulated primarily via the diversity created by APC subpopulations.

2 Aim of this study

White adipose tissue expands rapidly and massively at the early ages of life without causing any metabolic deterioration. However, if this expansion continues to adulthood, these individuals would develop obesity. We hypothesized that factors or subset of cells highly abundant at younger state of adipose tissue might be critical players of the healthy expansion and function of WAT. Thus, we aimed to understand the compositional differences between the young and adult state. To do this, we compared fat tissues of pre-weaned (2-weeks old) to adult (8-weeks old) wild-type mice. scRNA-seq analysis of three adipose depots (SCF, PGF and BAT) revealed *Igf2* and *Asc-1* as factors significantly highly expressed in pre-weaned subcutaneous depot compared to adult. IGF2 is a well-known fetal growth promoter and its postnatal role is not well studies. Therefore, **the first aim of this study was to unravel the function of IGF2 in adipose tissue expansion.** This was studied through preadipocyte proliferation and differentiation capacities. *In vitro* experiments were performed in two different culture conditions; normal cell culture (10% FBS) and physiological conditions (1% adult mouse serum), to mimic physiological conditions and eliminate excess exogenous IGF2. In the second part of this thesis, **we investigated the role of *Asc-1* in WAT function.** Since our group previously identified ASC-1 as a surface marker for white adipocytes, we studied fate of preadipocytes towards beige vs white adipocyte fate. Moreover, ASC-1 is an amino acid transporter, with high affinity to D-serine, to further characterize the mechanistic function of *Asc-1*; we linked it with regulation of D-serine metabolism.

3 Materials

3.1 List of Reagents and Chemicals

Table 1: List of reagents and chemicals

Product	Company	Catalog Number
3-Isobuthyl-1-methylxanthin (IBMX)	Sigma-Aldrich	I5869-1G
Seahorse XF DMEM Medium	Agilent	103575-100
A/G agarose beads	Santa Cruz Biotechnology	Sc-2003
Ammonium persulfate (APS)	Serva	13375.01
Antimycin A	Sigma Aldrich	A8674
autoMACS Running Buffer	Miltenyi Biotech	130-091-221
Beta-mercaptoethanol	Carl Roth	4227.3
Bovine serum albumin fraction V (BSA)	Carl Roth	T844.2
CellStripper	Corning	25-059-Cl
Chloroform	Carl Roth	4423.1
Collagenase type I	Gibco	17018029
Collagenase type IV	Gibco	17104019
Dako fluorescence mounting medium	Agilent Technologies	S302380-2
Diethyl pyrocarbonate	Sigma-Aldrich	D5758-25ML
Dexamethasone	Sigma-Aldrich	D4902
DMEM high-glucose + GlutaMAX	Life Technologies	31966021
EDTA disodium salt dihydrate	Carl Roth	8043.1
Ethanol (absolute)	Merck Millipore	UN1170
Ethanol (vergällt) 99.9%	Helmholtz Zentrum Muenchen	5000006
EZ-RUN Recombinant Protein Ladder	Fischer Scientific	10785674
Fetal bovine serum	Life Technologies	10270106
FCCP	R&D Systems	0453/10
Formaldehyde solution 37%	Carl Roth	4979.1
Glucose	Sigma Aldrich	49159
GlutaMAX	Gibco	350050038
Hydrochloric acid (HCl 37%)	Sigma-Aldrich	30721-1L-GL

ImmobilonTM Western Chemiluminescent HRP substrate	Merck Millipore	WBKLS0500
Insulin (cell culture)	Sigma-Aldrich	I9278
Insulin like growth factor 2 (IGF2)	Sigma-Aldrich	I8904
Isopropanol	Sigma-Aldrich	33539-2.5L
iTaq Universal SYBR® Green Supermix	BioRad	172-5124
Ketamine	Pharmanovo GmbH	
Lipofectamine™ RNAiMAX Transfektionsreagenz	Life Technologies	13778075
MACS G magnetic beads	Miltenyi Biotech	130-071-101
Matrigel	Corning	
Mayer's solution (Hematoxylin)	Merck	1092490500
Methanol	Merck Millipore	UN1230
MTT, Thiazolyl blue	Serva	20395.03
Normocin	InvivoGen	Ant-nr-1
Nuclease-free water	Qiagen GmbH	129114
OCT compound	Tissue Tek	4583
Oil Red O powder	Alfa Aesar	A12989
QIAzol	Qiagen GmbH	79306
Oligomycin	Sigma Aldrich	O4876
Opti-MEM™ I Serumreduziertes Medium	Gibco	31985062 and 31985070
Paraffin wax	Leica Surgipath	39601006
Paraformaldehyde	Th. Geyer	GE/00008416/000500
Penicillin/Streptomycin (Pen/Strep)	Life Technologies	15140-122
Phosphatase inhibitor cocktail II	Sigma-Aldrich	P5726-1mL
Phosphatase inhibitor cocktail III	Sigma-Aldrich	P0044-5mL
Phosphate buffer saline (PBS)	Life Technologies	14190-094
Sodium hydroxide (NaOH)	Roth	6771.3
Protease inhibitor cocktail	Sigma-Aldrich	P8340-5mL
Puromycin hydrochloride	Biomol	Cay13884-500
Rosiglitazone	Santa Cruz Biotechnology	Sc-202795
Rotenone	Sigma Aldrich	R8875

Roti®-Histokitt II	Carl Roth	T160.1
Sample buffer 4x	Life Technologies	NP0008
Sodium chloride (NaCl)	Carl Roth	3957.1
Sodium chloride solution 0.9%	Fresenius Kabi Deutschland GmbH	808765
Sodium dodecyl sulfate (SDS)	Carl Roth	CN30.3
Sodium hydroxide (NaOH)	Carl Roth	6771.3
StartingBlock™ T20 (TBS) Blocking Buffer	Thermo Fischer	37543
SuperSignal West FEMTO Max. Sensitivity Substrate	Fisher Scientific	10187393
Temed	AppliChem	A1148.0100
Thermo ScientificTM RestoreTM PLUS Western Blot Stripping Buffer	ThermoFischer Scientific	10016433
TRIS Pufferan	Carl Roth	4855.1
TritonTM X-100	Sigma-Aldrich	N150
Trypan blue solution	Sigma-Aldrich	93595
Trypsin, 0.05% EDTA, phenol red	Life Technologies	11580626
Tween-20	Santa Cruz Biotechnology	Sc-29113
Prozylaz	Belo-pharm	
Xylol	Carl Roth	9713.5

3.2 List of Buffers

Table 2: Buffer names and their composition

Buffer	Composition
1X Blotting buffer	1x Running buffer, 20% MeOH, MilliQ water
1x Running Buffer	1x Running Buffer, 0.1% SDS, MilliQ water
10x Running buffer	25 mM TRIS Pufferan, 192 mM Glycine, MilliQ water
20x MOPS-Running Buffer	1 M MOPS, 1 M TRIS Pufferan, 2% SDS, 20 mM EDTA, MilliQ water, pH: 7.4
Immunoprecipitation washing and lysis buffer	50 mM TRIS Pufferan, 150 mM NaCl, 2 mM EDTA, 1% TritonX-100, 1:100 Phosphatase buffer, 1:100 1:100 Protease Inhibitor Coctail II, 1:100 Protease Inhibitor Coctail III, MilliQ water, pH: 7.4

RIPA-buffer	50 mM TRIS Pufferan, 150 mM NaCl, 1 mM EDTA, 1% TritonX-100, MilliQ water, pH: 7.4
Protein lysis buffer	RIPA-buffer, 1:100 Phosphatase buffer, 1:100 1:100 Protease Inhibitor Coctail II, 1:100 Protease Inhibitor Coctail III, 0.1% SDS
Tissue digestion solution	1% BSA fraction V, 1mg/mL Collagenase type I, pure DMEM high-glucose + GlutaMAX
10x Tris-buffered saline (TBS)	10 mM TRIS Pufferan, 145 mM NaCl, MilliQ water, pH: 7.4
1x Tris-buffered saline Tween 20 (TBS-T)	1x TBS, 0.1% Tween 20, MilliQ water

3.3 List of Kits

Table 3: List of the kits used

Product	Company	Catalog Number
High-Capacity cDNA Reverse Transcription Kit	ThermoFischer Scientific	4368813
m/r/p/caIGF-II Qkit	R and D Systems	MG200
PierceTM BCATM Protein-Assay	ThermoFischer Scientific	23225
RNAscope Multiplex Fluorescent Assay Mm Fixed Frozen	Bio-techne	323133
RNeasy Mini Kit	Qiagen GmbH	74106
Ultra-Sensitive Mouse Insulin ELISA Kit	Crystal Chem	90080
TriFECTa DsiRNA Kit Srr	IDT	mm.Ri.Srr.13

3.4 List of Primary and Secondary Antibodies

Table 4: List of antibodies used

Antibody	Company	Catalog Number
ASC-1 (10A11)	In House	
AKT (pan) (11E7)	Cell Signalling	4685
Alexa Fluor 546 Phalloidin	Life Technologies	A22283

Alexa Fluor 647 Phalloidin	Life Technologies	A22287
β-Actin	Santa Cruz Biotechnology	Sc-47778
CD31	Merck Millipore	MAB1398Z
DAPI	Sigma-Aldrich	D9542
HCS LipidTOX green (lipid)	Life Technologies	H34475
Goat IgG (cell culture)	Invitrogen	31245
IGF-I Receptor β (D23H3) XP	Cell Signalling	9750
RNAscope® Probe - Mm-Igf2	Bio-techne	437671
IGF2 (neutralizing)	Thermo Fischer	PA5-47946
Insulin Receptor Beta (L55B10)	Cell Signalling	3020
GAPDH (6C5)	CalbioChem	CB1001
Mouse Alexa Fluor 594	Life Technologies	A21203
Mouse Alexa Fluor 594	Dinova	415-585-166
Mouse Alexa Fluor 488	Dinova	415-545-166
Mouse IgG-HRP	Santa Cruz Biotech	Sc-2005
KI67	Abcam	Ab15580
Lipitox Green	Life Technologies	H34475
p44/42 MAPK (Erk1/2) (137F5)	Cell Signalling	4695
PERILIPIN-1 (D1D8)	Cell Signalling	9349
Phospho-AKT (Ser 473)	Cell Signalling	9271
Phospho-p44/42 MAPK (Erk1/2) (197G2)	Cell Signalling	4377
Phospho-Tyrosine (P-Tyr-1000) MultiMab™	Cell Signalling	8954
PPARγ (81B8)	Cell Signalling	2443
Rabbit Alexa Fluor 594	Jackson ImmunoResearch	111-585-144
Rabbit Alexa Fluor 488	Abcam	Ab150073
Donkey Anti Rabbit Alexa Fluor 647	Invitrogen	A-31573
Goat Anti Rabbit Alexa Fluor 647	Life Technologies	A21245
Rabbit IgG-HRP	Cell Signaling	7074
UCP1 (for cells)	Abcam	Ab10983

3.5 List of RT-qPCR primers

Table 5:List of primer sequences used for RT-qPCR

Gene	Forward sequence	Reverse sequence
Adipq	GATGGCACTCCTGGAGAGAA	TCTCCAGGCTCTCCTTTCCT
Asc-1	AGTGTTCCAGGACACCCTTG	GGGTGGCACTCAAGAAAGAG
Fabp4	GATGCCTTTGTGGGAACCT	CTGTCGTCTGCGGTGATTT
Igf2	AGACATACTGTGCCACCCC	ATTGGAAGAACTTGCCCACG
Pparγ	CCCTGGCAAAGCATTTGTAT	GAAACTGGCACCCTTGAAAA
Pgc1α	AGCCGTGACCACTGACAACGAG	GCTGCATGGTTCTGAGTGCTAAG
Srr	AACTACGGCTTTGGGCTTCT	GGCGCAATCTTTTCTTCAAA
Tbp	ACCCTTCACCAATGACTCCTATG	TGACTGCAGCAAATCGCTTGG
Tfam	CAGGAGGCAAAGGATGATTC	CCAAGACTTCATTTCATTGTCG
Ucp1	CTGCCAGGACAGTACCCAAG	TCAGCTGTTCAAAGCACACA

3.6 List of Softwares

Table 6: List of Softwares used for analysis

Gimp 2.10.24
Fiji
Biorad CFX Manager 3.1
GraphPad Prism 9.4.0
Seahorse Wave Controller 2.6

4 Methods

4.1 *In vivo* experiments

4.1.1 Animal husbandary

Pre-weaned (15 ± 2 days old) and adult (58 ± 2 days old) C57BL/6J or C57BL/6N wild-type mice were bred and housed at constant ambient temperature of 22 ± 2°C, 45-65% humidity and a 12h light-dark cycle with *ad libitum* access to food and water. Preadipocyte transplanted Balb/c nude mice were single housed at 30°C. All the animal experiments were performed in a conventional animal facility of Helmholtz Zentrum Munich (Neuherberg, Germany).

4.1.2 Preadipocyte transplantation

For preadipocyte transplantation male Balb/c nude mice were used. shAsc-1 and shScr cells were collected in CellStripper buffer, washed once with DPBS and spun at 300 *× g* for 5 min. Cells were resuspended in 50% pure DMEM high-glucose + GlutaMAX and 50% Matrigel and injected at a cell density of 1×10^6 with a 25 G syringe on top of the sternum. Six-weeks post injection engrafted tissues were collected and fixed in 4% PFA. Animal experiments was conducted in accordance with the German animal welfare law, permission and relevant to the guidelines and regulations of the government of Upper Bavaria (Bavaria, Germany): ROB-55.2-2532.Vet_02-18-188, and ROB-55.2-2532.Vet_02-17-125.

4.2 Ex vivo measurement

4.2.1 Sacrifice and tissue collection

C57BL/6J or C57BL/6N wild-type mice were either killed by cervical dislocation or overdose with anesthesia (100 mg/kg Ketamine and 7 mg/kg Xylazine). Once anesthetized blood was withdrawn via heart puncture. Collected blood was kept at room temperature around 15 min and later on ice for at least 30 min. Blood serum was obtained by centrifugation at 10,000 × g for 5 min at room temperature and then stored at -80°C for ELISA or cell culture. We pooled 27 adult mouse serum (MS) to be used in cell culture media. After dissection, fat depots were collected and processed according to the experiment.

4.2.2 ELISAs

Blood serum insulin and IGF2 levels were measured using Ultra-Sensitive Mouse Insulin ELISA kit (Crystal Chem) and m/r/p/caIGF-II Qkit (R and D Systems), respectively, following manufacturer's instructions.

4.3 *In vitro* experiments

4.3.1 Magnetic-activated cell sorting (MACS) cell sorting of ASC-1+ cell population

Immortalized preadipocytes from adult mice were harvested in CellStripper (Corning), spin down at 500 x *g* at 4°C for 5 min and blocked in 1 mL MACS Running Buffer (Milteny Biotec) for 10 mins on ice. Cells were then incubated with 1 mL ASC-1 antibody (10A11; 1:2) for 30 min. Cells were then incubated with 25 µL protein G microbeads (Milteny Biotec) for 30 min. MS columns (Milteny Biotech) were equilibrated with 200 µL MACS Running Buffer. The flow through fraction was collected as the negative control depleted of the labelled cells. MACS column was washed three times with 200 µL MACS Running Buffer. The column was then removed from the magnetic field and retained cells were eluted in 500 µL MACS Running Buffer. Both flow through and eluted cells were seeded on 24 well plate in the growth medium. Cells were either supplemented with 170 µM insulin or induced in differentiation media or differentiation media with 1 µM rosiglitazone when reached 100% confluence. Preadipocytes two days prior to induction, on the day of induction (d0) and differentiated adipocytes on day 8 were harvested to be subjected to total RNA using RNeasy mini kit (Qiagen) according to the manufacture protocol.

4.3.2 siRNA Knockdown by Reverse Transfection

Previously published reverse transfection method was used for knockdown *Srr* (Isidor et al., 2016). Briefly, shAsc-1 and shScr cells were seeded in a 12-well plate in the presence of transfection mix containing 50 nM DiSrr (mm.Ri.Srr.13.3, IDT) or negative control (IDT) and Lipofectamine RNAiMAX (Invitrogen) in Opti-MEM (Gibco). Twenty-four hours post transfection, cells were re-seeded in a 24-well plate and induced to differentiation with 0.5 mM IBMX, 5 µM dexamethasone, and 100 nM insulin supplemented with 1 µM rosiglitazone after 48 hours. After 2 days, the medium was changed to culture medium containing only 100 nM insulin. The medium was changed every 2 days until day 8 of differentiation.

4.3.3 Primary preadipocyte isolation and culture

Subcutaneous preadipocytes were isolated from pre-weaned and adult male wild-type C57BL/6 mice. Freshly isolated SCF was chopped into small pieces and digested in tissue digestion solution at 37°C for 30-45 min at 1000 rpm. Digested cells were filtered through 100 µm cell strainer for preadipocyte collection. Filtered cell suspension was centrifuged at 500 × *g* for 5 min at room temperature (RT). Pelleted SVCs were either washed one time with DPBS and stored at -80°C for

total RNA isolation or washed one time with and cultured in normal growth media (DMEM high-glucose + GlutaMAX, 10% FBS, 1% PenStrep and 0.1 mg/mL Normocin) at 37°C and 5% CO_2.

4.3.3.1 IGF2 Stimulation

Cultured SVCs from adult mice were seeded on a 6-well plate and grown to 100% confluence. Cells were serum starved for 3 h in DMEM high-glucose + GlutaMAX. Time 0 was collected in protein lysis buffer after one-time ice cold DPBS wash. Cells were then treated with or without 10 nM IGF2 in DMEM high-glucose + GlutaMAX for 2, 5, 10, 20 and 60 min. Cells were frozen in protein lysis buffer at -20°C after one time ice cold DPBS wash.

4.3.3.2 IGF2 Supplementation

Cultured SVCs from adult mice were seeded on a 12-well plate and grown to 100% confluence. Cells were induced on day 0 with induction cocktail (0.5 mM 3-isobuthyl-1-methylxanthin (IBMX), 5 µM dexamethasone, and 100 nM insulin) in the presence or absence of 10 nM IGF2 in normal growth medium (DMEM high-glucose + GlutaMAX, 10% FBS, 1% PenStrep) or physiological mimetic media (Opti-MEM, 1% adult mouse serum, 1% PenStrep). After 2 days, the media were changed to corresponding continuum medium containing 100 nM insulin in the presence or absence of 10 nM IGF2. The media were changed every 2 days until day 8. Cells were harvested either for total RNA extraction, protein extraction, ORO quantifications or immunofluorescence staining.

4.3.3.3 IGF2 Neutralizing Antibody Treatment

Cultured SVCs from pre-weaned mice were seeded on a 12-well plate and grown to 100% confluence. Cells were induced on day 0 with induction cocktail in the presence of 1 µg/mL anti-IGF2 or Goat IgG (isotype control) antibodies in the normal growth medium (10% FBS) or physiological mimetic medium (1% Adult MS). After 2 days, the media were changed to corresponding continuum medium with 100 nM Insulin in the presence of 1 µg/mL anti-IGF2 or Goat IgG antibodies every 2 days until day 8.

4.3.4 MTT Assay

Isolated primary preadipocytes were seeded in a 96-well plates with at 1 x 10^4 cells per well. Separate plates were prepared for each day up to 7 days including the measurement on the day of seeding. MTT stock concentration of 5 mg/mL was prepared in 1 x PBS and filtered through 0.45 µm filter. Day 0 was incubated with MTT 3 hours post seeding. Initially, death control wells were treated with 0.03% Triton X-100 for 1 min at RT. Then MTT was directly diluted in the well with a final concentration of 0.5 mg/mL. After 2 h of incubation at 37°C, medium was replaced with 100 µl solubilization solution (10% Triton X-100 and 0.03% HCl in 100% isopropanol). The plate was

incubated at 24°C for 10 min at 700 rpm. The supernatant was then transferred into a fresh 96-well plate (Greiner, F-bottom) and its absorbance at 570 nm and 640 nm (as a background absorbance) was measured using Varioskan Lux plate reader.

4.3.5 Oil red O (ORO) staining

Differentiated adipocytes from preadipocytes of adult mice were fixed with 10% formalin at RT followed by washing with water. Cells were dehydrated with 60% isopropanol for 5 min and then air dried. Working solution of ORO was prepared by diluting 60% stock solution ORO in ddH_2O and filtering with 0.22 µm filter after 20 min. Cells were then treated with ORO for 10 min and washed with ddH_2O. Images were taken using an EVOS XL Core Cell Imaging System (Thermo Fisher Scientific). Cell number was measured after 5 min DAPI (1:5000) staining by measuring fluorescence intensity at 460 nm using PHERAstar FSX. Absorbance of ORO was measured at 500 nm after elution with 100% isopropanol.

4.3.6 Measurement of cellular oxygen consumption rate (OCR)

Primary cultured preadipocytes or pre-weaned mice were differentiated in the presence of 1 µg/mL anti-IGF2 antibody or IgG isotype as describes in section 4.3.4.3. On day 7 of differentiation, OCR was measured with a XF96 Extracellular Flux analyzer (Seahorse Bioscience). Cells were equilibrated in assay media (Agilent Seahorse XF DMEM supplemented with 0.2% fatty acid-free BSA, 25 mM glucose (Sigma Aldrich), 2 mM GlutaMAX (Gibco)) with 1 µg/mL anti-IGF2 antibody or IgG isotype 1 h prior to measurement at 37°C with 5% CO_2. Compounds were prepared at 10-times concentrated in respiration base media (assay media without FFA-free BSA) and loaded to the overnight equilibrated cartridge ports (A: 50 µM Oligomycin, B: 75 µM FCCP, C: 50 µM Antimycin A and 30 µM Rotenone, D: only respiration base media). The cartridge was equilibrated for at least 20 min in the XF96 Extracellular Flux analyzer. Each cycle was consisting of 4 min of mixing, and 2 min of measuring. Measurement was recorded before and after each injection for 3 cycles. Each cycle per biological replicate was averaged and plot on a graph against time.

4.4 Histology and imaging

4.4.1 Hematoxylin and Eosin (H&E) staining

Engrafted tissues from Balb/c mice were fixed in 4% PFA overnight at 4°C. They were then transferred into 70% ethanol and stored at 4°C until further use. For paraffin embedding, tissues were dehydrated in 80%, 90% and twice 100% ethanol for 1 h each consecutively. This was followed by 3 times 10 min xylol incubation. Subsequently, tissues were transferred to 2 times 1 hour in paraffin and then kept in paraffin overnight at 65°C. Next day, tissues were embedded in paraffin

using paraffin-embedding machine (Leica, EG1150). Tissue blocks were pre-cooled at -20°C before cutting 2 µm thick sections using microtome (Leica). Tissue sections on SuperFrost Plus glass slides (Thermo Fischer) were dried overnight at RT.

For H&E staining, tissue sections were rehydrated twice in xylol for 5 min each, then immersed in 100%, 90%, 70% ethanol (2 min each). This followed by transfer into Mayer solution (1:5, in water) for 1 min. Afterwards, sections were immediately washed under running tap water for 3 min and dehydrated by incubating in 96% and 100% ethanol for 2 min each. Tissues were stained with chromotope II R solution (100 mg chromotrope II R diluted in 100 mL of 95% ethanol, combined with 100 µL of acetic acid) for 3 min and immersed in 96% ethanol 3 times and moved into 100% ethanol for 1 min. At the final step, slides were incubated 2 times 5 min in xylol. Subsequently, sections were mounted using Roti-Histokkit II (Carl Roth); air dried and imaged using Nikon Eclipse Ci.

4.4.2 Cryosection

Pre-weaned and adult subcutaneous depots were isolated and fixed in 4% PFA overnight at 4°C. Tissues were washed once with 1 x PBS and transferred to initially 15% sucrose and then to 30% sucrose both overnight at 4°C. After washing 3 times with 1 x PBS, excess liquid was removed, and tissues were embedded in OCT compound (Tissue Tek). Tissue blocks were stored at -80°C. For both immunohistochemistry and RNAscope stainings 20 µm sections were cut using cryostat (Leica), except for engrafted tissue from Balb/c nude mice were cut in 30 µm thickness.

4.4.3 Immunofluorescent staining

Engrafted tissue sections were blocked in 3% BSA for 1 h at RT, permeabilized with 1% Triton-X100/PBS for 1 min on ice, incubated for UCP1 (1:250, Abcam) and PERILIPIN-1 (1:200, Cell Signalling) in 3% BSA/PBS overnight at 4°C. Section were washed three time 5 min each with 1 x PBS. Rabbit Alexa 594 (1:400, Jackson ImmunoResearch), BODIPY (1:2000) and DAPI (1:1000) were incubated for 1 h at RT. Washing step was repeated and sections were mounted using Dako fluorescence mounting medium and images were acquired using Leica SP5 Confocal microscope.

In vitro differentiated adipocytes were fixed with 10% Formalin for 10 min at RT, permeabilized 10 min with 0.1% Triton X-100/PBS. Fixed cells were incubated with Phalloidin 647 (1:40, Life Technologies) and Lipitox Green (1:200, Life Technologies) in 3% BSA, 0.03% Triton X-100/PBS for 1 h at RT. Sections were mounted using Dako fluorescence mounting medium and images were acquired using Leica SP8 X Confocal microscope.

4.4.4 Fluorescent *in situ* hybridization by RNAscope

RNAscope (Bio-techne) staining for *Igf2* (Atto 550) was performed on cryo-sections of pre-weaned and adult subcutaneous depots according to manufacturer's instructions (320535-TN and 320293-UM). Sections stained for KI67 (1:100, Abcam) were permeabilised with 0.1% Triton X-100 in DPBS for 5 min at RT and blocked in 1% BSA, 10% donkey serum, 0.1% Tween-20 in DPBS for 1 h at RT. For CD31 (1:100, Merck Millipore), sections were blocked in 3% BSA, 0.3% Tween-20 in DPBS for 1h at RT. Primary antibodies were added in the respective blocking solution for 2h at RT. This was followed by 3 times 5 min DPBS wash in dark and incubation with secondary antibodies (rabbit Alexa Fluor 647, Life Technologies and mouse Alexa, Fluor 488, Dinova, 1:400 both) in 1% BSA, 0.01% Tween-20 for 45 min at RT. Sections were washed 3 times for 5 min each with DPBS in dark and stained for DAPI from the RNAscope kit for 30 secs. As a control, 3-Plex Positive and Negative Control probes were used from the kit. Positive probe was targeting POLR2A in Channel 1, PPIB in Channel 2 and UBC in Channel 3. Dako fluorescence mounting medium was used for mounting. Images were acquired using Leica SP8 X Confocal microscope.

4.5 Molecular biologic analysis

4.5.1 RNA Isolation from whole tissue and cells

Whole tissue samples were lysed for 2 min at 30 Hz/sec in Qiazol (Qiagen) with metal beads using the TisseLyzer II (Qiagen). Samples were sit at RT for at least 5 min. Afterwards chloroform was added to the samples, shake for 15 sec and sit at RT for 3 min. Homogenates were then centrifuged at 12,000 x *g* for 15 min at 4°C. The clear aqueous phase is transferred to a fresh Eppendorf tube and mixed with same volume of 70% ethanol. RNA isolation was performed according to manufacturer's protocol using RNeasy Mini Kit (Qiagen).

Preadipocytes and differentiated adipocytes were freezed at -80°C in RLT buffer containing 25 µM dithiothreitol (DTT) until all biological replicates were collected. Homogenates thawed at RT were then mixed with the same volume of 70% ethanol followed by the transfer to RNeasy mini spin columns. Total RNA isolation was performed according to manufacturer's protocol using RNeasy Mini Kit (Qiagen).

Total RNA concentrations were measured at 260 nm using NanoDrop 2000 UV-Vis Spectrophotometer (Thermo Scientific).

4.5.2 cDNA synthesis and RT-qPCR Analysis

Depending on the availability, 500 ng of total RNA was converted to cDNA using High-Capacity cDNA Reverse Transcription Kit (Applied Biosystems) following manufacturer's protocol. Total RNA content used for each experimental set-up was kept constant between samples. Relative mRNA expression was quantified by Real-Time quantitative polymerase chain reaction (RT-qPCR). For this purpose, cDNA, iTaq Universal SYBR® Green Supermix (BioRad) and 300 nM forward and reverse primers (**Table 5**) mix was run in a C1000 Touch Thermal Cycler (BioRad) in duplicates or triplicates and quantified using Biorad CFX Manager 3.1 Program. All expressions levels were normalized to TATA-binding protein (*Tbp*). *Cq* value was set to 50 when there is no gene but *Tbp* expression was present.

4.5.3 Protein isolation and Western blot

Differentiated white adipocytes were washed with ice cold DPBS and frozen in protein lysis buffer (section 3.2). After one-time freeze-thaw cycle, cells were scraped from the plate, transferred into a tube and lysed using a 24G needle. Homogenates were incubated on ice for 10 min, centrifuged at 14,000 x *g* at 4°C for 10 min and supernatant were collected in a new tube. Until further use, the lysates were stored at -20°C.

BCA Protein Assay kit (Thermo Fisher Scientific) was used to quantify protein concentration. BSA dilution series (0, 0.25, 0.5, 1 and 2 mg/mL) were used as the standard curve. Protein samples were prepared in final concentration of 1 x NuPAGE Sample Buffer (Life Techonologies) containing 2.5% beta-mercaptoethanol (Carl Roth) and boiled for 5 min at 95°C following cooling on ice before loading on a SDS-PAGE gel (**Table 7**).

Table 7: SDS-PAGE gel recipe

Chemical Name	10% Resolving Gel	4% Stacking Gel
Water	4.1 mL	3 mL
Rotiphorese® Gel 30 acrylamide	3.3 mL	750 µL
1.5 M Tris-HCl pH: 8.8	2.6 mL	-
0.5 M Tris-HCl pH: 6.8	-	1.3 mL
10% SDS	100 µL	50 µL
10% APS	50 µL	25 µL
Temed	15 µL	10 µL

Protein samples were load on the SDS-PAGE gel and run in 1 x Running Buffer (section 3.2). Fisher BioReagentsTM EZ-RunTM Prestained Rec Protein Ladder (ThermoFischer Scientific) was used as

the molecular size marker. After the run, protein was blotted onto a 0.45 µm PVDF membrane for 1.5 h at 80 V or 1 h at 100 V in 1 x Blotting Buffer (section 3.2). Membrane was blocked using 5% BSA or non-fat dried milk in TBS-T (1 x TBS containing 0.1% Tween 20) at RT for 1 h, followed by incubation with primary antibodies (**Table 4**) overnight at 4°C by gentle shaking. Next day, membranes were washed with 1 x TBS-T for 3 times, incubated with HRP-conjugated secondary antibody for 1 h at RT and washed again with 1 x TBS-T prior to acquiring images. Western Blots were developed using Immobilon western HRP substrat (Merck Millipore) or SuperSignal™ West Femto Maximum Sensitivity Substrate (Fischer Scientific) by ChemiDocTM (BioRad).

4.5.4 Immunoprecipitation

Protein from primary SCF preadipocytes stimulated for 10 min with or without 10 nM IGF2 (section 4.3.4.1) was isolated as described in section 4.5.3, except that IP lysis buffer was used instead of protein lysis buffer (section 3.2). Protein concentration was quantified using BCA Protein Assay kit (Thermo Fisher Scientific). Two-hundred microgram protein lysate in 500 µL from each sample were separately incubated with anti-InsR and anti-IGF1R antibodies (1:100, Cell Signaling) overnight at 4°C by gentle rotation. Next day, 15 µL A/G agarose beads were added to the antibody-protein lysate mix and incubated for 1 h at 4°C by gentle rotation. This was followed by antibody-protein-bead mix was centrifuged at 1000 x *g* at 4°C for 5 min and washed three times with IP lysis buffer. After the final centrifugation step, the immune complex was eluted by mixing with a final concentration of 2 x NuPAGE Sample Buffer (Life Technologies) containing 5% beta-mercaptoethanol (Carl Roth) and boiling at 95°C for 5 min. Protein lysates were transferred into a new tube after centrifugation at 1000 x *g* at 4°C for 5 min. As an input control, 20 µg whole protein lysate was mixed with final concentration of 1 x NuPAGE Sample Buffer (Life Technologies) containing 2.5% beta-mercaptoethanol (Carl Roth), boiled for 5 min at 95°C and stored at -20°C.

Both IP and input samples were loaded on a NuPAGE 4 to 12%, Bis-Tris gels (Invitrogen) and run in 1 x MOPS Buffer (section 3.2) at 200 V. Western blot analysis was performed as described in section 4.5.3 with antibodies described in **Table 4**.

4.5.5 Single Cell RNA Sequencing (scRNA-seq) and analysis (collaboration)

Subcutaneous, perigonadal and interscapular brown adipose tissues were isolated from pre-weaned and adult mice. SVCs were isolated following the protocol similar in section 4.3.2, except the centrifugation step was performed at 800 x *g* and collagenase IV instead of I was used in digestion media. Live cells unstained 7-ADD from the SVCs were obtained by flow cytometry. Afterwards, cells were loaded on a 10x chip channel to produce Gel Bead-in-Emulsion and

generated using ChromiumTM Single-cell 3’ library and gel bead kit v2 (PN#120237) from 10x Genomics. This was followed by reverse transcription to barcode RNA before cleanup and cDNA amplification followed by enzymatic fragmentation and 5’ adaptor and sample index attachment. Libraries were sequenced on the HiSeq4000 (Illumina) with 150 bp paired-end sequencing of read2 and 50,000 reads per cell. The analysis was done by Dr. Viktorian Miok from the Institute of Diabetes and Obesity (Helmholtz Zentrum München). Workflow was performed using scanpy version 1.7.1. Briefly, UMI count and the fraction of mitochondrial DNA was used to filter cells. The remaining cell vectors were normalized to sum a total count of 1e4 by linear scaling. *t*-SNE and *k*-nearest neighbor (*k*NN) graph were computed based on top 50 PCs. Moreover, Louvain clustering was based on the *k*NN graph. Cell types were assigned according to the expression profiles of marker genes by cluster. Louvain cluster that correspond to preadipocytes was further evaluated.

4.5.6 Statistics

Differential gene expression analysis was performed between two age groups of each depot type separately. The analysis was done with Welch’s *t*-tests and performed multiple testing correction with the Benjamini–Hochberg correction. Gene Ontology (GO) and KEGG Pathways enrichment analysis were performed on the significantly differentially expressed genes (adjusted P-values <0.05) of SCF pre-weaned preadipocyte clusters identified by scRNA-seq analysis.

Data are shown as mean ± standard error mean (SEM). Statistical significance for multiple comparisons was determined by ordinary One-way ANOVA or Two-way ANOVA, with Tukey’s multiple comparisons test, or unpaired Two-Tailed t-test using GraphPad prism 9.4.0 program. Exact P-values were indicated in the figures and $P<0.05$ was considered as statistically significant.

5 Results

5.1 scRNA-seq analysis show distinct differences by age between pre-weaned and adult mice preadipocytes

Pre-weaned mice display massive and rapid expansion of adipose tissue compared to adult mice (**Fig. 4A**). SCF and PGF masses of pre-weaned mice showed around 2.5 and 15-fold increase, respectively, compared to adult (**Fig. 4B-C**). In order to understand the compositional differences between pre-weaned and adult mice and to identify factors that promote this healthy expansion, scRNA-seq analysis was perfomed on BAT (2,317 and 1,889 cells respectively), PGF (5,669 and 2,138 cells respectively) and SCF (3,790 and 4,936 cells respectively) depots' SVCs (**Fig. 4D**). Unlike many other studies, we sequenced the whole SVCs instead of only enriching for preadipocytes. Analysis of the whole dataset revealed 14 main louvain clusters. We assigned cell types according to the marker gene expression profiles and identified various cell types present in the stromal vascular fraction (**Fig. 4E**). Clusters 0,5,6 were high in mesenchymal progenitor cell markers (*Pdgfra, Fbn1, Cd34, Dlk1, Col4a1*), clusters 1 and 7 were high in T-cell markers (*Cd4, Cd3*), clusters 1, 7, 12 were high in markers for natural killer cells (*Nkr, Ly94*), clusters 3, 4, 8, 12, 13 were high for macrophages (*Adgre1, Lyz2*), clusters 2, 3, 4, 9 were for dentritic cells (*Cd74, Cd83*) and cluster 2 was for B-cells (*Cd19*). Some clusters were an overlap of several cell types such as clusters 1 and 7, which showed high expression levels for T-cell and natural killer cell markers, indicating that these cells have higher similarity in terms of the expression profiles. To identify differences between the depots, age was projected on the whole dataset (**Fig. 4F**). Interestingly, cells marked with *Pdgfra*, a fibroblast marker used widely to identify preadipocytes, showed distinct separations by age (**Fig. 4F-G**). Therefore, this cell population was further analyzed.

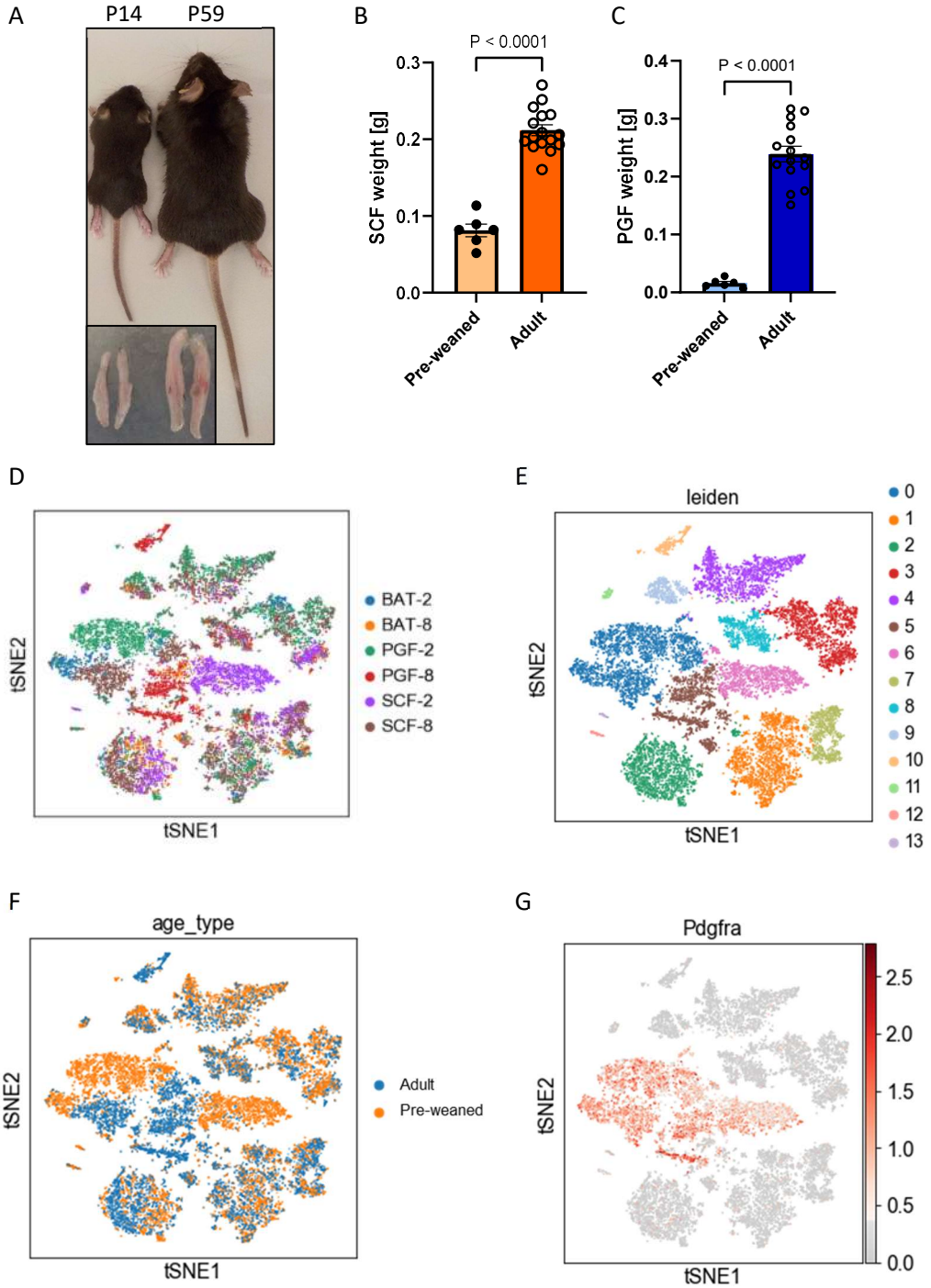

Figure 4: Single cell RNA sequencing analysis of stromal vascular cells of SCF, PGF and BAT. (A) Picture of 14 (pre-weaned) and 59 (adult) days old wild type C57BL/6J male mice and their isolated subcutaneous adipose tissues (SCF). Tissue weight of (B) SCF and (C) perigonadal adipose tissue (PGF) of pre-weaned (n= 6) and adult (n=15-16) wild-type C57BL/6J male mice. (D) t-distribution stochastic neighbor embedding (*t*-SNE) of three adipose depots (SCF, PGF, BAT) and two age groups (2 and 8 weeks old) showed (E) 14 clusters. *t*-SNE cluster projected by (F) age and (G) cell clusters positive for preadipocyte marker (*Pdgfra*). P values are indicated in the graph. Data analyzed by mean ± SEM. Analysis was done unpaired Two-Tailed *t*-test.

5.2 *Igf2* is one of the most differentially expressed gene in subcutaneous preadipocytes of pre-weaned mice

Unsupervised clustering of gene expression profiles of cells expressing *Pdgfra* revealed 12 clusters. *t*-SNE plots of preadipocytes showed that all the depots and their respective age groups were clearly separated from each other, indicating that with development gene expression profiles in adipose depots are changed (**Fig. 5A-B**). Interestingly, pre-weaned SCF (SCF-2) and adult BAT (BAT-8) showed overlaps in their gene expression profiles (Clusters 1 and 3) (**Fig. 5A-B**).

Further analysis of differential gene expression levels of pre-weaned vs. adult mice of each depot type separately showed that *Igf2* was one of the most differentially expressed gene in the subcutaneous preadipocytes in pre-weaned mice, which made it a potential candidate to study also because it is a well-known fetal growth promoter (Gicquel and Le Bouc, 2006) (**Fig. 5C-D**). Surprisingly, its expression was significantly higher in adult PGF and BAT compared to pre-weaned preadipocytes (**Fig. 5E-F**). PGF develops postnatally and the differences in *Igf2* expression might be due to the differences in the developmental stage of the tissue (Wang et al., 2013). Since among WAT depots SCF has more protective effects on metabolic syndrome compared to PGF tissue, we based our study focusing on SCF.

The mRNA expression level of *Igf2* was significantly lower in both whole tissue and isolated SVCs from SCF of adult compared to pre-weaned mice (**Fig. 5G-H**). This was also observed by fluorescent *in situ* hybridization staining of *Igf2* in SCF from pre-weaned and adult mice (**Fig. 5I**). Therefore, in order to investigate its role in adipose tissue function, we supplemented subcutaneous preadipocytes of adult mice with 10 nM IGF2. On the other hand, we treated subcutaneous preadipocytes of pre-weaned mice with IGF2 neutralizing antibody because they expressed significantly high levels of *Igf2* compared to adult and thus its function can be further confirmed by blocking receptor-ligand interaction.

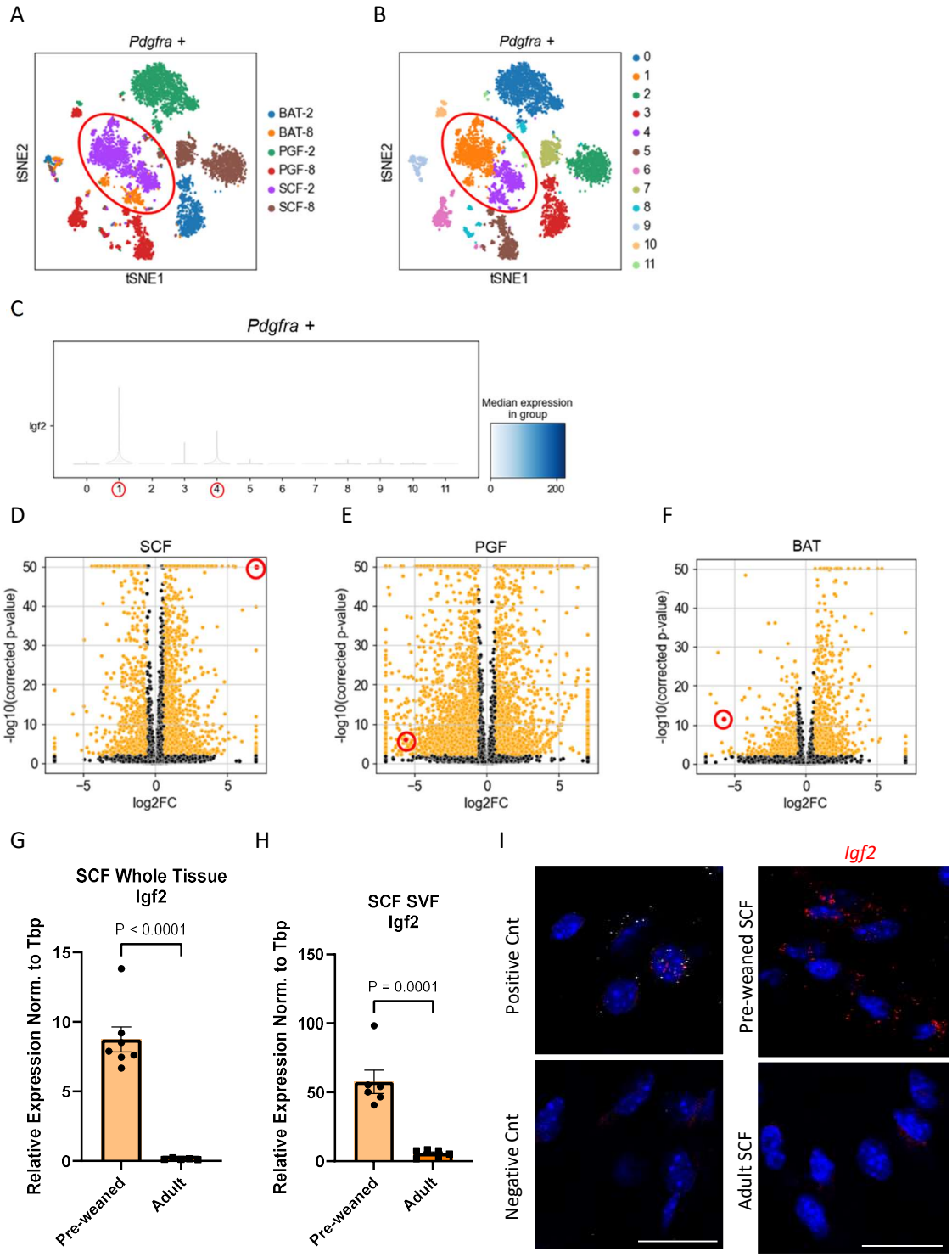

Figure 5: Single cell RNA sequencing analysis revealed *Igf2* as one of the significantly highly expressed gene in pre-weaned subcutaneous preadipocytes. (A) *t*-SNE plot of only *Pdgfra*$^{+}$ cells of three adipose depots (SCF, PGF, BAT) and two age groups (2 and 8 weeks old) revealed (B) 12 clusters. (C) Violin plot of *Igf2* expression in each cluster from figure B. Differential gene expression by comparing pre-weaned to adult (D) SCF, (E) PGF and (F) BAT. Red dots in red circle indicates *Igf2*. mRNA expression level of *Igf2* in (G) whole tissue (n=7 vs 5) and (H) stroma vascular fraction (n=6) of SCF from pre-weaned and adult wild-type C57BL/6 male mice. (I) Fluorescent *in situ* hybridization staining of *Igf2* (Red) in pre-weaned and adult mice SCF by RNAscope (n=3). Nucleus is stained by DAPI (blue). Scale bar 25 µm. Positive and negative controls from the kit are shown on the left. Red is the same channel as *Igf2* staining but stained for *Polr2a* and grey stained for *Ubc*. P values are indicated in the graph. Data showed mean ± SEM. Analysis was done using unpaired Two-Tailed *t*-test.

5.3 Studying the effect of IGF2 on preadipocyte differentiation

5.3.1 IGF2 enhances phosphorylation of ERK and AKT in subcutaneous preadipocytes of both pre-weaned and adult mice

Several studies have shown that IGF2 activates IGF1 (IGF1R) and insulin (InsR-β) receptors. Downstream of these receptors are MAPK/ERK and PI3K/AKT signaling pathways that regulate growth, survival and differentiation. To confirm whether the concentration of IGF2 used in this study can also activate these signaling pathways, we isolated and cultured primary subcutaneous preadipocytes of pre-weaned and adult wild-type mice. Adult cells were serum starved for 3 h and stimulated with 10 nM IGF2 for 10 min. Western blot analysis showed that phosphorylation of both AKT and ERK were higher in subcutaneous preadipocytes of adult mice supplemented with IGF2 (**Fig. 6A**). ERK was also phosphorylated in the untreated cells potentially due to media change for the stimulation, but this was independent of the InsR-β and IGF1R pathways (**Fig. 6A-C**).

Next, InsR-β and IGF1R receptors were pulled down from the protein lysates of pre-weaned and adult preadipocytes by immunoprecipitation (IP) (**Fig. 6B-C**). Since both receptors were tyrosine kinase receptors, we assessed their activation by checking phospho-Tyr (P-TYR) level (**Fig. 6B-C**). Western blot analysis revealed that both InsR-β and IGF1R IPs from IGF2 stimulated cells showed

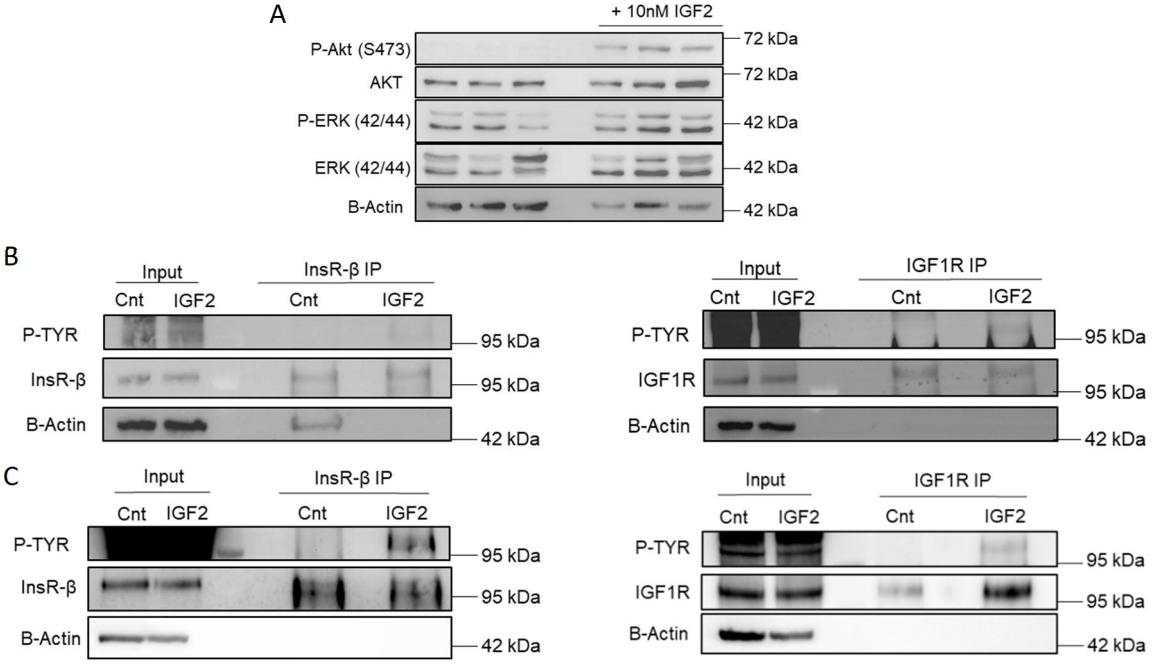

Figure 6: IGF2 activates both IGF1R and InsR in subcutaneous preadipocytes. Primary subcutaneous preadipocytes of adult wild-type C57BL/6 mouse were serum starved for 3 h and stimulated with 10nM IGF2 for 10 min. No treatment was used as control. (A) Western blot displaying phosphorylated (p) /total AKT and p/total ERK from whole cell lysate of preadipocytes of adult mice (n=3). Immunoprecipitation (IP) of InsR-β (left) and IGF1R (right) from (B) pre-weaned (n=1) and (C) adult (n=2) preadipocyte lysates. Immunoblotting with phospho-tyrosine (P-TYR) was used to analyze the phosphorylation of the receptors in the IP lysate.

higher P-TYR level, while untreated cells showed no phosphorylation. All together these results indicated that 10 nM IGF2 activates AKT and ERK through IGF1R and InsR-β pathways in both pre-weaned and adult SCF preadipocytes.

5.3.2 IGF2 supplemented subcutaneous preadipocytes of adult mice differentiated in a similar level to control condition

InsR and IGF1R play important roles in WAT formation and preadipocyte differentiation (Boucher et al., 2016, Boucher et al., 2010b). Since both receptors were activated by IGF2 stimulation (**Fig. 6**) and hyperplastic expansion was suggested to have a more protective effect on metabolism (Nunn et al., 2022, Kim et al., 2007), we next tested whether IGF2 supplementation can enhance the differentiation capacity of subcutaneous preadipocytes of adult mice. Primary preadipocytes were differentiated in the presence of 10 nM IGF2 (Dif. Adipocytes + 10 nM IGF2) under normal cell culture conditions (10% FBS). Control cells (Dif. Adipocytes) received no supplementation. *Igf2* mRNA levels remained unchanged upon differentiation or supplementation (**Fig. 7A**). There was no difference in the mRNA and protein expression levels of adipogenic markers (**Fig. 7B-C**). Consistently, Oil red O staining (ORO) and fluorescence staining of lipids did not show differences between IGF2 supplemented and untreated condition in terms of lipid content (**Fig. 7D-E**)

Xue *et al.* reported a peak in *Ucp1* expression between P10 and P30 in retroperitoneal fat (Xue et al., 2007). Since *Igf2* expression is significantly higher in pre-weaned mice (P15 ± 2 days), we wanted to check if supplementation of IGF2 could induce beiging. Even though, *Tfam* and *Ucp1* levels were slightly downregulated in IGF2 supplemented compared to untreated cells, this did not reach statistical significance. *Pgc1α* expression was unchanged between two conditions (**Fig. 8F**). Altogether these findings indicate that under established *in vitro* culture conditions IGF2 neither enhanced adipogenic capacity nor induced beiging.

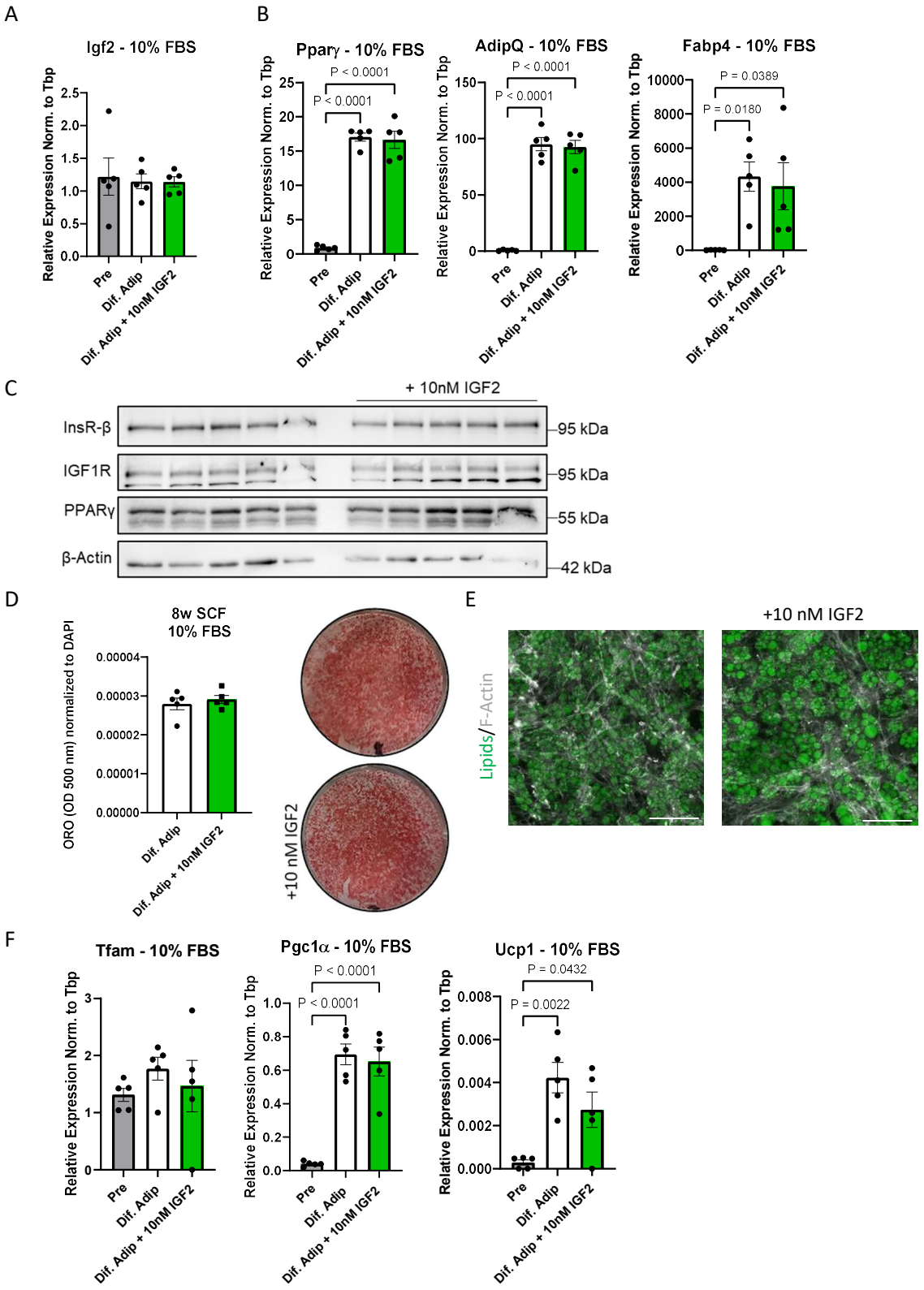

Figure 7: IGF2 supplementation does not alter adipogenesis in SCF preadipocytes of adult mice cultured in 10% FBS. Primary adult preadipocytes (Pre) were differentiated in the presence (Dif. Adip + 10 nM IGF2) or absence (Dif. Adip) of 10 nM IGF2 for 8 days (d8). mRNA expression levels of (A) *Igf2* and (B) adipogenic markers (n=5). (C) Western blot of differentiated cells in the presence (+10 nM IGF2) or absence of IGF2 (n=5). (D) Quantitative lipid accumulation measured at 500 nm absorbance after elution of the Oil Red O (ORO) staining (left) and representative images (right) (n=5). (E) Fluorescent staining of lipids (green) and F-actin (grey) (n=3). Scale bar 100 µm. (F) mRNA expression levels of

beiging markers (n=5). Data analyzed by mean ± SEM. Analysis was done using One-Way ANOVA, with Tukey's multiple comparisons test.

5.3.3 Adult mice have significantly lower circulating IGF2 levels

IGFs play an important role in the development. IGF1 and IGF2 are functionally similar in mammals. Studies showed that *Igf1* null mice and IGF1R knockout mice show profound growth retardation similar to *Igf2* null mice. Some mice die after birth because of respiratory failure and delayed development of organs (Liu et al., 1993). In contrast, insulin deficient mice also display growth retardation but die shortly after suckling milk due to hyperglycemia and diabetic ketoacidosis (Duvillie et al., 1997). Since insulin does not affect the development in early ages, we checked whether IGF2 might be a substitution for insulin. However, serum insulin levels of random-fed mice were comparable between pre-weaned (0.55 ± 0.05 ng/mL) and adult (0.57 ± 0.08 ng/mL) mice (**Fig. 8A**). Interestingly, serum IGF2 levels were more than 20-fold higher in pre-weaned mice (239.4 ± 28.2 ng/mL) compared to adult (9.0 ± 0.6 ng/mL) and were significantly down-regulated in the adult mice compared to the pre-weaned pups (**Fig. 8B**). These findings support the developmental role of IGF2 during early ages. We have also collected cell supernatants of preadipocytes after overnight serum starvation to measure IGF2 secretion. Cells from pre-weaned mice secreted slightly more IGF2 compared to that from adult (**Fig. 8C**), indicating a potential autocrine or paracrine role of IGF2 in preadipocytes.

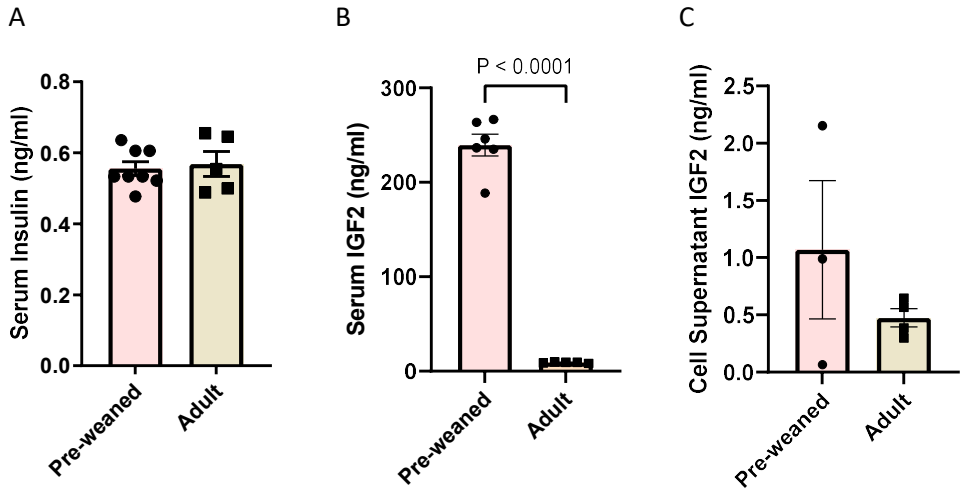

Figure 8: Serum IGF2 levels are significantly less in adult mice compared to pre-weaned. (A) Serum insulin (ng/ml) levels of pre-weaned (n=8) and adult (n=5) C57BL/6 wild-type mice. (B) Serum IGF2 levels (ng/ml) of pre-weaned (n=6) and adult (n=5) mice. (C) Cell supernatant IGF2 levels (ng/ml) obtained from 12-hour serum starved pre-weaned (n=3) and adult (n=4) subcutaneous preadipocytes. P values are indicated in the graph. Data analyzed by ±SEM. Analysis was done using unpaired Two-Tailed *t*-test.

5.3.4 Substitution of FBS with mouse serum did not alter adipogenesis upon IGF2 supplementation

Fetal bovine serum (FBS) contains fetal growth factors including IGF2, which might be a limitation in studying its effect on adipogenesis (Honegger and Humbel, 1986). Therefore next, we substituted FBS with adult mouse serum (MS) for two reasons: i) to investigate the real effect of endogenous IGF2 and ii) to mimic physiological conditions free from fetal growth factors. In contrast to normal culture conditions, *Igf2* mRNA expression levels were downregulated significantly upon differentiation under physiological mimetic culture conditions (1% Adult MS) (**Fig. 7A and Fig. 9A**). However, mRNA and protein levels of adipogenesis markers were unaltered by IGF2 supplementation (**Fig. 9 B-C**). Lipid quantification by ORO staining was in line with these findings (**Fig. 9D**). Interestingly, even though the experiments of normal and physiological cell culture conditions ran at the same time with the same biological samples, the number of cells that accumulated lipids were less when cultured with mouse serum, as depicted by immunofluorescence staining of lipids (**Fig. 7E and Fig. 9E**). On the other hand, *Tfam* and *Ucp1* expression levels were similar between preadipocytes differentiated in the presence or absence of IGF2. There was a slight increase in *Pgc1α* mRNA levels; however, this did not reach significance compared to untreated cells (**Fig. 9F**).

All together these data imply that IGF2 has no effect on adipogenesis or beiging in preadipocytes of adult mice *in vitro*. Furthermore, reduction in *Igf2* expression levels in adipocytes cultured under physiological mimetic (1% Adult MS) compared to normal (10% FBS) culture conditions suggest that there might be certain factors in the adult mouse serum that blunt IGF2 expression. However, this needs further investigation.

5.3.1 Neutralization of IGF2 activity does not alter adipogenesis in subcutaneous preadipocyte of pre-weaned mice regardless of the culture conditions

Next, to study the role of IGF2 in pre-weaned mice, where it is expressed significantly higher compared to subcutaneous preadipocytes of adult mice, ligand-receptor interaction of IGF2 was blocked. Specificity of the neutralizing antibody (Neut Ab) was confirmed by western blot. For this purpose, pre-weaned SCF preadipocytes were overnight serum starved with IGF2 neutralizing antibody or isotype (IgG) Control. Western blot analysis revealed reduced AKT and ERK phosphorylation (**Fig. 10A**), which were enhanced by IGF2 supplementation as shown before (**Fig. 6A**), suggesting that IGF2 could act in autocrine and paracrine fashion.

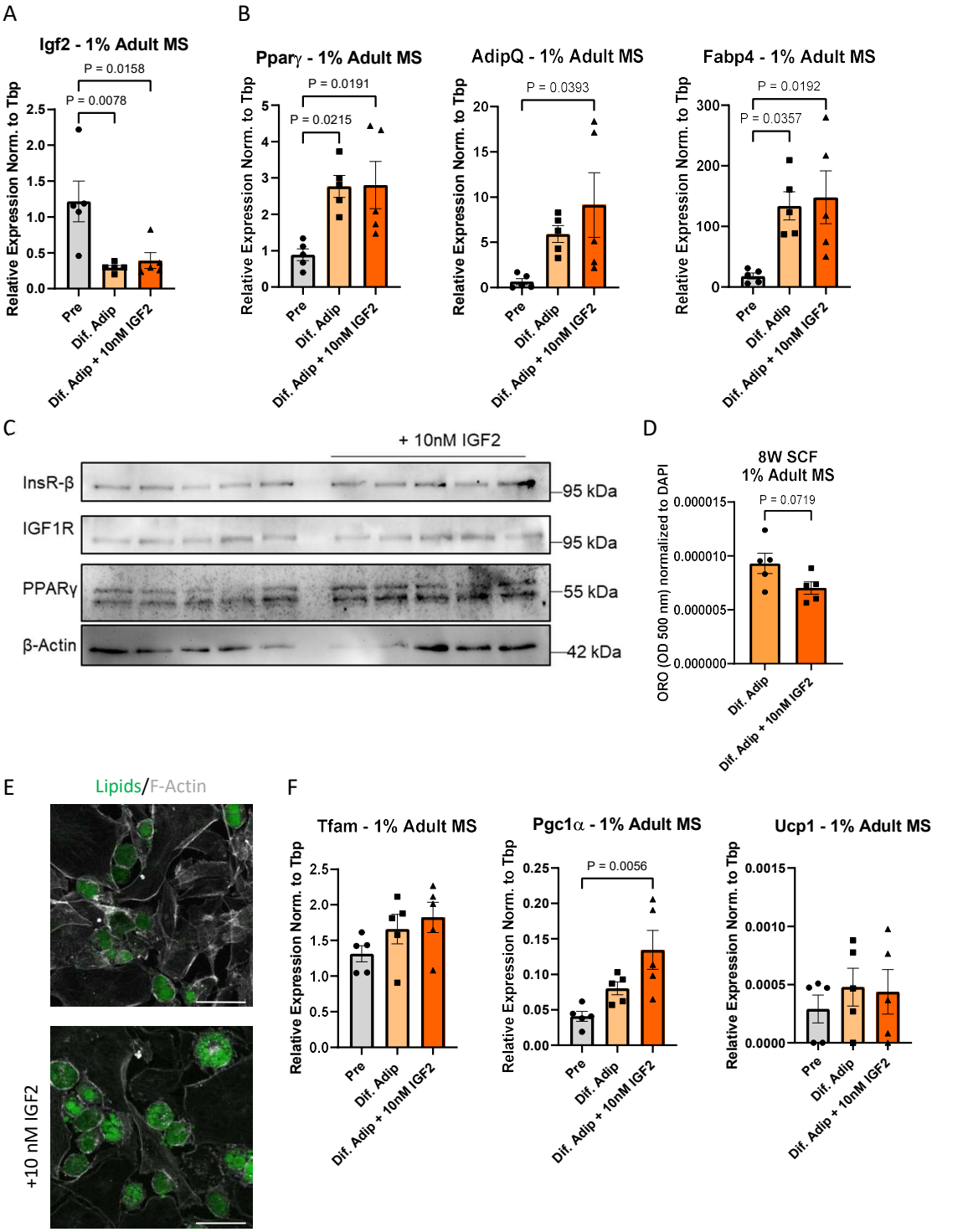

Figure 9: IGF2 supplementation does not affect adipogenic capacity of subcutaneous preadipocytes of adult mice cultured in 1% adult mouse serum (MS). Primary adult preadipocytes (Pre) were isolated from C57BL/6 wild-type mice and differentiated in the presence (Dif. Adip + 10 nM IGF2) or absence (Dif. Adip) of 10 nM IGF2 for 8 days (d8). mRNA expression levels of (A) *Igf2* and (B) adipogenic markers (n=5). (C) Western blot of differentiated cells in the presence (+ 10 nM IGF2) or absence of IGF2 (n=5). (D) Quantitative lipid accumulation measured at 500 nm absorbance after elution of the Oil Red O (ORO) staining (n=5). (E) Immunocytochemistry of lipids (green) and F-actin (grey) of differentiated adult preadipocytes (n=4). Scale bar 100 µm. (F) mRNA expression levels of beiging markers (n=5). Preadipocyte samples for mRNA expression levels were same for 10% FBS and 1% Adult MS experiments. P values are indicated in the graph. Data analyzed by mean ± SEM. Analysis was done using One-Way ANOVA, with Tukey's multiple comparisons test.

Afterwards, subcutaneous preadipocytes of pre-weaned wild-type mice were treated with 1 µg/mL IGF2 neutralizing antibody (Dif Adip + IGF2 Ab) starting from the day of induction for 8 days. Control cells received 1 µg/mL IgG isotype control (Dif Adip + IgG Cnt). Preadipocytes were differentiated under both normal and physiological mimetic culture conditions. Regardless of the culture conditions or treatment type, *Igf2* mRNA levels were significantly downregulated in adipocytes (Dif Adip) compared to preadipocytes (Pre) (**Fig. 10B-C**). Furthermore, even though there was a slight tendency for an increase in the expression of adipogenesis markers under normal culture conditions with IGF2 neutralizing antibody compared to IgG control, this did not reach to significance (**Fig. 10D**). In line with this, mRNA expression levels of *Pparγ*, *Adipq* and *Fabp4* were similar between IGF2 neutralizing antibody and IgG Control under physiological mimetic culture conditions (**Fig. 10E**).

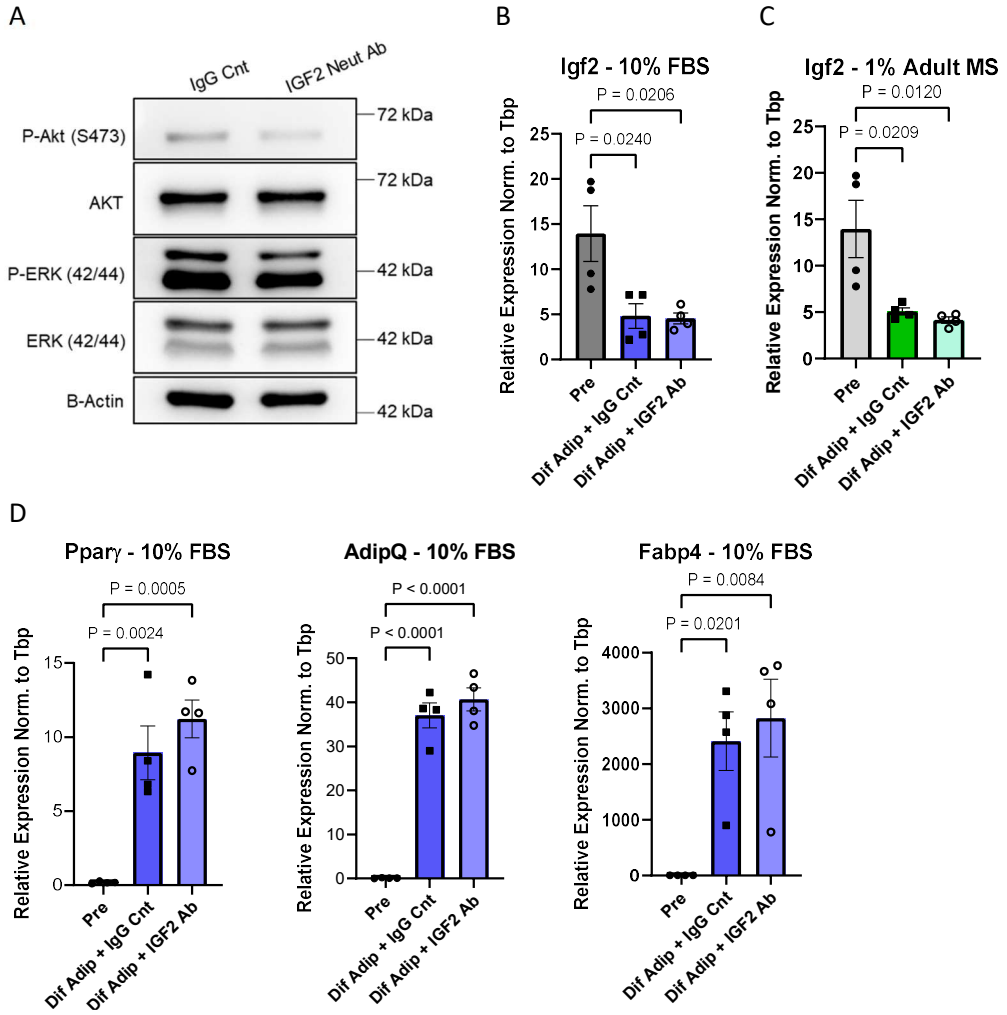

E

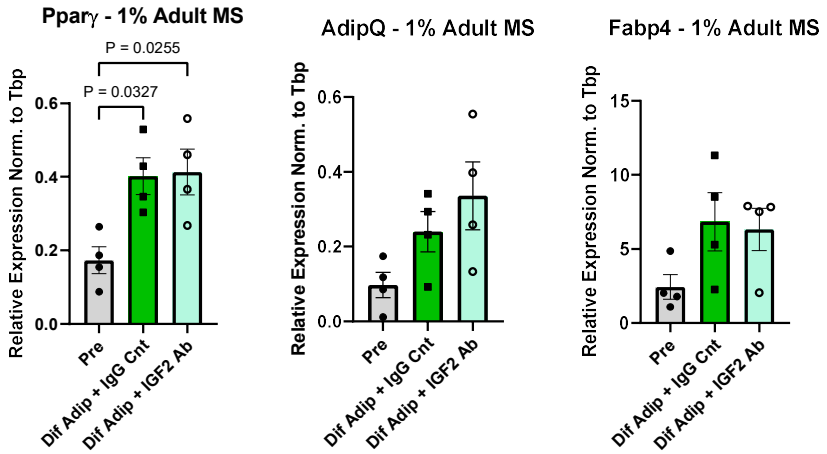

Figure 10: Blocking of IGF2 does not alter adipogenesis in subcutaneous preadipocytes of pre-weaned mice. (A) Western blot of p/total AKT and p/total ERK of 24 h serum starved pre-weaned subcutaneous preadipocytes in the presence of 1 µg/mL IgG (IgG Cnt) or IGF2 neutralizing antibody (IGF2 neutalising antibody) (n=1). Primary adult preadipocytes (Pre) were isolated from C57BL/6 wild-type mice and differentiated in the presence of 1 µg/mL IGF2 neutralizing antibody (Dif Adip + IGF2 neutalising antibody) for 8 days. As a control condition 1 µg/mL IgG isotype control was used (Dif Adip + IgG Cnt). *Igf2* mRNA expression level of cells differentiated in (B) 10% FBS or (C) 1% Adult MS culture conditions (n=4). Adipogenesis marker expression levels of cells differentiated in (D) 10% FBS or (E) 1% Adult MS culture conditions (n=4). P values are indicated in the graph. Data analyzed by mean ± SEM. Analysis was done using One-Way ANOVA, with Tukey's multiple comparisons test.

5.4 Neutralization of IGF2 affect neither the beiging nor the mitochondrial function of pre-weaned subcutaneous preadipocytes

Interestingly under normal culture conditions (10% FBS) *Tfam* and *Ucp1* mRNA levels were slightly upregulated in IGF2 neutralizing antibody compared to IgG Control treated pre-weaned adipocytes, but this did not reach statistical significance (**Fig 11A left and middle panels**). There was also no difference in *Pgc1α* expression levels (**Fig. 11A right panel**). Similar to this, expression level of beiging markers were unchanged under physiological mimetic culture conditions (1% Adult MS) (**Fig. 11B**). To understand the effect of IGF2 on mitochondrial function further, we performed seahorse extracellular flux analysis on pre-weaned preadipocytes differentiated under normal cell culture conditions. However, there was no difference between differentiated adipocytes with IGF2 neutralizing antibody or IgG Control in terms of oxygen consumption rate (OCR) (**Fig. 11C**). Preadipocytes differentiated in the presence of 1% Adult MS culture condition also did not show differences in the OCR between treatment conditions (**Fig. 11D**).

Taken together, consistent with adult preadipocytes, these data indicate that IGF2 does not regulate either the adipogenesis or mitochondrial function in pre-weaned preadipocytes.

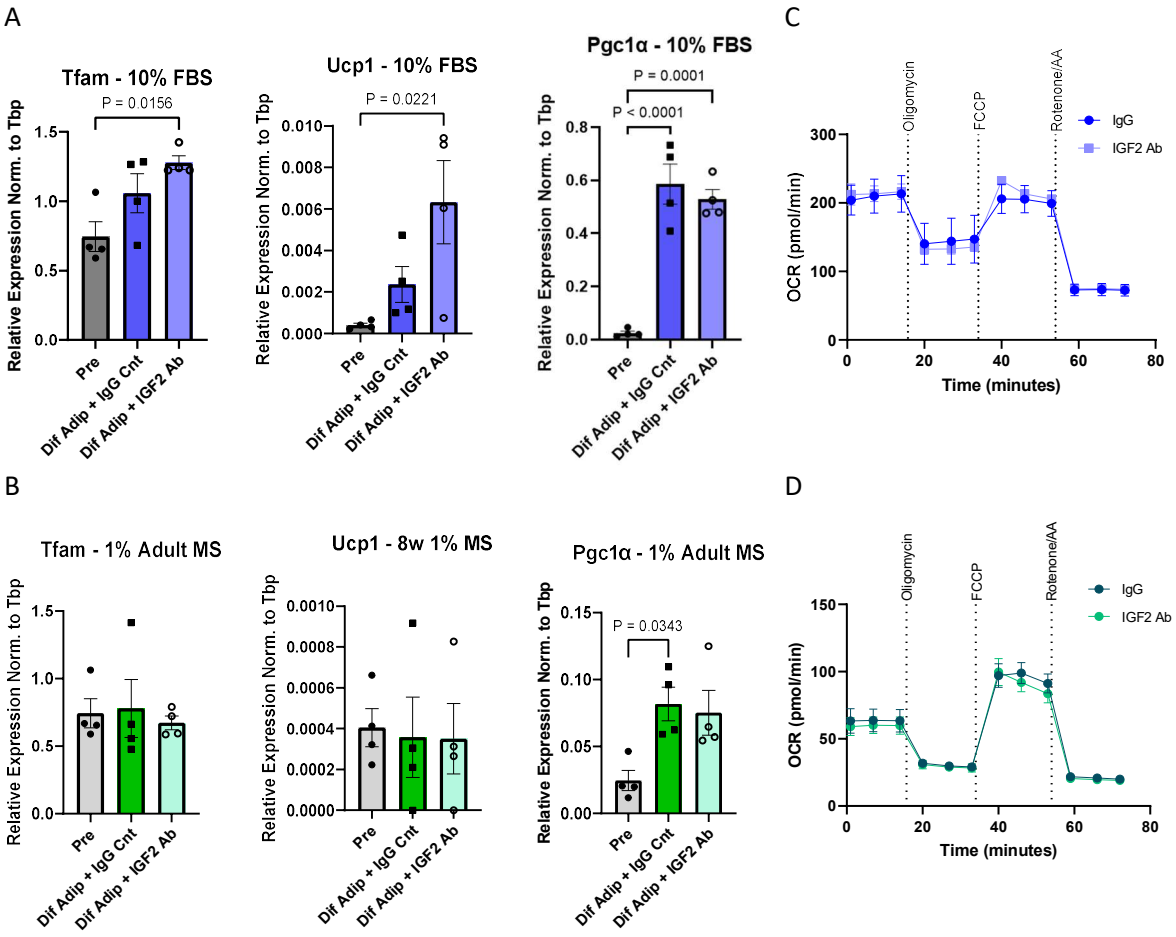

Figure 11: IGF2 does not affect mitochondrial function. Primary adult preadipocytes (Pre) were isolated from C57BL/6 wild-type mice and differentiated in the presence of 1 µg/mL IGF2 neutralizing antibody (Dif Adip + IGF2 neutalizing antibody) for 8 days. As a control condition 1 µg/mL Goat IgG was used (Dif Adip + IgG Cnt). mRNA expression level of beiging markers of cells differentiated in (A) 10% FBS or (B) 1% Adult MS culture conditions (n=4). OCR plot of differentiated adipocytes in (C) 10% FBS and (D) 1% Adult MS culture conditions (n=3). P values are indicated in the graph. Data analyzed by mean ± SEM. Analysis was done using One-Way ANOVA, with Tukey's multiple comparisons test.

5.5 IGF2 enhances proliferation of adult subcutaneous preadipocytes

To investigate the function of IGF2 in preadipocytes, further analysis was performed on the scRNA-seq data. We identified two main clusters in pre-weaned SCF preadipocytes, from which *Igf2* expressing cells were enriched in cluster 0 (P value of 4.07E-13, *t*-test). There were 2,561 differentially expressed genes between these clusters (**Fig. 12A**). Gene set enrichment analysis for KEGG Pathways showed that PI3K/Akt and MAPK signaling pathways were upregulated in *Igf2* enriched cells (**Fig. 12B**), which was in line with the data shown above (**Fig. 6A**). This was further confirmed by checking the phosphorylation state of AKT and ERK, downstream components of MAPK and PI3K pathways. Subcutaneous preadipocytes of adult preadipocytes were stimulated with 10 nM IGF2 over a time course (2, 5, 10, 20 and 60 min). Western blot analysis of phospho-AKT (P-AKT) and phosphor-ERK (P-ERK) showed that even though media change induced a basal

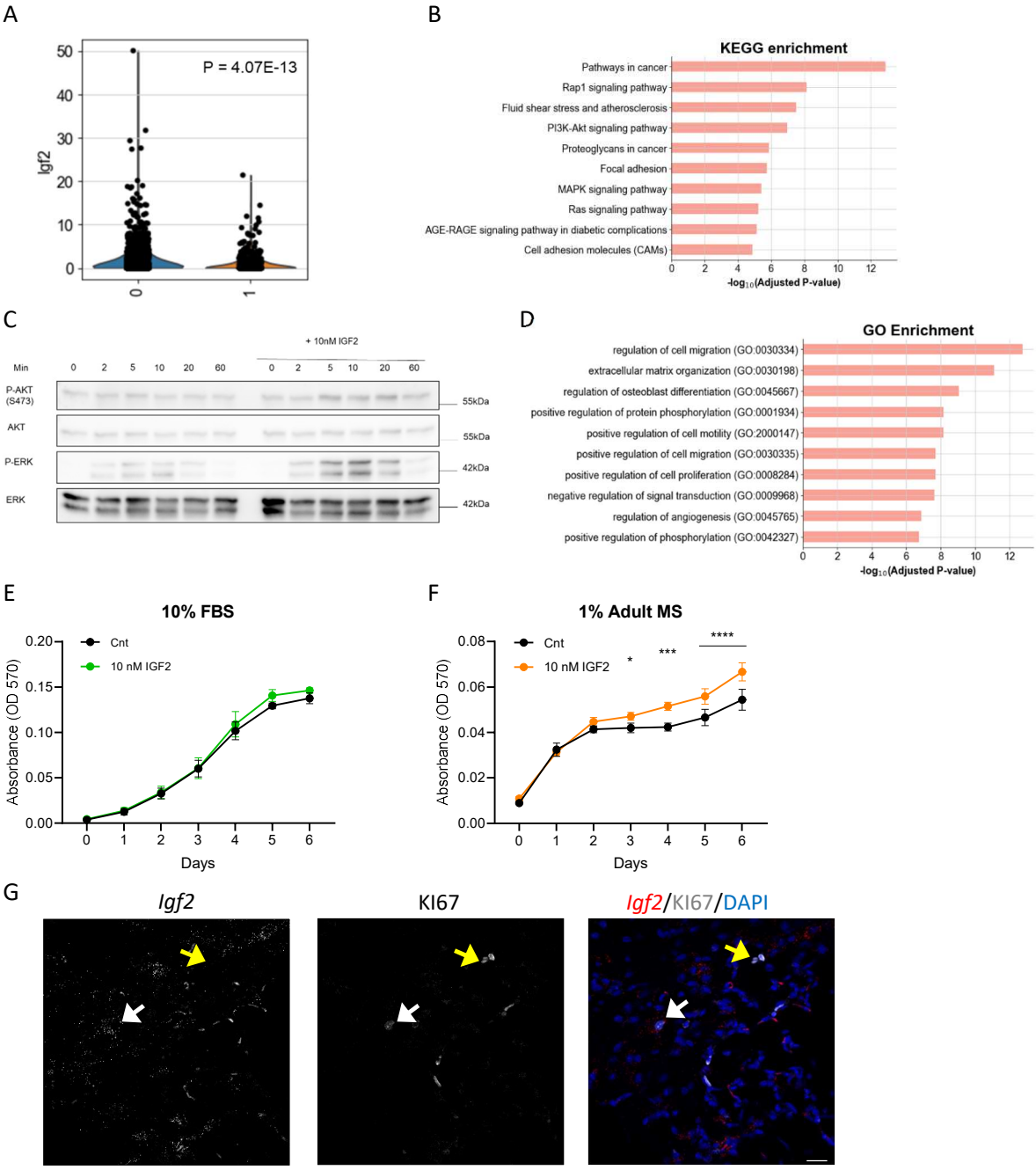

Figure 12: IGF2 enhances proliferation of adult SCF preadipocytes. Re-clustering of *Pdgfra*⁺ pre-weaned SCF cells revealed two cluster (0 and 1). (A) *Igf2* expression represented as violin plot in these two clusters. Gene enrichment analysis of *Igf2* high vs low cell clusters (from Figure A) for (B) KEGG pathways. (C) Western blot of adult preadipocytes stimulated with 10 nM IGF2 over a time course (n=3). Gene enrichment analysis of *Igf2* enriched vs low cell clusters (from Figure A) for (D) GO terms. MTT assay represented as Absorbance (OD 570) vs time (days) of adult SCF preadipocytes cultured in (E) 10% FBS (n=3) and (F) 1% Adult MS (n=5) supplemented with or without 10 nM IGF2. (G) Fluorescent *in situ* hybridization by RNAscope staining of *Igf2* (Red) and immunofluorescence staining of KI67 (grey) of pre-weaned SCF depot (n=3). *Igf2*⁺KI67⁺ cells were pointed with white arrow, only *Igf2*⁻KI67⁺ cells were pointed with yellow arrow. Scale bar 25 µm. *=0.0222, ***=0.0002 ****<0.0001. Data analyzed by mean ± SEM. Analysis was done using Two-Way ANOVA, with Tukey's multiple comparisons test.

level of phosphorylation, IGF2 treatment upregulated this (**Fig. 12C**). Moreover, Gene ontology (GO) analysis identified enrichment of terms associated with cell proliferation and extracellular matrix remodeling indicating a potential role of *Igf2* in niche formation (**Fig. 12D**). Therefore, we

performed a MTT assay to investigate whether IGF2 affects preadipocyte proliferation. Adult SCF preadipocytes were cultured with or without 10nM IGF2 under normal (10% FBS) or physiological mimetic culture conditions (1% Adult MS). Interestingly, while there was no difference observed in cells cultured under normal culture conditions, IGF2 supplemented cells were significantly more proliferative compared to control under physiological conditions (Fig. 12E-F). Next, we co-stained cryo-sections of pre-weaned SCF with *Igf2* (RNAscope) and a proliferation marker (KI67). Surprisingly, only few of the *Igf2* expressing cells were KI67 positive (Fig. 12G).

5.5.1 Some of the *Igf2* expressing cells sit in close proximity to vasculature

Next, since GO enrichment analysis identified terms related to angiogenesis and cell mobility, we visualize the location of some of the *Igf2* expressing cells in the tissue. Fluorescent *in situ* hybridization of *Igf2* was performed on subcutaneous cryo-sections of pre-weaned mice. These sections were then co-stained with endothelial marker (CD31) because several proliferating adipocyte progenitor cells were reported to reside in a vascular niche (Jiang et al., 2017, Tang et al., 2008). We have identified some of the *Igf2* expressing cells sitting in close proximity to vasculature (Fig. 13). Together these data propose a potential role of IGF2 on supporting or acting on adipose progenitor niches through upregulating the proliferative capacity of APCs.

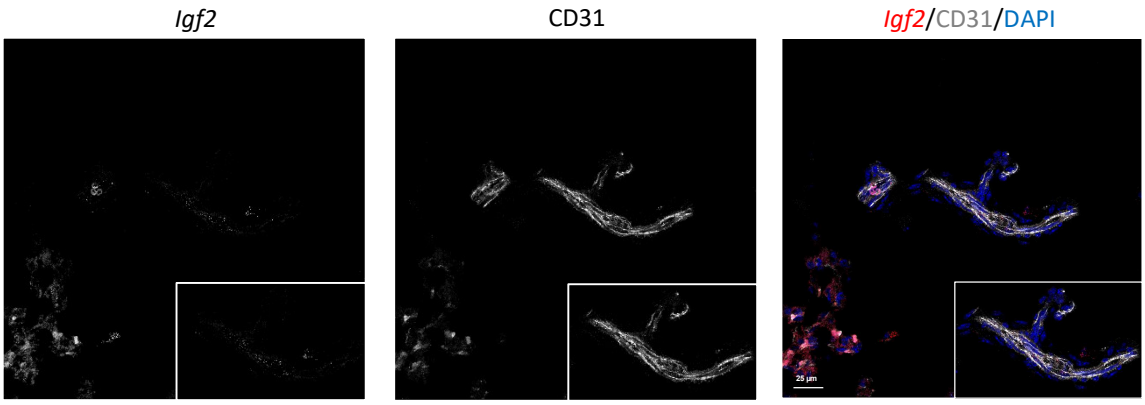

Figure 13: *Igf2*⁺ cells sit close to blood vessels. Fluorescent *in situ* hybridization by RNAscope staining of *Igf2* (Red) and immunofluorescence staining of CD31 (grey) of pre-weaned SCF depot (n=2). Scale bar 25 µm.

5.6 ASC-1 regulates beige vs white lineage decision of subcutaneous preadipocytes

ASC-1 was identified as a surface marker for mature white adipocytes (Ussar et al., 2014). scRNA-seq data showed that it was one of the most differentially expressed genes in pre-weaned SCF preadipocytes similar to *Igf2* (Fig 14A-B). In the second part of this thesis, we aimed to further study the function of *Asc-1* in WAT. For this purpose, immortalized subcutaneous preadipocytes were infected with lentivirus carrying shAsc-1 expressing plasmid (Dr. Lisa Siu-Lan Lehmann generated this cell line). Non-targeting shScr was used as control. All parts of this chapter were already recently published (Suwandhi et al., 2021).

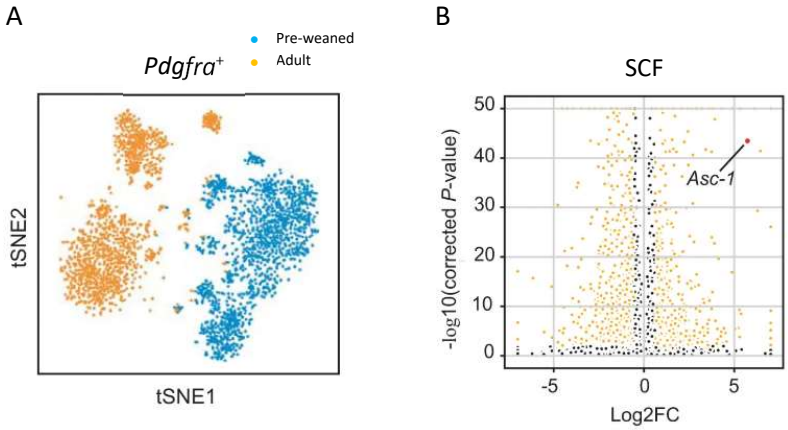

Figure 14: *Asc-1* is differentially highly expressed in SCF preadipocytes of pre-weaned mice. (A) *t*-SNE plot of *Pdgfra*$^+$ SCF cells marked by age. Blue cells are from pre-weaned and yellow cells are from adult C57BL/6 wild-type mice. (B) Differential gene expression analysis of SCF preadipocytes represented as a volcano plot. *Asc-1* is marked by a red dot.

5.6.1 ASC-1$^+$ cells differentiate into white adipocytes

Initially, since ASC-1 is a surface protein immortalized subcutaneous preadipocytes were sorted by MACS with an ASC-1 antibody. *Asc-1* mRNA expression levels were confirmed in ASC-1$^+$ and ASC-1$^-$ cells (**Fig. 15A**). However, further passaging resulted in re-expression of *Asc*-1 in ASC-1$^-$ cells (**Fig. 15B**). Sorted cells were differentiated in three different differentiation protocols: only insulin (insulin), standard differentiation cocktail with (+Rosi) or without (Adipo) rosiglitazone. *Pparγ* expression levels, a marker for adipogenesis, did not show differences between the cell populations (**Fig. 15C**). ASC-1$^-$ cells induced with the PPARγ agonist (rosiglitazone) showed increased *Ucp1* expression, whereas this was blunted in ASC-1$^+$ cells (**Fig. 15D**). These findings indicate that *Asc-1* favor white over beige adipocyte differentiation.

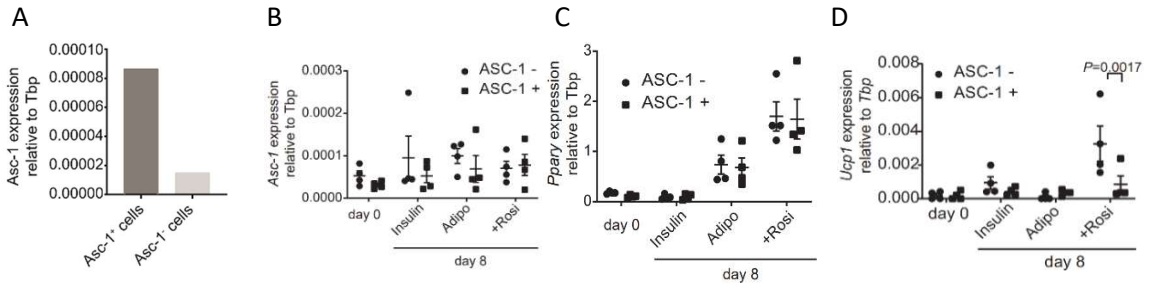

Figure 15: Subpopulation of cells expressing ASC-1 differentiate into white adipocytes. Immortalized subcutaneous preadipocytes were sorted with ASC-1 antibody (10A11). (A) *Asc-1* expression level of sorted cells (n=1). Relative (B) *Asc-1*, (C) *Ppary* and (D) *Ucp-1* expression of ASC-1^{+} and ASC-1^{-} cells differentiated with only insulin or normal differentiation media (Adipo) with or without rosiglitazone (+Rosi) for 8 days (d8) (n=4). Day 0 is the preadipocyte on the day of induction. P values are indicated in the graph. Data analyzed by ±SEM. Analysis was done using Two-Way Anova with Turkey's multiple comparison post hoc test.

5.6.2 Loss of *Asc-1* induced differentiation of UCP1 expressing adipocytes *in vivo*

Next, we aimed to perform a functional study. *Asc-1* expression was significantly upregulated upon differentiation. In contrary, treatment with rosiglitazone significantly reduced its expression in shScr cells (**Fig. 16A**). On the other hand, *Ucp1* mRNA expression levels showed indirect correlation with *Asc-1* expression. Its expression was significantly increased with both differentiation and rosiglitazone treatment in shAsc-1 compared to shScr cells (**Fig. 16B**), which was in line with the findings of the sorted cells above (**Fig. 16D**).

In order to characterize the behavior of *Asc-1* deficient cells *in vivo*, shAsc-1 and shScr cells were injected into Balb/c nude mice over the sternum. These mice were housed at thermoneutrality due to the regulation from our animal protocol, which normally negatively affect beiging. Nevertheless, both histology and PERILIPIN-1 staining revealed smaller and multilocular lipid droplet formation in shAsc-1 transplants, whereas shScr cells showed predominantly unilocular and bigger lipids (**Fig. 16C-D**). Moreover, UCP1 staining of engrafted tissue sections confirmed formation of UCP1 expressing adipocytes in shAsc-1 transplants, which was absent in shScr (**Fig. 16E**). These findings further demonstrate the role of *Asc-1* in in white adipocyte formation.

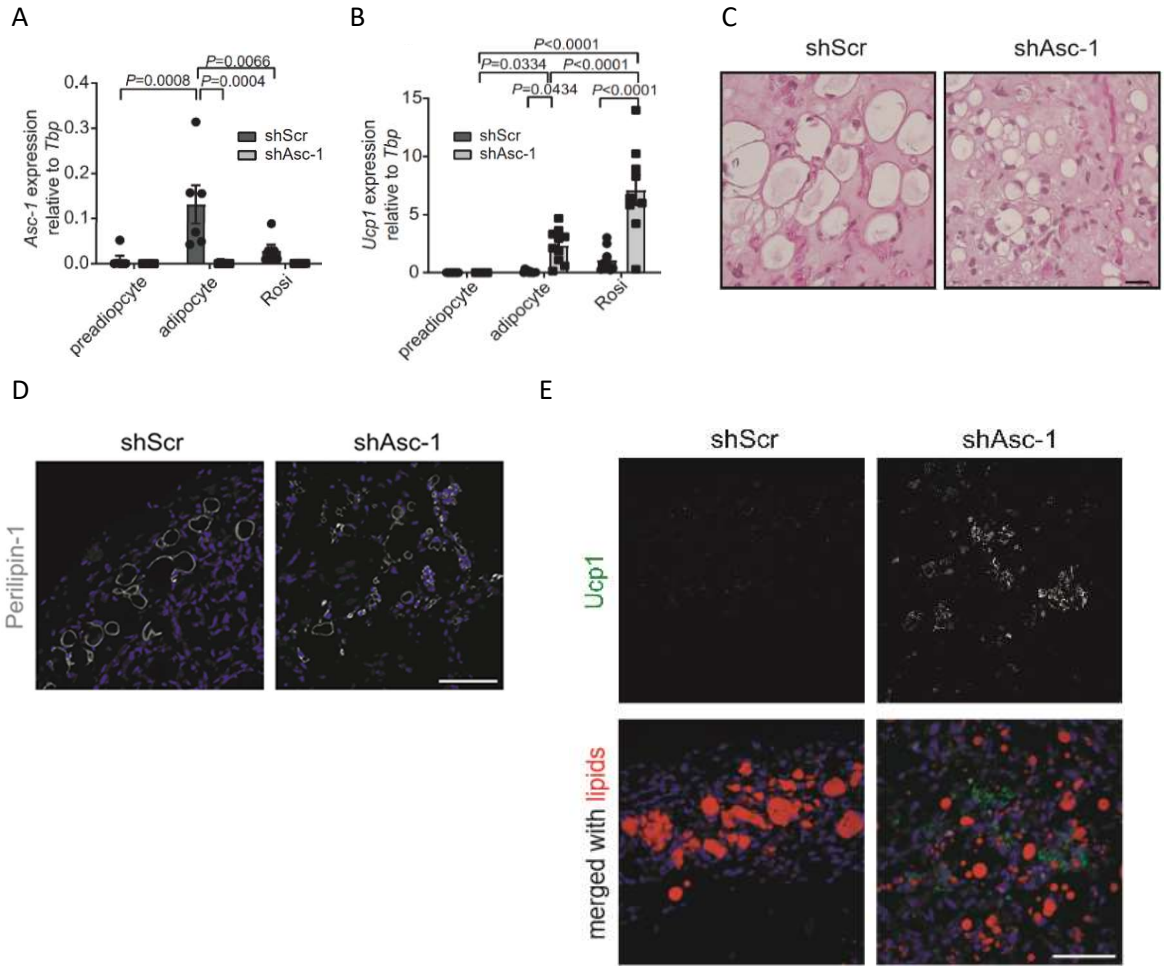

Figure 16: Transplanted shAsc-1 preadipocyte differentiate into beige adipocytes. Asc-1 was knockdown (shAsc-1) in immortalized subcutaneous preadipocytes. Control cells were transfected with scramble shRNA (shScr). Relative (A) *Asc-1* (n=6, only shAsc-1 preadipocytes n=5) and (B) *Ucp1* (n=10, only shScr preadipocytes and shAsc-1 Rosi n=9) expression levels of shAsc-1 and shScr cells differentiated with normal differentiation media (Adipocyte) with or without rosiglitazone (Rosi). Total RNA of preadipocytes were collected on the day of induction. (C) Balb/c nude mice were injected with shAsc-1 or shScr preadipocytes. H&E staining of engrafted tissue (n=1). Scale bar 20 µm. Immunofluorescence staining of (D) PERILIPIN-1 (grey, n=1 for shScr and n=2 for shAsc-1) and (E) UCP1 (green) with lipids (red) (n=2). Scale bar 100 µm. Figure A and B were generated by Dr. Lisa Siu-Lan Lehmann.

5.6.3 D-serine regulates beige vs white adipocyte fate decision

In our publication, we have shown that transport activity of ASC-1 in proliferating preadipocytes is essential for inhibiting differentiation of white preadipocytes into beige adipocytes (Data generated by Dr. Lisa Siu-Lan Lehmann) (Suwandhi et al., 2021). Next, since ASC-1 transports D-serine with high affinity, intracellular and extracellular D-serine levels were measured in subconfluent and confluent preadipocytes. Interestingly, while intracellular D-serine levels were very high in proliferating shAsc-1 compared to shScr preadipocytes, after reaching confluence this effect was blunted (Data generated by Dr. Lisa Siu-Lan Lehmann) (Suwandhi et al., 2021). In order

to test if intracellular D-serine levels regulate beiging *in vitro*, the enzyme (serine racemase, *Srr*) that converts L-serine to D-serine was transiently knockdown in proliferating shAsc-1 and shScr cells (**Fig. 17A and D**). Cells were differentiated in the presence of rosiglitazone to further induce beiging. *Srr* knockdown (DsiSrr) did not alter differentiation capacity of both shAsc-1 and shScr compared to transfection control (Control) (**Fig. 17B and E**). In line with the findings above, *Srr* knockdown significantly reduced *Ucp1* expression in shAsc-1 compared to Control (**Fig. 17C**). Moreover, it had no effect on shScr *Ucp1* mRNA levels, potentially due to low intracellular D-serine levels (**Fig. 17F**). These findings imply that loss of *Asc-1* increase intracellular D-serine accumulation, which contributes to commitment of subpopulation of SCF preadipocytes to beige adipocytes.

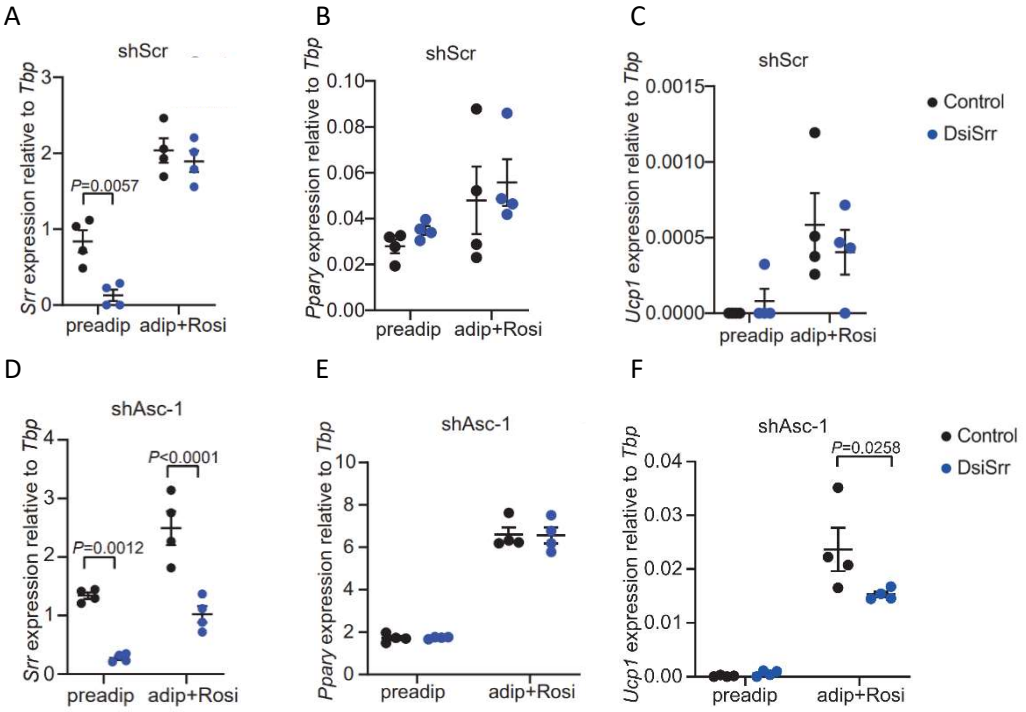

Figure 17: Transient knockdown of serine racemase (DsiSrr) reduced *Ucp1* expression only in shAsc-1 cells. shAsc-1 and shScr cells were reverse transfected with either DsiSrr or control siRNA (control). Relative (A/D) *Srr*, (B/E) *Pparγ* and (C/F) *Ucp1* expression levels in shScr (top) and shAsc-1 (bottom) cells differentiated in normal differentiation with rosiglitazone (adip+Rosi) (n=4). RNA of preadipocytes (preadip) were collected on the day of induction. P values are indicated in the graph. Data analyzed by mean ± SEM. Analysis was done using Two-Way ANOVA with Turkey's multiple comparison post hoc test.

6 Discussion

Adipose tissue (AT) is an endocrine organ that is critical for energy homeostasis and insulin signaling (Friedman, 2019, Scheja and Heeren, 2019). Therefore, its proper development is crucial for a functional metabolism. Metabolic syndrome arises from massive AT expansion in overweight and obese individuals. Despite this, there are several animal and human studies reporting MHO (Ahl et al., 2015, Kloting et al., 2010, Kim et al., 2007, Franckhauser et al., 2002). A common phenotype in MHO is a higher fat accumulation in legs and hips, indicating an enhanced fat storage capacity of subcutaneous depot and increased adiponectin levels. Moreover, these individuals displayed insulin sensitivity, no hypertension, lower inflammation and did not show lipid accumulation in the liver (Ahl et al., 2015, Primeau et al., 2011, Kloting et al., 2010). Many researchers aim to understand ways to improve unhealthy metabolism by identifying potential pathophysiological pathways during the 'disease' progression. However, there are other ways one can learn about the mechanisms regulating healthy expansion of the tissue that naturally occur upon development.

Studies have reported a rapid fat mass increase of infants in the first few months post-birth that does not cause any metabolic deterioration (Orsso et al., 2020, Wells et al., 2020, Fomon et al., 1982). High amounts of fat accumulation resulting in massive expansion of AT is crucial for the healthy development of human infants and mouse pups for adaptation of the body temperature to the temperature changes between the womb and outside world (Bruder and Fromme, 2022, Orsso et al., 2020). In this thesis, we also showed a similar phenomenon in mice. Pre-weaned mice (15 ± 2 days old) showed 2.5 and 15-fold increase in SCF and PGF tissue weights, respectively, compared to adult mice (58 ± 2 days old). Despite this massive expansion, mouse pups were metabolically healthy. Adult mice in our study were also metabolically healthy when fed a regular chow diet, but were predisposed to become metabolically unhealthy when fed with a high-fat diet (Buettner et al., 2007). Thus, in this study, we aimed to understand the compositional differences between pre-weaned and adult adipose depots to identify factors that can contribute to a metabolically healthier adipose tissue expansion and function. We focused on SCF since it has been reported to have a more protective effect on metabolism than PGF (Vishvanath and Gupta, 2019).

6.1 IGF2 does not alter adipogenesis in subcutaneous preadipocytes

Our scRNA-seq analysis of SCF, PGF and BAT of pre-weaned and adult SVC revealed 14 clusters, which consisted of various cell types including endothelial cell, immune cells and preadipocytes. Interestingly projection of age showed distinct separation of *Pdgfra*$^{+}$ cells, which is a commonly used marker for fibroblasts and preadipocytes (Sakers et al., 2022, Berry and Rodeheffer, 2013).

Further re-clustering of only *Pdgfra*$^{+}$ cells and differential gene expression analysis of each depot individually revealed *Igf2* as one of the most differentially expressed gene in subcutaneous preadipocytes of pre-weaned mice. Interestingly, according to the differential gene expression analysis, *Igf2* was also differentially expressed in PGF and BAT preadipocytes of adult mice. One explanation for the case of PGF might be because of the differences in the developmental stage. Even though BAT and SCF develop prenatally in mice, PGF develops postnatally (Wang et al., 2013). Thus, at birth it is very immature. This might be delaying the gene expression profiles of certain genes responsible for tissue expansion. In the case of BAT, it is harder to explain the difference in gene expression profiles of *Igf2* compared to SCF, since both depots develop prenatally and are derived from different lineages. However, this finding propose that there might be depot specific actions of IGF2, which requires further evaluation.

IGF2 is a well-known fetal growth promoter. It regulates placental growth and nutrient transfer (Gicquel and Le Bouc, 2006). Thus, making it a strong candidate in studying 'healthy' adipose tissue expansion. Depletion or knockout of *Igf2* in mice results in growth retardation and reduction in body weight (Lopez et al., 2018, DeChiara et al., 1990). In contrast, overexpression of IGF2 during embryonic development leads to overgrowth and increased birth weight (Sun et al., 1997). These findings indicate a potential correlation between IGF2 levels and body weight. Nevertheless, there is still little known about the postnatal role of IGF2, which is a recently emerging research field.

InsR and IGF1R are tyrosine kinases expressed in both preadipocyte and adipocytes but with different expression profiles (Boucher et al., 2010b, Back and Arnqvist, 2009). They carry a similar structural homology and are reported to regulate adipogenesis (Boucher et al., 2010b). IGF2 binds to both IGF1R and InsR with high affinity (Kadakia and Josefson, 2016). In line with the literature, immunoprecipitation of 10 nM IGF2 stimulated preadipocytes showed activation of both receptors. Moreover, insulin promotes differentiation of committed preadipocytes to adipocytes. Insulin activates InsR inducing glucose uptake and activating AKT pathway, which inhibits lipolysis and induces lipogenesis (Cignarelli et al., 2019, Kadakia and Josefson, 2016, Kahn and Flier, 2000). Thus, these findings indicate a potential role of IGF2 in promoting preadipocyte differentiation through InsR and IGF1R pathways. In order to study this, we supplemented primary subcutaneous preadipocytes of adult mice with 10 nM (75 ng/mL) recombinant IGF2. Our data showed that supplementation has no effect on differentiation capacity of subcutaneous preadipocytes from adult mice compared to untreated cells when cultured in normal cell culture conditions (10% FBS). This was confirmed by mRNA and protein levels of adipogenic markers (*Pparγ*, *Adipq* and *Fabp4*), immunofluorescence staining of lipids and lipid quantification by ORO. Interestingly, there are

some contradictory data in literature on this topic. Alfares *et al.* showed treatment of normal weight children SCF preadipocytes with recombinant IGF2 enhanced differentiation capacity in a dose dependent manner (7.5 and 62.5 ng/mL). Same study also reported an inhibitory effect of IGF2 on vWAT adipogenesis through downregulation of GLUT4 and InsR-A expression levels (Alfares et al., 2018). Moreover, recombinant IGF2 treatment increased adipogenic differentiation of patient derived hemangioma-derived stem cells (Zhang et al., 2019). In contrast, a 4.5-year follow-up study on non-diabetic individuals reported a negative correlation between circulating IGF2 levels and weight gain and development of obesity (Sandhu et al., 2003). Furthermore, comparison of First-Degree Relatives of T2D (FDR) to no family history of T2D patients revealed reduced differentiation of adipose precursor cells of FDRs in the presence of 100 ng/mL IGF2. They also found a negative correlation between adipogenesis and *Igf2* mRNA levels (Mirra et al., 2021). The opposing findings to the literature could be due to several reasons: (i) some studies focused on the young state while we studied adult state. (ii) We based our study on primary mouse preadipocytes, while others studied human preadipocytes, which highlights the complexities between species that might play a role in IGF2 function. (iii) *In vitro* culture systems use FBS as a media supplement, which contains high levels of fetal growth hormones including IGF2 that might have blunted the real effect in our study.

Harcuch and Green discussed in 1978 that adipogenic factors present in the serum regulates the extend of differentiation in 3T3-F442A cells. They showed that cells cultured under 10% calf serum yielded in less lipid accumulation compared to 10% fetal calf serum (Kuri-Harcuch and Green, 1978). In other words, circulating adipogenic factors were higher prenatally compared to postnatal. In order to reduce the impact of unknown factors contained in the FBS, we this time performed the same experiment of IGF2 supplementation in 1% mouse serum from adult mice (physiological mimetic culture conditions), since adult (9.0 ± 0.6 ng/mL) mice had significantly lower circulating IGF2 compared to pre-weaned mice (239.4 ± 28.2 ng/mL). This also allowed the mimicry of *in vivo* conditions. We pooled 27 C57BL/6 wild-type adult male mice to obtain a batch of mouse serum, which the availability and the quantity of mouse serum were one of the limitations of this study. Moreover, we substituted DMEM+GlutaMAX with Opti-MEM in the mouse serum culture conditions because our preliminary observations showed better differentiation capacity of the immortalized subcutaneous preadipocytes (**Fig. 18, Appendix**). Interestingly, immunofluorescence staining of lipids showed less number of cells that accumulated lipid droplets under physiological mimetic (1% Adult MS) compared to normal culture conditions (10% FBS). Nevertheless, similar to

10% FBS experiment, cells supplemented with 10 nM IGF2 under 1% Adult MS did not show differences in their differentiation capacity compared to no treatment.

Whole body *Igf2* knockout (*Igf2*$^{-/-}$) mice, despite born with decreased body weight (40% reduction) compared to wild-type littermates displayed increased hepatic triglyceride levels possibly due to an upregulation in genes associated with lipid metabolism in the liver, especially the master regulator of hepatic lipid content (peroxisome proliferator-activated receptor alpha, *Ppara*) (Lopez et al., 2018). Thus, to further evaluate the correlation between IGF2 and adipogenic capacity, subcutaneous preadipocytes of pre-weaned mice were this time treated with 1 µg/mL anti-IGF2 neutralizing antibody (IGF2 neutralizing antibody) due to their significantly high *Igf2* expression compared to adult mice. In line with the supplementation experiments, cells treated with the IGF2 neutralizing antibody differentiated similarly to control. Altogether, these findings indicate that IGF2 does not promote adipogenesis in primary murine subcutaneous preadipocytes.

6.2 IGF2 does not affect mitochondrial activity

Several studies imply the role of IGF2 in mitochondrial function and biogenesis. Knockdown of *Igf2* in skeletal muscle cells from 2-5 days old mice significantly reduced mitochondrial respiration, mass and mtDNA levels suggesting impaired mitochondrial function in a SIRT1-PGC1α dependent pathway (Zhu et al., 2021). In line with this, loss of *Igf2* function in HepG2 and AML12 cell lines disrupted mitochondrial biogenesis by significantly downregulating the expression levels of genes related to mitochondrial function, such as; *Sirt1*, *Tfam* and *Pgc1α,* as well as mtDNA numbers (Gui et al., 2021b). Even though overexpression of IGF2 in breast cancer cells did not affect *Pgc1α* expression levels, 10 nM IGF2 supplementation to cells overexpressing InsR in the absence of IGF1R (MCF7$^{IGF1R\text{-}ve}$/IR-A) upregulated *Pgc1α* significantly more than insulin. Overall, IGF2 contributed to increased mitochondrial biogenesis markers and activity in breast cancer cell line (Vella et al., 2019). Since it was also shown that retroperitoneal fat displays increased *Ucp1* expression between P10 and P30 (Xue et al., 2007), which is around similar time points as upregulated *Igf2* expression in pre-weaned mice, along with the findings discussed above, we investigated the effect of both IGF2 supplementation and neutralization on *Tfam*, *Pgc1α* and *Ucp1* mRNA expression levels. There was no difference in their mRNA expression levels when subcutaneous preadipocytes of adult mice were supplemented with 10 nM IGF2 regardless of the serum conditions. In contrast to what has been reported in the literature, there was no significant difference in beiging markers *(Tfam, Pgc1α and Ucp1)* expression levels in pre-weaned mice treated with IGF2 neutralizing antibody compared to the control regardless of the culture conditions. Furthermore, seahorse analysis also did not show differences in mitochondrial respiration between IGF2 neutralizing antibody and IgG

treatments. Since AT is more susceptible to insulin resistance, presence of insulin might suppress the signaling transduction of IGF2-InsR axis in preadipocytes and thus, might blunt changes in mitochondrial function by IGF2 supplementation or neutralization in contrast to reported previously (Vella et al., 2019, Turner et al., 2013). Furthermore, it was shown that even though the differentiation yield is very low, some 3T3-L1 cells could still differentiate in the absence of insulin. However, studies in brown preadipocytes showed that between 172-860 nM insulin significantly enhances adipogenesis and depot specific gene expression profiles compared to only IBMX and dexamethasone (Wang et al., 2018). Therefore, insulin is essential in the induction and differentiation media for evaluation of adipogenesis and function. Presence of insulin was one of the potential limitations of this study. Nevertheless, together these data show that IGF2 does not regulate mitochondrial activity in subcutaneous preadipocytes, subsequently indicating increased pre-weaned subcutaneous AT beiging is not associated with *Igf2*.

6.3 IGF2 supplementation enhances proliferative capacity of preadipocytes potentially via PI3K/AKT and ERK pathways

Obesity related complications are attributed to hypertrophic expansion of AT. Adipocyte size is positively correlated with insulin resistance and chronic inflammation. In contrast to MUO, MHO individuals display increased recruitment of new fat cells (Vishvanath and Gupta, 2019, Longo et al., 2019, Gustafson et al., 2009). Furthermore, adipocyte turnover is around 10% annually and is tightly regulated by death or generation of adipocytes (Spalding et al., 2008). This highlights the importance of APC niche maintenance that give rise to committed preadipocytes later differentiating into adipocytes. This is also important to overcome the exhaustion on lipid storage capacity of the mature adipocytes during tissue expansion (Altun et al., 2022). Over activation of APCs and maintenance of healthy tissue function are regulated through several processes, one of which is through induction or inhibition of proliferation.

In accordance with our findings, studies showed that IGF2 activates both PI3K/AKT and MAPK/ERK pathways in various cell types (Zhu et al., 2014, Hamamura et al., 2008). These pathways have been associated with many biological processes including cell proliferation and survival (Yu and Cui, 2016, Zhang and Liu, 2002). Furthermore, studies showed that IGF2 stimulates proliferation in various cell types. *Igf2* overexpression in breast cancer cell line (MCF7) or 10 nM supplementation in IGF1R-ablated MCF7 IR-A overexpressing cell ($MCF7^{IGF1R\text{-}ve}$/IR-A) stimulated proliferation and invasion. This was due to increased glycolysis and mitochondrial respiration (Vella et al., 2019). Moreover, Giudice and colleagues showed that IGF2 promoted InsR isoform B (InsR-B) internalization in HeLa cells, which stimulated cell proliferation. In contrast, insulin binding to the

IR-B maintained it in the cell membrane and facilitated metabolic regulation (Giudice et al., 2013). Along with these findings and since adipose tissue express more IR-B than IR-A (Westermeier et al., 2016), we investigated whether *Igf2* promotes hyperplastic adipose tissue expansion via preadipocyte proliferation. For this purpose, primary subcutaneous preadipocytes of adult mice were supplemented with 10 nM IGF2 in either normal (10%) or physiological mimentic (1% Adult MS) culture conditions for several days. MTT assay was performed to evaluate proliferation capacity. Similar to what was reported, we have shown that adult preadipocytes supplemented with 10 nM IGF2 proliferated significantly more compared to without IGF2. This was observed only when cells cultured with 1% Adult MS, where there were no excess fetal growth hormones like in FBS.

KI67 is highly expressed in cells going through mid-G1 and early M phase, therefore it is a well-accepted marker for studying proliferative cells (Zhang et al., 2021). Co-staining of pre-weaned SCF cryo-sections with *Igf2* and KI67 surprisingly showed that while few *Igf2*$^{+}$ cells were KI67 positive, majority of the *Igf2*$^{+}$ cells were KI67 negative *in vivo*, indicating that majority of the *Igf2* expressing cells do not proliferate. This highlights a more complex regulatory mechanism of IGF2 in tissue expansion, potentially implying a regulatory role of secreted IGF2 in the mitogenic activity of SVCs. Furthermore, CD31 staining revealed that some of the *Igf2* expressing cells were sitting in close proximity to blood vessels. Several APC populations have been reported to reside in a vascular niche (Jiang et al., 2017, Tang et al., 2008). Furthermore, a study also showed that interaction of APCs with vasculature is necessary for the maintenance and expansion of the progenitor niche (Jiang et al., 2017). Circulating IGF2 levels in mouse embryos positively correlated with endothelial cell proliferation. Fetal endothelial specific *Igf2* deletion resulted in disrupted placental microvasculature expansion (Sandovici et al., 2022). Thus, due to the localization of *Igf2* expressing cells and IGF2 enhancing proliferation capacity of preadipocytes *in vitro* might suggest that these cells regulate APC pool expansion in subcutaneous white adipose tissue.

6.4 ASC-1 expressing preadipocyte differentiate into white adipocytes

Here, like *Igf2*, we have detected *Asc-1* as one of the differentially expressed gene in SCF preadipocytes of pre-weaned mice. In addition to this, our group previously identified ASC-1 as a surface marker for white adipocytes (Ussar et al., 2014). Moreover, its physiological role is well studied in the brain (Ehmsen et al., 2016, Safory et al., 2015, Rutter et al., 2007, Matsuo et al., 2004), however little is known about its role in adipose tissue. This made it a strong candidate to further unravel its function in white adipose tissue. We initially sorted immortalized subcutaneous preadipocytes with an ASC-1 antibody. We did not see differences in the differentiation capacity of

ASC-1^{+} and ASC-1^{-} cells. In line with this, stable knockdown (shAsc-1) in immortalized subcutaneous preadipocytes and overexpression of Asc-1 (Asc-1-HA-2a-4F2HC) in immortalized brown preadipocytes, or treatment of preadipocytes with ASC-1 inhibitor (BMS-466422) during differentiation did not show differences in their adipogenic capacity compared to their respective control conditions measured by mRNA expression levels (Suwandhi et al., 2021). In contrast to this, Jersin *et al.* showed that treatment of preadipocytes with BMS-466422 increased lipid accumulation quantified by ORO. This difference might be because we have studied physiological function of *Asc-1* in preadipocytes with stable cell lines while Jersin *et al.* studied transport activity of ASC-1 after the induction of 3T3-L1 and human adipose stromal cells (Jersin et al., 2021).

Since *Asc-1* was not involved in adipogenesis in our study, we wanted to further investigate its function in white adipocytes. Interestingly, sorted ASC-1^{+} cells showed significant reduction in *Ucp1* expression compared to ASC-1^{-} cells when induced with rosiglitazone, which enhances beiging. Moreover, stable knockdown of *Asc-1* in subcutaneous preadipocytes induced beige adipocyte formation, that was assessed by browning markers including *Ucp1* (Suwandhi et al., 2021). Addition to this, injection of shAsc-1 preadipocytes over the sternum of Balb/c nude mice gave rise to multilocular adipocyte formation that expressed UCP1 compared to shScr cells, which showed unilocular fat cells. These findings indicated that *Asc-1* is involved in beige vs white adipocyte commitment in our study.

The cell-fate decision is tightly regulated in the proliferating preadipocytes. Inhibition of ASC-1 with BMS-466422 in sub-confluent preadipocytes 2 days before reaching confluency induced beige adipocyte formation. However, this effect was gone when confluent preadipocytes on the day of induction were treated with the ASC-1 inhibitor (Suwandhi et al., 2021). Therefore, the timing of intervention to ASC-1 function could lead to different findings in adipocytes, Arianti *et al.* also showed that BMS-466422 treatment of mature adipocytes alone compared to untreated condition did not affect mitochondrial respiration. However, when the cells were treated with cAMP to induce thermogenesis, addition of ASC-1 inhibitor reduced mitochondrial respiration in differentiated subcutaneous adipocytes of humans (Arianti et al., 2021). In contrast to this, we have shown that stable knockdown of *Asc-1* in preadipocytes increased basal respiration (Suwandhi et al., 2021). Moreover, another study showed that overexpression of *Asc-1* in 3T3-L1 cell line after induction significantly increased mitochondrial respiration (Jersin et al., 2021). Although these findings highlight the differences between preadipocyte and adipocyte cell programing, the discrepancy between our findings and literature might be due to the difference in adipocyte models used: we used established cell lines, whereas others used primary cells or the location of the

depot's cells were isolated from: abdominal vs deep neck (Jersin et al., 2022). Nevertheless, our results show an important role of *Asc-1* in a subtype of preadipocytes regulating white vs beige adipocyte differentiation.

6.5 Intracellular D-serine accumulation is one of the key players in determining white vs beige adipocyte fate decision

ASC-1 is a neutral amino acid transporter. It has high affinity to alanine, cysteine, glycine and serine (Rutter et al., 2007, Fukasawa et al., 2000). Analysis of amino acid levels showed reduced intracellular and extracellular D-serine in shAsc-1 preadipocytes compared to shScr (Suwandhi et al., 2021). In line with this, Arianti *et al*. and colleagues showed significantly reduced serine consumption of human deep neck subcutaneous adipocytes 10 h after BMS-466422 treatment compared to control (Arianti et al., 2021). This shows that similar to brain, ASC-1 play an important role in bidirectional D-serine transport in adipose tissue.

Next, the mechanism behind the ASC-1 transport activity on beige vs white adipocyte commitment was tested. Depletion of cargo amino acids; glycine, alanine, glutamine and serine, did not influence the differentiation capacity or beiging markers (*Ucp1* and *Pgc1α*) expression in shAsc-1 cells compared to control medium condition. However, 10 g/L D-serine supplementation in drinking water of CD fed wild-type mice showed reduced *Ucp1* expression in BAT compared to control mice (Suwandhi et al., 2021). This result along with increased intracellular D-serine accumulation in shAsc-1 cells encouraged further studying of D-serine metabolism. Serine racemase (*Srr*) is an important enzyme that converts L-serine to D-serine (Graham et al., 2019). Knockdown of *Srr* in shAsc-1 and shScr cells did not alter adipogenesis compared to knockdown control. It significantly reduced *Ucp1* expression in shAsc-1 cells compared to knockdown control, while shScr cells did not show any difference in *Ucp1* expression with *Srr* knockdown. This was in line with the intracellular D-serine levels discussed above (Suwandhi et al., 2021). Altogether, these data suggest that loss of *Asc-1* function induces intracellular D-serine accumulation and regulates beiging of subpopulation of SCF preadipocytes. However, it is important highlight here that ASC-1 has other cargo amino acids and their role in the observed beiging needs further investigation.

7 Conclusion and Outlook

Obesity is a worldwide epidemic. It has major health and economic burdens on the society. Therefore, it attracts great attention of public health system. Over the past decade researchers have tried to find mechanisms to improve obesity related comorbidities by studying animal models that compare diseased state to healthy state. There have been several potential treatment options found, however either these are costly or decrease life quality of the patients. Therefore, new treatment strategies need to be found.

In this study, we aimed to understand the naturally occurring developmental state of adipose tissue and therefore, compared compositional differences of pre-weaned and adult mice adipose depots. Both mice were metabolically healthy; however, the major difference was that pre-weaned mice displayed rapid and massive expansion of AT without any metabolic deterioration. If the same expansion was induced in adult mice by HFD feeding, then these mice would become metabolically unhealthy, which has been the animal model studied in the field. Single cell RNA sequencing analysis of whole SVCs revealed distinct separation by age between preadipocytes. Comprehensive analysis of these cells showed *Igf2* and *Asc-1* as one of the abundantly expressed genes in SCF preadipocytes of pre-weaned mice.

We have shown here that IGF2 did not alter adipogenic capacity of the preadipocytes but increased preadipocyte proliferation. These findings indicated a potential role of IGF2 in regulating hyperplasia via inducing preadipocyte pool expansion. However, a deeper understanding of molecular mechanism by stable cell lines and transplantation of these subpopulation of cells is required.

Moreover, *Asc-1* was also identified as one of the differentially expressed genes in pre-weaned SCF compared to adult. Here we showed that *Asc-1* plays an essential role on white adipocyte formation and loss of *Asc-1* function induces beiging both *in vivo* and *in vitro*. The fact that there is a peak UCP1 expression levels between postnatal days (P) 10 and 30 in SCF combined with our findings indicate that *Asc-1* plays an important role in the development of white adipose tissue. Most importantly, it regulates white vs beige fate decision during differentiation partly by ASC-1 mediated D-serine transport in the preadipocytes. However, the role of other ASC-1 cargos on beiging is still not well known, which requires further investigation.

Our findings highlight the heterogeneity in SCF preadipocytes. We propose here naturally occurring mechanisms that enable healthy tissue remodeling. Thus, these results have major impacts on the treatment of obesity and associated metabolic syndromes.

8 References

ACCILI, D., DRAGO, J., LEE, E. J., JOHNSON, M. D., COOL, M. H., SALVATORE, P., ASICO, L. D., JOSE, P. A., TAYLOR, S. I. & WESTPHAL, H. 1996. Early neonatal death in mice homozygous for a null allele of the insulin receptor gene. *Nat Genet,* 12**,** 106-9.

AGROGIANNIS, G. D., SIFAKIS, S., PATSOURIS, E. S. & KONSTANTINIDOU, A. E. 2014. Insulin-like growth factors in embryonic and fetal growth and skeletal development (Review). *Mol Med Rep,* 10**,** 579-84.

AHL, S., GUENTHER, M., ZHAO, S., JAMES, R., MARKS, J., SZABO, A. & KIDAMBI, S. 2015. Adiponectin Levels Differentiate Metabolically Healthy vs Unhealthy Among Obese and Nonobese White Individuals. *J Clin Endocrinol Metab,* 100**,** 4172-80.

ALBERTI, K. G. & ZIMMET, P. Z. 1998. Definition, diagnosis and classification of diabetes mellitus and its complications. Part 1: diagnosis and classification of diabetes mellitus provisional report of a WHO consultation. *Diabet Med,* 15**,** 539-53.

ALFARES, M. N., PERKS, C. M., HAMILTON-SHIELD, J. P. & HOLLY, J. M. P. 2018. Insulin-like growth factor-II in adipocyte regulation: depot-specific actions suggest a potential role limiting excess visceral adiposity. *Am J Physiol Endocrinol Metab,* 315**,** E1098-E1107.

ALTUN, I., YAN, X. & USSAR, S. 2022. Immune Cell Regulation of White Adipose Progenitor Cell Fate. *Front Endocrinol (Lausanne),* 13**,** 859044.

ANDERSEN, M., NORGAARD-PEDERSEN, D., BRANDT, J., PETTERSSON, I. & SLAABY, R. 2017. IGF1 and IGF2 specificities to the two insulin receptor isoforms are determined by insulin receptor amino acid 718. *PLoS One,* 12**,** e0178885.

APPLETON, S. L., SEABORN, C. J., VISVANATHAN, R., HILL, C. L., GILL, T. K., TAYLOR, A. W., ADAMS, R. J. & NORTH WEST ADELAIDE HEALTH STUDY, T. 2013. Diabetes and cardiovascular disease outcomes in the metabolically healthy obese phenotype: a cohort study. *Diabetes Care,* 36**,** 2388-94.

ARGYROPOULOS, G. & HARPER, M. E. 2002. Uncoupling proteins and thermoregulation. *J Appl Physiol (1985),* 92**,** 2187-98.

ARIANTI, R., VINNAI, B. A., TOTH, B. B., SHAW, A., CSOSZ, E., VAMOS, A., GYORY, F., FISCHER-POSOVSZKY, P., WABITSCH, M., KRISTOF, E. & FESUS, L. 2021. ASC-1 transporter-dependent amino acid uptake is required for the efficient thermogenic response of human adipocytes to adrenergic stimulation. *FEBS Lett,* 595**,** 2085-2098.

ASHTON, I. K., ZAPF, J., EINSCHENK, I. & MACKENZIE, I. Z. 1985. Insulin-like growth factors (IGF) 1 and 2 in human foetal plasma and relationship to gestational age and foetal size during midpregnancy. *Acta Endocrinol (Copenh),* 110**,** 558-63.

BACK, K. & ARNQVIST, H. J. 2009. Changes in insulin and IGF-I receptor expression during differentiation of human preadipocytes. *Growth Horm IGF Res,* 19**,** 101-11.

BARAL, K. & ROTWEIN, P. 2019. The insulin-like growth factor 2 gene in mammals: Organizational complexity within a conserved locus. *PLoS One,* 14**,** e0219155.

BARTELT, A. & HEEREN, J. 2014. Adipose tissue browning and metabolic health. *Nat Rev Endocrinol,* 10**,** 24-36.

BARTHOLDI, D., KRAJEWSKA-WALASEK, M., OUNAP, K., GASPAR, H., CHRZANOWSKA, K. H., ILYANA, H., KAYSERILI, H., LURIE, I. W., SCHINZEL, A. & BAUMER, A. 2009. Epigenetic mutations of the imprinted IGF2-H19 domain in Silver-Russell syndrome (SRS): results from a large cohort of patients with SRS and SRS-like phenotypes. *J Med Genet,* 46**,** 192-7.

BEFORT, C. A., NAZIR, N. & PERRI, M. G. 2012. Prevalence of obesity among adults from rural and urban areas of the United States: findings from NHANES (2005-2008). *J Rural Health,* 28**,** 392-7.

BERGHOFER, A., PISCHON, T., REINHOLD, T., APOVIAN, C. M., SHARMA, A. M. & WILLICH, S. N. 2008. Obesity prevalence from a European perspective: a systematic review. *BMC Public Health,* 8**,** 200.

BERRY, R. & RODEHEFFER, M. S. 2013. Characterization of the adipocyte cellular lineage in vivo. *Nat Cell Biol,* 15**,** 302-8.

BIANCO, M. E. & JOSEFSON, J. L. 2019. Hyperglycemia During Pregnancy and Long-Term Offspring Outcomes. *Curr Diab Rep,* 19**,** 143.

BLUHER, M. 2020. Metabolically Healthy Obesity. *Endocr Rev,* 41.

BLUHER, M., MICHAEL, M. D., PERONI, O. D., UEKI, K., CARTER, N., KAHN, B. B. & KAHN, C. R. 2002. Adipose tissue selective insulin receptor knockout protects against obesity and obesity-related glucose intolerance. *Dev Cell,* 3**,** 25-38.

BOOTH, A. D., MAGNUSON, A. M., FOUTS, J., WEI, Y., WANG, D., PAGLIASSOTTI, M. J. & FOSTER, M. T. 2018. Subcutaneous adipose tissue accumulation protects systemic glucose tolerance and muscle metabolism. *Adipocyte,* 7**,** 261-272.

BORENSZTEIN, M., VIENGCHAREUN, S., MONTARRAS, D., JOURNOT, L., BINART, N., LOMBES, M. & DANDOLO, L. 2012. Double Myod and Igf2 inactivation promotes brown adipose tissue development by increasing Prdm16 expression. *FASEB J,* 26**,** 4584-91.

BOUCHER, J., MACOTELA, Y., BEZY, O., MORI, M. A., KRIAUCIUNAS, K. & KAHN, C. R. 2010a. A kinase-independent role for unoccupied insulin and IGF-1 receptors in the control of apoptosis. *Sci Signal,* 3**,** ra87.

BOUCHER, J., MORI, M. A., LEE, K. Y., SMYTH, G., LIEW, C. W., MACOTELA, Y., ROURK, M., BLUHER, M., RUSSELL, S. J. & KAHN, C. R. 2012. Impaired thermogenesis and adipose tissue development in mice with fat-specific disruption of insulin and IGF-1 signalling. *Nat Commun,* 3**,** 902.

BOUCHER, J., SOFTIC, S., EL OUAAMARI, A., KRUMPOCH, M. T., KLEINRIDDERS, A., KULKARNI, R. N., O'NEILL, B. T. & KAHN, C. R. 2016. Differential Roles of Insulin and IGF-1 Receptors in Adipose Tissue Development and Function. *Diabetes,* 65**,** 2201-13.

BOUCHER, J., TSENG, Y. H. & KAHN, C. R. 2010b. Insulin and insulin-like growth factor-1 receptors act as ligand-specific amplitude modulators of a common pathway regulating gene transcription. *J Biol Chem,* 285**,** 17235-45.

BROWN, J., JONES, E. Y. & FORBES, B. E. 2009. Interactions of IGF-II with the IGF2R/cation-independent mannose-6-phosphate receptor mechanism and biological outcomes. *Vitam Horm,* 80**,** 699-719.

BRUDER, J. & FROMME, T. 2022. Global Adipose Tissue Remodeling During the First Month of Postnatal Life in Mice. *Front Endocrinol (Lausanne),* 13**,** 849877.

BUETTNER, R., SCHOLMERICH, J. & BOLLHEIMER, L. C. 2007. High-fat diets: modeling the metabolic disorders of human obesity in rodents. *Obesity (Silver Spring),* 15**,** 798-808.

BUNNER, A. E., CHANDRASEKERA, P. C. & BARNARD, N. D. 2014. Knockout mouse models of insulin signaling: Relevance past and future. *World J Diabetes,* 5**,** 146-59.

CAPODAGLIO, P. & LIUZZI, A. 2013. Obesity: a disabling disease or a condition favoring disability? *Eur J Phys Rehabil Med,* 49**,** 395-8.

CARPENTIER, A. C., BLONDIN, D. P., VIRTANEN, K. A., RICHARD, D., HAMAN, F. & TURCOTTE, E. E. 2018. Brown Adipose Tissue Energy Metabolism in Humans. *Front Endocrinol (Lausanne),* 9**,** 447.

CHANG, S., WU, X., YU, H. & SPITZ, M. R. 2002. Plasma concentrations of insulin-like growth factors among healthy adult men and postmenopausal women: associations with body composition, lifestyle, and reproductive factors. *Cancer Epidemiol Biomarkers Prev,* 11**,** 758-66.

CHAO, W. & D'AMORE, P. A. 2008. IGF2: epigenetic regulation and role in development and disease. *Cytokine Growth Factor Rev,* 19**,** 111-20.

CHU, A. Y., DENG, X., FISHER, V. A., DRONG, A., ZHANG, Y., FEITOSA, M. F., LIU, C. T., WEEKS, O., CHOH, A. C., DUAN, Q., DYER, T. D., EICHER, J. D., GUO, X., HEARD-COSTA, N. L., KACPROWSKI, T., KENT, J. W., JR., LANGE, L. A., LIU, X., LOHMAN, K., LU, L., MAHAJAN, A., O'CONNELL, J. R., PARIHAR, A., PERALTA, J. M., SMITH, A. V., ZHANG, Y., HOMUTH, G., KISSEBAH, A. H., KULLBERG, J., LAQUA, R., LAUNER, L. J., NAUCK, M., OLIVIER, M., PEYSER, P. A., TERRY, J. G., WOJCZYNSKI, M. K., YAO, J., BIELAK, L. F., BLANGERO, J., BORECKI, I. B., BOWDEN, D. W., CARR, J. J., CZERWINSKI, S. A., DING, J., FRIEDRICH, N., GUDNASON, V., HARRIS, T. B., INGELSSON, E., JOHNSON, A. D., KARDIA, S. L., LANGEFELD, C. D., LIND, L., LIU, Y., MITCHELL, B. D., MORRIS, A. P., MOSLEY, T. H., JR., ROTTER, J. I., SHULDINER, A. R., TOWNE, B., VOLZKE, H., WALLASCHOFSKI, H., WILSON, J. G., ALLISON, M., LINDGREN, C. M., GOESSLING, W., CUPPLES, L. A., STEINHAUSER, M. L. & FOX, C. S. 2017. Multiethnic genome-wide meta-analysis of ectopic fat depots identifies loci associated with adipocyte development and differentiation. *Nat Genet,* 49**,** 125-130.

CIGNARELLI, A., GENCHI, V. A., PERRINI, S., NATALICCHIO, A., LAVIOLA, L. & GIORGINO, F. 2019. Insulin and Insulin Receptors in Adipose Tissue Development. *Int J Mol Sci,* 20.

COULTER, A. A., BEARDEN, C. M., LIU, X., KOZA, R. A. & KOZAK, L. P. 2003. Dietary fat interacts with QTLs controlling induction of Pgc-1 alpha and Ucp1 during conversion of white to brown fat. *Physiol Genomics,* 14**,** 139-47.

COUSIN, B., CINTI, S., MORRONI, M., RAIMBAULT, S., RICQUIER, D., PENICAUD, L. & CASTEILLA, L. 1992. Occurrence of brown adipocytes in rat white adipose tissue: molecular and morphological characterization. *J Cell Sci,* 103 (Pt 4)**,** 931-42.

CUSHMAN, S. W. & WARDZALA, L. J. 1980. Potential mechanism of insulin action on glucose transport in the isolated rat adipose cell. Apparent translocation of intracellular transport systems to the plasma membrane. *J Biol Chem,* 255**,** 4758-62.

CYPESS, A. M., LEHMAN, S., WILLIAMS, G., TAL, I., RODMAN, D., GOLDFINE, A. B., KUO, F. C., PALMER, E. L., TSENG, Y. H., DORIA, A., KOLODNY, G. M. & KAHN, C. R. 2009. Identification and importance of brown adipose tissue in adult humans. *N Engl J Med,* 360**,** 1509-17.

DECHIARA, T. M., EFSTRATIADIS, A. & ROBERTSON, E. J. 1990. A growth-deficiency phenotype in heterozygous mice carrying an insulin-like growth factor II gene disrupted by targeting. *Nature,* 345**,** 78-80.

DECHIARA, T. M., ROBERTSON, E. J. & EFSTRATIADIS, A. 1991. Parental imprinting of the mouse insulin-like growth factor II gene. *Cell,* 64**,** 849-59.

DEMETRIOU, C., ABU-AMERO, S., THOMAS, A. C., ISHIDA, M., AGGARWAL, R., AL-OLABI, L., LEON, L. J., STAFFORD, J. L., SYNGELAKI, A., PEEBLES, D., NICOLAIDES, K. H., REGAN, L., STANIER, P. & MOORE, G. E. 2014. Paternally expressed, imprinted insulin-like growth factor-2 in chorionic villi correlates significantly with birth weight. *PLoS One,* 9**,** e85454.

DESOYE, G. & HERRERA, E. 2021. Adipose tissue development and lipid metabolism in the human fetus: The 2020 perspective focusing on maternal diabetes and obesity. *Prog Lipid Res,* 81**,** 101082.

DUVILLIE, B., CORDONNIER, N., DELTOUR, L., DANDOY-DRON, F., ITIER, J. M., MONTHIOUX, E., JAMI, J., JOSHI, R. L. & BUCCHINI, D. 1997. Phenotypic alterations in insulin-deficient mutant mice. *Proc Natl Acad Sci U S A,* 94**,** 5137-40.

EHMSEN, J. T., LIU, Y., WANG, Y., PALADUGU, N., JOHNSON, A. E., ROTHSTEIN, J. D., DU LAC, S., MATTSON, M. P. & HOKE, A. 2016. The astrocytic transporter SLC7A10 (Asc-1) mediates glycinergic inhibition of spinal cord motor neurons. *Sci Rep,* 6**,** 35592.

ENTINGH-PEARSALL, A. & KAHN, C. R. 2004. Differential roles of the insulin and insulin-like growth factor-I (IGF-I) receptors in response to insulin and IGF-I. *J Biol Chem,* 279**,** 38016-24.

FABBRINI, E., YOSHINO, J., YOSHINO, M., MAGKOS, F., TIEMANN LUECKING, C., SAMOVSKI, D., FRATERRIGO, G., OKUNADE, A. L., PATTERSON, B. W. & KLEIN, S. 2015. Metabolically normal obese people are protected from adverse effects following weight gain. *J Clin Invest,* 125**,** 787-95.

FAJAS, L. 2003. Adipogenesis: a cross-talk between cell proliferation and cell differentiation. *Ann Med,* 35**,** 79-85.

FOMON, S. J., HASCHKE, F., ZIEGLER, E. E. & NELSON, S. E. 1982. Body composition of reference children from birth to age 10 years. *Am J Clin Nutr,* 35**,** 1169-75.

FOX, C. S., LIU, Y., WHITE, C. C., FEITOSA, M., SMITH, A. V., HEARD-COSTA, N., LOHMAN, K., CONSORTIUM, G., CONSORTIUM, M., CONSORTIUM, G., JOHNSON, A. D., FOSTER, M. C., GREENAWALT, D. M., GRIFFIN, P., DING, J., NEWMAN, A. B., TYLAVSKY, F., MILJKOVIC, I., KRITCHEVSKY, S. B., LAUNER, L., GARCIA, M., EIRIKSDOTTIR, G., CARR, J. J., GUDNASON, V., HARRIS, T. B., CUPPLES, L. A. & BORECKI, I. B. 2012. Genome-wide association for abdominal subcutaneous and visceral adipose reveals a novel locus for visceral fat in women. *PLoS Genet,* 8**,** e1002695.

FOX, C. S., MASSARO, J. M., HOFFMANN, U., POU, K. M., MAUROVICH-HORVAT, P., LIU, C. Y., VASAN, R. S., MURABITO, J. M., MEIGS, J. B., CUPPLES, L. A., D'AGOSTINO, R. B., SR. & O'DONNELL, C. J. 2007. Abdominal visceral and subcutaneous adipose tissue

compartments: association with metabolic risk factors in the Framingham Heart Study. *Circulation,* 116**,** 39-48.

FRANCKHAUSER, S., MUNOZ, S., PUJOL, A., CASELLAS, A., RIU, E., OTAEGUI, P., SU, B. & BOSCH, F. 2002. Increased fatty acid re-esterification by PEPCK overexpression in adipose tissue leads to obesity without insulin resistance. *Diabetes,* 51**,** 624-30.

FRIEDMAN, J. M. 2019. Leptin and the endocrine control of energy balance. *Nat Metab,* 1**,** 754-764.

FRUH, S. M. 2017. Obesity: Risk factors, complications, and strategies for sustainable long-term weight management. *J Am Assoc Nurse Pract,* 29**,** S3-S14.

FUKASAWA, Y., SEGAWA, H., KIM, J. Y., CHAIROUNGDUA, A., KIM, D. K., MATSUO, H., CHA, S. H., ENDOU, H. & KANAI, Y. 2000. Identification and characterization of a Na(+)-independent neutral amino acid transporter that associates with the 4F2 heavy chain and exhibits substrate selectivity for small neutral D- and L-amino acids. *J Biol Chem,* 275**,** 9690-8.

FUNCKE, J. B. & SCHERER, P. E. 2019. Beyond adiponectin and leptin: adipose tissue-derived mediators of inter-organ communication. *J Lipid Res,* 60**,** 1648-1684.

GEHART, H., KUMPF, S., ITTNER, A. & RICCI, R. 2010. MAPK signalling in cellular metabolism: stress or wellness? *EMBO Rep,* 11**,** 834-40.

GICQUEL, C. & LE BOUC, Y. 2006. Hormonal regulation of fetal growth. *Horm Res,* 65 Suppl 3**,** 28-33.

GIUDICE, J., BARCOS, L. S., GUAIMAS, F. F., PENAS-STEINHARDT, A., GIORDANO, L., JARES-ERIJMAN, E. A. & COLUCCIO LESKOW, F. 2013. Insulin and insulin like growth factor II endocytosis and signaling via insulin receptor B. *Cell Commun Signal,* 11**,** 18.

GRAHAM, D. L., BEIO, M. L., NELSON, D. L. & BERKOWITZ, D. B. 2019. Human Serine Racemase: Key Residues/Active Site Motifs and Their Relation to Enzyme Function. *Front Mol Biosci,* 6**,** 8.

GUI, W., LIANG, J., LIN, X., SHI, N., ZHU, Y., TAN, B. & LI, H. 2021a. Association of Genetic Variants in IGF2-Related Genes With Risk of Metabolic Syndrome in the Chinese Han Population. *Front Endocrinol (Lausanne),* 12**,** 654747.

GUI, W., ZHU, Y., SUN, S., ZHU, W., TAN, B., ZHAO, H., SHANG, C., ZHENG, F., LIN, X. & LI, H. 2021b. Knockdown of insulin-like growth factor 2 gene disrupts mitochondrial functions in the liver. *J Mol Cell Biol*.

GUSTAFSON, B., GOGG, S., HEDJAZIFAR, S., JENNDAHL, L., HAMMARSTEDT, A. & SMITH, U. 2009. Inflammation and impaired adipogenesis in hypertrophic obesity in man. *Am J Physiol Endocrinol Metab,* 297**,** E999-E1003.

GUTIN, I. 2018. In BMI We Trust: Reframing the Body Mass Index as a Measure of Health. *Soc Theory Health,* 16**,** 256-271.

HAKUNO, F. & TAKAHASHI, S. I. 2018. IGF1 receptor signaling pathways. *J Mol Endocrinol,* 61**,** T69-T86.

HAMAMURA, K., ZHANG, P. & YOKOTA, H. 2008. IGF2-driven PI3 kinase and TGFbeta signaling pathways in chondrogenesis. *Cell Biol Int,* 32**,** 1238-46.

HAMER, M., BELL, J. A., SABIA, S., BATTY, G. D. & KIVIMAKI, M. 2015. Stability of metabolically healthy obesity over 8 years: the English Longitudinal Study of Ageing. *Eur J Endocrinol,* 173**,** 703-8.

HARDY, O. T., CZECH, M. P. & CORVERA, S. 2012. What causes the insulin resistance underlying obesity? *Curr Opin Endocrinol Diabetes Obes,* 19**,** 81-7.

HARING, H. U. 1991. The insulin receptor: signalling mechanism and contribution to the pathogenesis of insulin resistance. *Diabetologia,* 34**,** 848-61.

HEID, I. M., JACKSON, A. U., RANDALL, J. C., WINKLER, T. W., QI, L., STEINTHORSDOTTIR, V., THORLEIFSSON, G., ZILLIKENS, M. C., SPELIOTES, E. K., MAGI, R., WORKALEMAHU, T., WHITE, C. C., BOUATIA-NAJI, N., HARRIS, T. B., BERNDT, S. I., INGELSSON, E., WILLER, C. J., WEEDON, M. N., LUAN, J., VEDANTAM, S., ESKO, T., KILPELAINEN, T. O., KUTALIK, Z., LI, S., MONDA, K. L., DIXON, A. L., HOLMES, C. C., KAPLAN, L. M., LIANG, L., MIN, J. L., MOFFATT, M. F., MOLONY, C., NICHOLSON, G., SCHADT, E. E., ZONDERVAN, K. T., FEITOSA, M. F., FERREIRA, T., LANGO ALLEN, H., WEYANT, R. J., WHEELER, E., WOOD, A. R., MAGIC, ESTRADA, K., GODDARD, M. E., LETTRE, G., MANGINO, M., NYHOLT, D. R., PURCELL, S., SMITH, A. V., VISSCHER, P. M., YANG, J., MCCARROLL, S. A., NEMESH, J., VOIGHT, B. F., ABSHER, D., AMIN, N., ASPELUND, T., COIN, L., GLAZER, N. L., HAYWARD, C., HEARD-COSTA, N. L., HOTTENGA, J. J., JOHANSSON, A., JOHNSON, T., KAAKINEN, M., KAPUR, K., KETKAR, S., KNOWLES, J. W., KRAFT, P., KRAJA, A. T., LAMINA, C., LEITZMANN, M. F., MCKNIGHT, B., MORRIS, A. P., ONG, K. K., PERRY, J. R., PETERS, M. J., POLASEK, O., PROKOPENKO, I., RAYNER, N. W., RIPATTI, S., RIVADENEIRA, F., ROBERTSON, N. R., SANNA, S., SOVIO, U., SURAKKA, I., TEUMER, A., VAN WINGERDEN, S., VITART, V., ZHAO, J. H., CAVALCANTI-PROENCA, C., CHINES, P. S., FISHER, E., KULZER, J. R., LECOEUR, C., NARISU, N., SANDHOLT, C., SCOTT, L. J., SILANDER, K., STARK, K., et al. 2010. Meta-analysis identifies 13 new loci associated with waist-hip ratio and reveals sexual dimorphism in the genetic basis of fat distribution. *Nat Genet,* 42**,** 949-60.

HOCKING, S., SAMOCHA-BONET, D., MILNER, K. L., GREENFIELD, J. R. & CHISHOLM, D. J. 2013. Adiposity and insulin resistance in humans: the role of the different tissue and cellular lipid depots. *Endocr Rev,* 34**,** 463-500.

HOLLY, J. M. P., BIERNACKA, K. & PERKS, C. M. 2019. The Neglected Insulin: IGF-II, a Metabolic Regulator with Implications for Diabetes, Obesity, and Cancer. *Cells,* 8.

HONEGGER, A. & HUMBEL, R. E. 1986. Insulin-like growth factors I and II in fetal and adult bovine serum. Purification, primary structures, and immunological cross-reactivities. *J Biol Chem,* 261**,** 569-75.

HOWLADER, M., SULTANA, M. I., AKTER, F. & HOSSAIN, M. M. 2021. Adiponectin gene polymorphisms associated with diabetes mellitus: A descriptive review. *Heliyon,* 7**,** e07851.

HRUBY, A. & HU, F. B. 2015. The Epidemiology of Obesity: A Big Picture. *Pharmacoeconomics,* 33**,** 673-89.

HUANG, X., LIU, G., GUO, J. & SU, Z. 2018. The PI3K/AKT pathway in obesity and type 2 diabetes. *Int J Biol Sci,* 14**,** 1483-1496.

HUDDA, M. T., NIGHTINGALE, C. M., DONIN, A. S., OWEN, C. G., RUDNICKA, A. R., WELLS, J. C. K., RUTTER, H., COOK, D. G. & WHINCUP, P. H. 2018. Patterns of childhood body mass index (BMI), overweight and obesity in South Asian and black participants in the English National child measurement programme: effect of applying BMI adjustments standardising for ethnic differences in BMI-body fatness associations. *Int J Obes (Lond),* 42**,** 662-670.

HURT, R. T., KULISEK, C., BUCHANAN, L. A. & MCCLAVE, S. A. 2010. The obesity epidemic: challenges, health initiatives, and implications for gastroenterologists. *Gastroenterol Hepatol (N Y),* 6**,** 780-92.

IACOBELLIS, G., RIBAUDO, M. C., ZAPPATERRENO, A., IANNUCCI, C. V. & LEONETTI, F. 2005. Prevalence of uncomplicated obesity in an Italian obese population. *Obes Res,* 13**,** 1116-22.

ISIDOR, M. S., WINTHER, S., BASSE, A. L., PETERSEN, M. C., CANNON, B., NEDERGAARD, J. & HANSEN, J. B. 2016. An siRNA-based method for efficient silencing of gene expression in mature brown adipocytes. *Adipocyte,* 5**,** 175-85.

IWAYAMA, T., STEELE, C., YAO, L., DOZMOROV, M. G., KARAMICHOS, D., WREN, J. D. & OLSON, L. E. 2015. PDGFRalpha signaling drives adipose tissue fibrosis by targeting progenitor cell plasticity. *Genes Dev,* 29**,** 1106-19.

JERSIN, R. A., JONASSEN, L. R. & DANKEL, S. N. 2022. The neutral amino acid transporter SLC7A10 in adipose tissue, obesity and insulin resistance. *Front Cell Dev Biol,* 10**,** 974338.

JERSIN, R. A., TALLAPRAGADA, D. S. P., MADSEN, A., SKARTVEIT, L., FJAERE, E., MCCANN, A., DYER, L., WILLEMS, A., BJUNE, J. I., BJUNE, M. S., VAGE, V., NIELSEN, H. J., THORSEN, H. L., NEDREBO, B. G., BUSCH, C., STEEN, V. M., BLUHER, M., JACOBSON, P., SVENSSON, P. A., FERNO, J., RYDEN, M., ARNER, P., NYGARD, O., CLAUSSNITZER, M., ELLINGSEN, S., MADSEN, L., SAGEN, J. V., MELLGREN, G. & DANKEL, S. N. 2021. Role of the Neutral Amino Acid Transporter SLC7A10 in Adipocyte Lipid Storage, Obesity, and Insulin Resistance. *Diabetes,* 70**,** 680-695.

JIANG, Y., BERRY, D. C., JO, A., TANG, W., ARPKE, R. W., KYBA, M. & GRAFF, J. M. 2017. A PPARgamma transcriptional cascade directs adipose progenitor cell-niche interaction and niche expansion. *Nat Commun,* 8**,** 15926.

JIANG, Y., BERRY, D. C., TANG, W. & GRAFF, J. M. 2014. Independent stem cell lineages regulate adipose organogenesis and adipose homeostasis. *Cell Rep,* 9**,** 1007-22.

JOSHI, R. L., LAMOTHE, B., CORDONNIER, N., MESBAH, K., MONTHIOUX, E., JAMI, J. & BUCCHINI, D. 1996. Targeted disruption of the insulin receptor gene in the mouse results in neonatal lethality. *EMBO J,* 15**,** 1542-7.

KADAKIA, R. & JOSEFSON, J. 2016. The Relationship of Insulin-Like Growth Factor 2 to Fetal Growth and Adiposity. *Horm Res Paediatr,* 85**,** 75-82.

KAHN, B. B. & FLIER, J. S. 2000. Obesity and insulin resistance. *J Clin Invest,* 106**,** 473-81.

KARLINA, R., LUTTER, D., MIOK, V., FISCHER, D., ALTUN, I., SCHOTTL, T., SCHORPP, K., ISRAEL, A., CERO, C., JOHNSON, J. W., KAPSER-FISCHER, I., BOTTCHER, A., KEIPERT, S., FEUCHTINGER, A., GRAF, E., STROM, T., WALCH, A., LICKERT, H., WALZTHOENI, T., HEINIG, M., THEIS, F. J., GARCIA-CACERES, C., CYPESS, A. M. & USSAR, S. 2021. Identification and characterization of distinct brown adipocyte subtypes in C57BL/6J mice. *Life Sci Alliance,* 4.

KARPE, F. & PINNICK, K. E. 2015. Biology of upper-body and lower-body adipose tissue--link to whole-body phenotypes. *Nat Rev Endocrinol,* 11**,** 90-100.

KERSHAW, E. E. & FLIER, J. S. 2004. Adipose tissue as an endocrine organ. *J Clin Endocrinol Metab,* 89**,** 2548-56.

KIM, J. Y., VAN DE WALL, E., LAPLANTE, M., AZZARA, A., TRUJILLO, M. E., HOFMANN, S. M., SCHRAW, T., DURAND, J. L., LI, H., LI, G., JELICKS, L. A., MEHLER, M. F., HUI, D. Y., DESHAIES, Y., SHULMAN, G. I., SCHWARTZ, G. J. & SCHERER, P. E. 2007. Obesity-associated improvements in metabolic profile through expansion of adipose tissue. *J Clin Invest,* 117**,** 2621-37.

KITAMURA, T., KAHN, C. R. & ACCILI, D. 2003. Insulin receptor knockout mice. *Annu Rev Physiol,* 65**,** 313-32.

KLOTING, N., FASSHAUER, M., DIETRICH, A., KOVACS, P., SCHON, M. R., KERN, M., STUMVOLL, M. & BLUHER, M. 2010. Insulin-sensitive obesity. *Am J Physiol Endocrinol Metab,* 299**,** E506-15.

KROOK, A., BRUETON, L. & O'RAHILLY, S. 1993. Homozygous nonsense mutation in the insulin receptor gene in infant with leprechaunism. *Lancet,* 342**,** 277-8.

KRYCER, J. R., QUEK, L. E., FRANCIS, D., ZADOORIAN, A., WEISS, F. C., COOKE, K. C., NELSON, M. E., DIAZ-VEGAS, A., HUMPHREY, S. J., SCALZO, R., HIRAYAMA, A., IKEDA, S., SHOJI, F., SUZUKI, K., HUYNH, K., GILES, C., VARNEY, B., NAGARAJAN, S. R., HOY, A. J., SOGA, T., MEIKLE, P. J., COONEY, G. J., FAZAKERLEY, D. J. & JAMES, D. E. 2020. Insulin signaling requires glucose to promote lipid anabolism in adipocytes. *J Biol Chem,* 295**,** 13250-13266.

KURI-HARCUCH, W. & GREEN, H. 1978. Adipose conversion of 3T3 cells depends on a serum factor. *Proc Natl Acad Sci U S A,* 75**,** 6107-9.

LASSARRE, C., HARDOUIN, S., DAFFOS, F., FORESTIER, F., FRANKENNE, F. & BINOUX, M. 1991. Serum insulin-like growth factors and insulin-like growth factor binding proteins in the human fetus. Relationships with growth in normal subjects and in subjects with intrauterine growth retardation. *Pediatr Res,* 29**,** 219-25.

LEE, K. Y., LUONG, Q., SHARMA, R., DREYFUSS, J. M., USSAR, S. & KAHN, C. R. 2019. Developmental and functional heterogeneity of white adipocytes within a single fat depot. *EMBO J,* 38.

LIU, C., WANG, C., GUAN, S., LIU, H., WU, X., ZHANG, Z., GU, X., ZHANG, Y., ZHAO, Y., TSE, L. A. & FANG, X. 2019. The Prevalence of Metabolically Healthy and Unhealthy Obesity according to Different Criteria. *Obes Facts,* 12**,** 78-90.

LIU, J. P., BAKER, J., PERKINS, A. S., ROBERTSON, E. J. & EFSTRATIADIS, A. 1993. Mice carrying null mutations of the genes encoding insulin-like growth factor I (Igf-1) and type 1 IGF receptor (Igf1r). *Cell,* 75**,** 59-72.

LONGO, M., ZATTERALE, F., NADERI, J., PARRILLO, L., FORMISANO, P., RACITI, G. A., BEGUINOT, F. & MIELE, C. 2019. Adipose Tissue Dysfunction as Determinant of Obesity-Associated Metabolic Complications. *Int J Mol Sci,* 20.

LOPEZ, M. F., ZHENG, L., MIAO, J., GALI, R., GORSKI, G. & HIRSCHHORN, J. N. 2018. Disruption of the Igf2 gene alters hepatic lipid homeostasis and gene expression in the newborn mouse. *Am J Physiol Endocrinol Metab,* 315**,** E735-E744.

LOTTA, L. A., GULATI, P., DAY, F. R., PAYNE, F., ONGEN, H., VAN DE BUNT, M., GAULTON, K. J., EICHER, J. D., SHARP, S. J., LUAN, J., DE LUCIA ROLFE, E., STEWART, I. D., WHEELER, E., WILLEMS, S. M., ADAMS, C., YAGHOOTKAR, H., CONSORTIUM, E. P.-I., CAMBRIDGE, F. C., FOROUHI, N. G., KHAW, K. T., JOHNSON, A. D., SEMPLE, R. K., FRAYLING, T., PERRY, J. R., DERMITZAKIS, E., MCCARTHY, M. I., BARROSO, I., WAREHAM, N. J., SAVAGE, D. B., LANGENBERG, C., O'RAHILLY, S. & SCOTT, R. A. 2017. Integrative genomic analysis implicates limited peripheral adipose storage capacity in the pathogenesis of human insulin resistance. *Nat Genet,* 49**,** 17-26.

LUONG, Q., HUANG, J. & LEE, K. Y. 2019. Deciphering White Adipose Tissue Heterogeneity. *Biology (Basel),* 8.

MAGKOS, F. 2019. Metabolically healthy obesity: what's in a name? *Am J Clin Nutr,* 110**,** 533-539.

MARCELIN, G., FERREIRA, A., LIU, Y., ATLAN, M., ARON-WISNEWSKY, J., PELLOUX, V., BOTBOL, Y., AMBROSINI, M., FRADET, M., ROUAULT, C., HENEGAR, C., HULOT, J. S., POITOU, C., TORCIVIA, A., NAIL-BARTHELEMY, R., BICHET, J. C., GAUTIER, E. L. & CLEMENT, K. 2017. A PDGFRalpha-Mediated Switch toward CD9(high) Adipocyte Progenitors Controls Obesity-Induced Adipose Tissue Fibrosis. *Cell Metab,* 25**,** 673-685.

MATSUO, H., KANAI, Y., TOKUNAGA, M., NAKATA, T., CHAIROUNGDUA, A., ISHIMINE, H., TSUKADA, S., OOIGAWA, H., NAWASHIRO, H., KOBAYASHI, Y., FUKUDA, J. & ENDOU, H. 2004. High affinity D- and L-serine transporter Asc-1: cloning and dendritic localization in the rat cerebral and cerebellar cortices. *Neurosci Lett,* 358**,** 123-6.

MERRICK, D., SAKERS, A., IRGEBAY, Z., OKADA, C., CALVERT, C., MORLEY, M. P., PERCEC, I. & SEALE, P. 2019. Identification of a mesenchymal progenitor cell hierarchy in adipose tissue. *Science,* 364.

MIRRA, P., DESIDERIO, A., SPINELLI, R., NIGRO, C., LONGO, M., PARRILLO, L., D'ESPOSITO, V., CARISSIMO, A., HEDJAZIFAR, S., SMITH, U., FORMISANO, P., MIELE, C., RACITI, G. A. & BEGUINOT, F. 2021. Adipocyte precursor cells from first degree relatives of type 2 diabetic patients feature changes in hsa-mir-23a-5p, -193a-5p, and -193b-5p and insulin-like growth factor 2 expression. *FASEB J,* 35**,** e21357.

MONK, D., SANCHES, R., ARNAUD, P., APOSTOLIDOU, S., HILLS, F. A., ABU-AMERO, S., MURRELL, A., FRIESS, H., REIK, W., STANIER, P., CONSTANCIA, M. & MOORE, G. E. 2006. Imprinting of IGF2 P0 transcript and novel alternatively spliced INS-IGF2 isoforms show differences between mouse and human. *Hum Mol Genet,* 15**,** 1259-69.

NORDIN, M., BERGMAN, D., HALJE, M., ENGSTROM, W. & WARD, A. 2014. Epigenetic regulation of the Igf2/H19 gene cluster. *Cell Prolif,* 47**,** 189-99.

NUNN, E. R., SHINDE, A. B. & ZAGANJOR, E. 2022. Weighing in on Adipogenesis. *Front Physiol,* 13**,** 821278.

O'DELL, S. D., MILLER, G. J., COOPER, J. A., HINDMARSH, P. C., PRINGLE, P. J., FORD, H., HUMPHRIES, S. E. & DAY, I. N. 1997. Apal polymorphism in insulin-like growth factor II (IGF2) gene and weight in middle-aged males. *Int J Obes Relat Metab Disord,* 21**,** 822-5.

OGDEN, C. L., CARROLL, M. D., KIT, B. K. & FLEGAL, K. M. 2013. Prevalence of obesity among adults: United States, 2011-2012. *NCHS Data Brief***,** 1-8.

ORSSO, C. E., COLIN-RAMIREZ, E., FIELD, C. J., MADSEN, K. L., PRADO, C. M. & HAQQ, A. M. 2020. Adipose Tissue Development and Expansion from the Womb to Adolescence: An Overview. *Nutrients,* 12.

PAJUNEN, P., KOTRONEN, A., KORPI-HYOVALTI, E., KEINANEN-KIUKAANNIEMI, S., OKSA, H., NISKANEN, L., SAARISTO, T., SALTEVO, J. T., SUNDVALL, J., VANHALA, M., UUSITUPA, M. & PELTONEN, M. 2011. Metabolically healthy and unhealthy obesity phenotypes in the general population: the FIN-D2D Survey. *BMC Public Health,* 11**,** 754.

PELLEGRINELLI, V., CAROBBIO, S. & VIDAL-PUIG, A. 2016. Adipose tissue plasticity: how fat depots respond differently to pathophysiological cues. *Diabetologia,* 59**,** 1075-88.

PETRUS, P., MEJHERT, N., CORRALES, P., LECOUTRE, S., LI, Q., MALDONADO, E., KULYTE, A., LOPEZ, Y., CAMPBELL, M., ACOSTA, J. R., LAURENCIKIENE, J., DOUAGI, I., GAO, H., MARTINEZ-ALVAREZ, C., HEDEN, P., SPALDING, K. L., VIDAL-PUIG, A., MEDINA-GOMEZ, G., ARNER, P. & RYDEN, M. 2018. Transforming Growth Factor-beta3 Regulates Adipocyte Number in Subcutaneous White Adipose Tissue. *Cell Rep,* 25**,** 551-560 e5.

POISSONNET, C. M., BURDI, A. R. & BOOKSTEIN, F. L. 1983. Growth and development of human adipose tissue during early gestation. *Early Hum Dev,* 8**,** 1-11.

PRAKASH, J., SRIVASTAVA, N., AWASTHI, S., AGARWAL, C., NATU, S., RAJPAL, N. & MITTAL, B. 2012. Association of PPAR-gamma gene polymorphisms with obesity and obesity-associated phenotypes in North Indian population. *Am J Hum Biol,* 24**,** 454-9.

PRIMEAU, V., CODERRE, L., KARELIS, A. D., BROCHU, M., LAVOIE, M. E., MESSIER, V., SLADEK, R. & RABASA-LHORET, R. 2011. Characterizing the profile of obese patients who are metabolically healthy. *Int J Obes (Lond),* 35**,** 971-81.

PU, R., SHI, D., GAN, T., REN, X., BA, Y., HUO, Y., BAI, Y., ZHENG, T. & CHENG, N. 2020. Effects of metformin in obesity treatment in different populations: a meta-analysis. *Ther Adv Endocrinol Metab,* 11**,** 2042018820926000.

RANDALL, J. C., WINKLER, T. W., KUTALIK, Z., BERNDT, S. I., JACKSON, A. U., MONDA, K. L., KILPELAINEN, T. O., ESKO, T., MAGI, R., LI, S., WORKALEMAHU, T., FEITOSA, M. F.,

CROTEAU-CHONKA, D. C., DAY, F. R., FALL, T., FERREIRA, T., GUSTAFSSON, S., LOCKE, A. E., MATHIESON, I., SCHERAG, A., VEDANTAM, S., WOOD, A. R., LIANG, L., STEINTHORSDOTTIR, V., THORLEIFSSON, G., DERMITZAKIS, E. T., DIMAS, A. S., KARPE, F., MIN, J. L., NICHOLSON, G., CLEGG, D. J., PERSON, T., KROHN, J. P., BAUER, S., BUECHLER, C., EISINGER, K., CONSORTIUM, D., BONNEFOND, A., FROGUEL, P., INVESTIGATORS, M., HOTTENGA, J. J., PROKOPENKO, I., WAITE, L. L., HARRIS, T. B., SMITH, A. V., SHULDINER, A. R., MCARDLE, W. L., CAULFIELD, M. J., MUNROE, P. B., GRONBERG, H., CHEN, Y. D., LI, G., BECKMANN, J. S., JOHNSON, T., THORSTEINSDOTTIR, U., TEDER-LAVING, M., KHAW, K. T., WAREHAM, N. J., ZHAO, J. H., AMIN, N., OOSTRA, B. A., KRAJA, A. T., PROVINCE, M. A., CUPPLES, L. A., HEARD-COSTA, N. L., KAPRIO, J., RIPATTI, S., SURAKKA, I., COLLINS, F. S., SARAMIES, J., TUOMILEHTO, J., JULA, A., SALOMAA, V., ERDMANN, J., HENGSTENBERG, C., LOLEY, C., SCHUNKERT, H., LAMINA, C., WICHMANN, H. E., ALBRECHT, E., GIEGER, C., HICKS, A. A., JOHANSSON, A., PRAMSTALLER, P. P., KATHIRESAN, S., SPELIOTES, E. K., PENNINX, B., HARTIKAINEN, A. L., JARVELIN, M. R., GYLLENSTEN, U., BOOMSMA, D. I., CAMPBELL, H., WILSON, J. F., CHANOCK, S. J., FARRALL, M., GOEL, A., MEDINA-GOMEZ, C., RIVADENEIRA, F., ESTRADA, K., UITTERLINDEN, A. G., et al. 2013. Sex-stratified genome-wide association studies including 270,000 individuals show sexual dimorphism in genetic loci for anthropometric traits. *PLoS Genet,* 9**,** e1003500.

REIK, W. & MAHER, E. R. 1997. Imprinting in clusters: lessons from Beckwith-Wiedemann syndrome. *Trends Genet,* 13**,** 330-4.

RIGAMONTI, A., BRENNAND, K., LAU, F. & COWAN, C. A. 2011. Rapid cellular turnover in adipose tissue. *PLoS One,* 6**,** e17637.

RINDERKNECHT, E. & HUMBEL, R. E. 1976. Polypeptides with nonsuppressible insulin-like and cell-growth promoting activities in human serum: isolation, chemical characterization, and some biological properties of forms I and II. *Proc Natl Acad Sci U S A,* 73**,** 2365-9.

RINDERKNECHT, E. & HUMBEL, R. E. 1978. Primary structure of human insulin-like growth factor II. *FEBS Lett,* 89**,** 283-6.

RODEHEFFER, M. S., BIRSOY, K. & FRIEDMAN, J. M. 2008. Identification of white adipocyte progenitor cells in vivo. *Cell,* 135**,** 240-9.

ROGLER, C. E., YANG, D., ROSSETTI, L., DONOHOE, J., ALT, E., CHANG, C. J., ROSENFELD, R., NEELY, K. & HINTZ, R. 1994. Altered body composition and increased frequency of diverse malignancies in insulin-like growth factor-II transgenic mice. *J Biol Chem,* 269**,** 13779-84.

ROSEN, E. D. & SPIEGELMAN, B. M. 2006. Adipocytes as regulators of energy balance and glucose homeostasis. *Nature,* 444**,** 847-53.

ROSSETTI, L., BARZILAI, N., CHEN, W., HARRIS, T., YANG, D. & ROGLER, C. E. 1996. Hepatic overexpression of insulin-like growth factor-II in adulthood increases basal and insulin-stimulated glucose disposal in conscious mice. *J Biol Chem,* 271**,** 203-8.

ROTH, S. M., SCHRAGER, M. A., METTER, E. J., RIECHMAN, S. E., FLEG, J. L., HURLEY, B. F. & FERRELL, R. E. 2002. IGF2 genotype and obesity in men and women across the adult age span. *Int J Obes Relat Metab Disord,* 26**,** 585-7.

RUTTER, A. R., FRADLEY, R. L., GARRETT, E. M., CHAPMAN, K. L., LAWRENCE, J. M., ROSAHL, T. W. & PATEL, S. 2007. Evidence from gene knockout studies implicates Asc-1 as the primary transporter mediating d-serine reuptake in the mouse CNS. *Eur J Neurosci,* 25**,** 1757-66.

RYTKA, J. M., WUEEST, S., SCHOENLE, E. J. & KONRAD, D. 2011. The portal theory supported by venous drainage-selective fat transplantation. *Diabetes,* 60**,** 56-63.

SAFORY, H., NEAME, S., SHULMAN, Y., ZUBEDAT, S., RADZISHEVSKY, I., ROSENBERG, D., SASON, H., ENGELENDER, S., AVITAL, A., HULSMANN, S., SCHILLER, J. & WOLOSKER, H. 2015. The alanine-serine-cysteine-1 (Asc-1) transporter controls glycine levels in the brain and is required for glycinergic inhibitory transmission. *EMBO Rep,* 16**,** 590-8.

SAKAGUCHI, M., FUJISAKA, S., CAI, W., WINNAY, J. N., KONISHI, M., O'NEILL, B. T., LI, M., GARCIA-MARTIN, R., TAKAHASHI, H., HU, J., KULKARNI, R. N. & KAHN, C. R. 2017. Adipocyte Dynamics and Reversible Metabolic Syndrome in Mice with an Inducible Adipocyte-Specific Deletion of the Insulin Receptor. *Cell Metab,* 25**,** 448-462.

SAKERS, A., DE SIQUEIRA, M. K., SEALE, P. & VILLANUEVA, C. J. 2022. Adipose-tissue plasticity in health and disease. *Cell,* 185**,** 419-446.

SALTIEL, A. R. & KAHN, C. R. 2001. Insulin signalling and the regulation of glucose and lipid metabolism. *Nature,* 414**,** 799-806.

SANCHEZ-GURMACHES, J. & GUERTIN, D. A. 2014. Adipocytes arise from multiple lineages that are heterogeneously and dynamically distributed. *Nat Commun,* 5**,** 4099.

SANDHU, M. S., GIBSON, J. M., HEALD, A. H., DUNGER, D. B. & WAREHAM, N. J. 2003. Low circulating IGF-II concentrations predict weight gain and obesity in humans. *Diabetes,* 52**,** 1403-8.

SANDOVICI, I., GEORGOPOULOU, A., PEREZ-GARCIA, V., HUFNAGEL, A., LOPEZ-TELLO, J., LAM, B. Y. H., SCHIEFER, S. N., GAUDREAU, C., SANTOS, F., HOELLE, K., YEO, G. S. H., BURLING, K., REITERER, M., FOWDEN, A. L., BURTON, G. J., BRANCO, C. M., SFERRUZZI-PERRI, A. N. & CONSTANCIA, M. 2022. The imprinted Igf2-Igf2r axis is critical for matching placental microvasculature expansion to fetal growth. *Dev Cell,* 57**,** 63-79 e8.

SANTORO, A., MCGRAW, T. E. & KAHN, B. B. 2021. Insulin action in adipocytes, adipose remodeling, and systemic effects. *Cell Metab,* 33**,** 748-757.

SCHEJA, L. & HEEREN, J. 2019. The endocrine function of adipose tissues in health and cardiometabolic disease. *Nat Rev Endocrinol,* 15**,** 507-524.

SCHOETTL, T., FISCHER, I. P. & USSAR, S. 2018. Heterogeneity of adipose tissue in development and metabolic function. *J Exp Biol,* 221.

SEALE, P., BJORK, B., YANG, W., KAJIMURA, S., CHIN, S., KUANG, S., SCIME, A., DEVARAKONDA, S., CONROE, H. M., ERDJUMENT-BROMAGE, H., TEMPST, P., RUDNICKI, M. A., BEIER, D. R. & SPIEGELMAN, B. M. 2008. PRDM16 controls a brown fat/skeletal muscle switch. *Nature,* 454**,** 961-7.

SELENOU, C., BRIOUDE, F., GIABICANI, E., SOBRIER, M. L. & NETCHINE, I. 2022. IGF2: Development, Genetic and Epigenetic Abnormalities. *Cells,* 11.

SHIN, S., PANG, Y., PARK, J., LIU, L., LUKAS, B. E., KIM, S. H., KIM, K. W., XU, P., BERRY, D. C. & JIANG, Y. 2020. Dynamic control of adipose tissue development and adult tissue homeostasis by platelet-derived growth factor receptor alpha. *Elife,* 9.

SMITH, U. & KAHN, B. B. 2016. Adipose tissue regulates insulin sensitivity: role of adipogenesis, de novo lipogenesis and novel lipids. *J Intern Med,* 280**,** 465-475.

SONG, A., DAI, W., JANG, M. J., MEDRANO, L., LI, Z., ZHAO, H., SHAO, M., TAN, J., LI, A., NING, T., MILLER, M. M., ARMSTRONG, B., HUSS, J. M., ZHU, Y., LIU, Y., GRADINARU, V., WU, X., JIANG, L., SCHERER, P. E. & WANG, Q. A. 2020. Low- and high-thermogenic brown adipocyte subpopulations coexist in murine adipose tissue. *J Clin Invest,* 130**,** 247-257.

SONG, Z., XIAOLI, A. M. & YANG, F. 2018. Regulation and Metabolic Significance of De Novo Lipogenesis in Adipose Tissues. *Nutrients,* 10.

SPALDING, K. L., ARNER, E., WESTERMARK, P. O., BERNARD, S., BUCHHOLZ, B. A., BERGMANN, O., BLOMQVIST, L., HOFFSTEDT, J., NASLUND, E., BRITTON, T., CONCHA, H., HASSAN, M., RYDEN, M., FRISEN, J. & ARNER, P. 2008. Dynamics of fat cell turnover in humans. *Nature,* 453**,** 783-7.

SPARAGO, A., CERRATO, F., VERNUCCI, M., FERRERO, G. B., SILENGO, M. C. & RICCIO, A. 2004. Microdeletions in the human H19 DMR result in loss of IGF2 imprinting and Beckwith-Wiedemann syndrome. *Nat Genet,* 36**,** 958-60.

STANFORD, K. I., MIDDELBEEK, R. J., TOWNSEND, K. L., AN, D., NYGAARD, E. B., HITCHCOX, K. M., MARKAN, K. R., NAKANO, K., HIRSHMAN, M. F., TSENG, Y. H. & GOODYEAR, L. J. 2013. Brown adipose tissue regulates glucose homeostasis and insulin sensitivity. *J Clin Invest,* 123**,** 215-23.

STEFAN, N., KANTARTZIS, K., MACHANN, J., SCHICK, F., THAMER, C., RITTIG, K., BALLETSHOFER, B., MACHICAO, F., FRITSCHE, A. & HARING, H. U. 2008. Identification and characterization of metabolically benign obesity in humans. *Arch Intern Med,* 168**,** 1609-16.

STEFKOVICH, M., TRAYNOR, S., CHENG, L., MERRICK, D. & SEALE, P. 2021. Dpp4+ interstitial progenitor cells contribute to basal and high fat diet-induced adipogenesis. *Mol Metab,* 54**,** 101357.

STEINER, B. M. & BERRY, D. C. 2022. The Regulation of Adipose Tissue Health by Estrogens. *Front Endocrinol (Lausanne),* 13**,** 889923.

SUMMERS, S. A., WHITEMAN, E. L. & BIRNBAUM, M. J. 2000. Insulin signaling in the adipocyte. *Int J Obes Relat Metab Disord,* 24 Suppl 4**,** S67-70.

SUN, F. L., DEAN, W. L., KELSEY, G., ALLEN, N. D. & REIK, W. 1997. Transactivation of Igf2 in a mouse model of Beckwith-Wiedemann syndrome. *Nature,* 389**,** 809-15.

SUWANDHI, L., ALTUN, I., KARLINA, R., MIOK, V., WIEDEMANN, T., FISCHER, D., WALZTHOENI, T., LINDNER, C., BOTTCHER, A., HEINZMANN, S. S., ISRAEL, A., KHALIL, A., BRAUN, A., PRAMME-STEINWACHS, I., BURTSCHER, I., SCHMITT-KOPPLIN, P., HEINIG, M., ELSNER, M., LICKERT, H., THEIS, F. J. & USSAR, S. 2021. Asc-1 regulates white versus beige adipocyte fate in a subcutaneous stromal cell population. *Nat Commun,* 12**,** 1588.

TAKAHASHI, Y., KADOWAKI, H., MOMOMURA, K., FUKUSHIMA, Y., ORBAN, T., OKAI, T., TAKETANI, Y., AKANUMA, Y., YAZAKI, Y. & KADOWAKI, T. 1997. A homozygous kinase-defective mutation in the insulin receptor gene in a patient with leprechaunism. *Diabetologia,* 40**,** 412-20.

TANG, W., ZEVE, D., SUH, J. M., BOSNAKOVSKI, D., KYBA, M., HAMMER, R. E., TALLQUIST, M. D. & GRAFF, J. M. 2008. White fat progenitor cells reside in the adipose vasculature. *Science,* 322**,** 583-6.

TINT, M. T., SADANANTHAN, S. A., SOH, S. E., ARIS, I. M., MICHAEL, N., TAN, K. H., SHEK, L. P. C., YAP, F., GLUCKMAN, P. D., CHONG, Y. S., GODFREY, K. M., VELAN, S. S., CHAN, S. Y., ERIKSSON, J. G., FORTIER, M. V., ZHANG, C. & LEE, Y. S. 2020. Maternal glycemia during pregnancy and offspring abdominal adiposity measured by MRI in the neonatal period and preschool years: The Growing Up in Singapore Towards healthy Outcomes (GUSTO) prospective mother-offspring birth cohort study. *Am J Clin Nutr,* 112**,** 39-47.

TOWNSEND, K. L. & TSENG, Y. H. 2014. Brown fat fuel utilization and thermogenesis. *Trends Endocrinol Metab,* 25**,** 168-77.

TURNER, N., KOWALSKI, G. M., LESLIE, S. J., RISIS, S., YANG, C., LEE-YOUNG, R. S., BABB, J. R., MEIKLE, P. J., LANCASTER, G. I., HENSTRIDGE, D. C., WHITE, P. J., KRAEGEN, E. W.,

MARETTE, A., COONEY, G. J., FEBBRAIO, M. A. & BRUCE, C. R. 2013. Distinct patterns of tissue-specific lipid accumulation during the induction of insulin resistance in mice by high-fat feeding. *Diabetologia,* 56**,** 1638-48.

USSAR, S., LEE, K. Y., DANKEL, S. N., BOUCHER, J., HAERING, M. F., KLEINRIDDERS, A., THOMOU, T., XUE, R., MACOTELA, Y., CYPESS, A. M., TSENG, Y. H., MELLGREN, G. & KAHN, C. R. 2014. ASC-1, PAT2, and P2RX5 are cell surface markers for white, beige, and brown adipocytes. *Sci Transl Med,* 6**,** 247ra103.

VAN VLIET-OSTAPTCHOUK, J. V., NUOTIO, M. L., SLAGTER, S. N., DOIRON, D., FISCHER, K., FOCO, L., GAYE, A., GOGELE, M., HEIER, M., HIEKKALINNA, T., JOENSUU, A., NEWBY, C., PANG, C., PARTINEN, E., REISCHL, E., SCHWIENBACHER, C., TAMMESOO, M. L., SWERTZ, M. A., BURTON, P., FERRETTI, V., FORTIER, I., GIEPMANS, L., HARRIS, J. R., HILLEGE, H. L., HOLMEN, J., JULA, A., KOOTSTRA-ROS, J. E., KVALOY, K., HOLMEN, T. L., MANNISTO, S., METSPALU, A., MIDTHJELL, K., MURTAGH, M. J., PETERS, A., PRAMSTALLER, P. P., SAARISTO, T., SALOMAA, V., STOLK, R. P., UUSITUPA, M., VAN DER HARST, P., VAN DER KLAUW, M. M., WALDENBERGER, M., PEROLA, M. & WOLFFENBUTTEL, B. H. 2014. The prevalence of metabolic syndrome and metabolically healthy obesity in Europe: a collaborative analysis of ten large cohort studies. *BMC Endocr Disord,* 14**,** 9.

VAN WYK, J. J. & SMITH, E. P. 1999. Insulin-like growth factors and skeletal growth: possibilities for therapeutic interventions. *J Clin Endocrinol Metab,* 84**,** 4349-54.

VELLA, V., NICOLOSI, M. L., GIULIANO, M., MORRIONE, A., MALAGUARNERA, R. & BELFIORE, A. 2019. Insulin Receptor Isoform A Modulates Metabolic Reprogramming of Breast Cancer Cells in Response to IGF2 and Insulin Stimulation. *Cells,* 8.

VIRTANEN, K. A., LIDELL, M. E., ORAVA, J., HEGLIND, M., WESTERGREN, R., NIEMI, T., TAITTONEN, M., LAINE, J., SAVISTO, N. J., ENERBACK, S. & NUUTILA, P. 2009. Functional brown adipose tissue in healthy adults. *N Engl J Med,* 360**,** 1518-25.

VISHVANATH, L. & GUPTA, R. K. 2019. Contribution of adipogenesis to healthy adipose tissue expansion in obesity. *J Clin Invest,* 129**,** 4022-4031.

VON RUESTEN, A., STEFFEN, A., FLOEGEL, A., VAN DER, A. D., MASALA, G., TJONNELAND, A., HALKJAER, J., PALLI, D., WAREHAM, N. J., LOOS, R. J., SORENSEN, T. I. & BOEING, H. 2011. Trend in obesity prevalence in European adult cohort populations during follow-up since 1996 and their predictions to 2015. *PLoS One,* 6**,** e27455.

WAKEFIELD, J. 2004. Fighting obesity through the built environment. *Environ Health Perspect,* 112**,** A616-8.

WAKELING, E. L., BRIOUDE, F., LOKULO-SODIPE, O., O'CONNELL, S. M., SALEM, J., BLIEK, J., CANTON, A. P., CHRZANOWSKA, K. H., DAVIES, J. H., DIAS, R. P., DUBERN, B., ELBRACHT, M., GIABICANI, E., GRIMBERG, A., GRONSKOV, K., HOKKEN-KOELEGA, A. C., JORGE, A. A., KAGAMI, M., LINGLART, A., MAGHNIE, M., MOHNIKE, K., MONK, D., MOORE, G. E., MURRAY, P. G., OGATA, T., PETIT, I. O., RUSSO, S., SAID, E., TOUMBA, M., TUMER, Z., BINDER, G., EGGERMANN, T., HARBISON, M. D., TEMPLE, I. K., MACKAY, D. J. & NETCHINE, I. 2017. Diagnosis and management of Silver-Russell syndrome: first international consensus statement. *Nat Rev Endocrinol,* 13**,** 105-124.

WANG, Q. A., TAO, C., GUPTA, R. K. & SCHERER, P. E. 2013. Tracking adipogenesis during white adipose tissue development, expansion and regeneration. *Nat Med,* 19**,** 1338-44.

WANG, X., YOU, L., CUI, X., LI, Y., WANG, X., XU, P., ZHU, L., WEN, J., PANG, L., GUO, X. & JI, C. 2018. Evaluation and optimization of differentiation conditions for human primary brown adipocytes. *Sci Rep,* 8**,** 5304.

WELLS, J. C. K., DAVIES, P. S. W., FEWTRELL, M. S. & COLE, T. J. 2020. Body composition reference charts for UK infants and children aged 6 weeks to 5 years based on measurement of total body water by isotope dilution. *Eur J Clin Nutr,* 74**,** 141-148.

WERTHEIMER, E., LU, S. P., BACKELJAUW, P. F., DAVENPORT, M. L. & TAYLOR, S. I. 1993. Homozygous deletion of the human insulin receptor gene results in leprechaunism. *Nat Genet,* 5**,** 71-3.

WESTERMEIER, F., SAEZ, T., ARROYO, P., TOLEDO, F., GUTIERREZ, J., SANHUEZA, C., PARDO, F., LEIVA, A. & SOBREVIA, L. 2016. Insulin receptor isoforms: an integrated view focused on gestational diabetes mellitus. *Diabetes Metab Res Rev,* 32**,** 350-65.

WHITE, V., JAWERBAUM, A., MAZZUCCO, M. B., GAUSTER, M., DESOYE, G. & HIDEN, U. 2018. IGF2 stimulates fetal growth in a sex- and organ-dependent manner. *Pediatr Res,* 83**,** 183-189.

WIDDOWSON, E. M. 1950. Chemical composition of newly born mammals. *Nature,* 166**,** 626-8.

WILDMAN, R. P., MUNTNER, P., REYNOLDS, K., MCGINN, A. P., RAJPATHAK, S., WYLIE-ROSETT, J. & SOWERS, M. R. 2008. The obese without cardiometabolic risk factor clustering and the normal weight with cardiometabolic risk factor clustering: prevalence and correlates of 2 phenotypes among the US population (NHANES 1999-2004). *Arch Intern Med,* 168**,** 1617-24.

WU, J., BOSTROM, P., SPARKS, L. M., YE, L., CHOI, J. H., GIANG, A. H., KHANDEKAR, M., VIRTANEN, K. A., NUUTILA, P., SCHAART, G., HUANG, K., TU, H., VAN MARKEN LICHTENBELT, W. D., HOEKS, J., ENERBACK, S., SCHRAUWEN, P. & SPIEGELMAN, B. M. 2012. Beige adipocytes are a distinct type of thermogenic fat cell in mouse and human. *Cell,* 150**,** 366-76.

XIA, C. L., LYU, Y., LI, C., LI, H., ZHANG, Z. T., YIN, S. W., MAO, Y., LI, W., KONG, L. Y., LIANG, B., JIANG, H. K., LI-LING, J., LIU, C. X. & WEI, J. 2019. Rare De Novo IGF2 Variant on the Paternal Allele in a Patient With Silver-Russell Syndrome. *Front Genet,* 10**,** 1161.

XIE, X., DUMAS, T., TANG, L., BRENNAN, T., REEDER, T., THOMAS, W., KLEIN, R. D., FLORES, J., O'HARA, B. F., HELLER, H. C. & FRANKEN, P. 2005. Lack of the alanine-serine-cysteine transporter 1 causes tremors, seizures, and early postnatal death in mice. *Brain Res,* 1052**,** 212-21.

XUE, B., RIM, J. S., HOGAN, J. C., COULTER, A. A., KOZA, R. A. & KOZAK, L. P. 2007. Genetic variability affects the development of brown adipocytes in white fat but not in interscapular brown fat. *J Lipid Res,* 48**,** 41-51.

YONESHIRO, T., AITA, S., MATSUSHITA, M., KAYAHARA, T., KAMEYA, T., KAWAI, Y., IWANAGA, T. & SAITO, M. 2013. Recruited brown adipose tissue as an antiobesity agent in humans. *J Clin Invest,* 123**,** 3404-8.

YU, J. S. & CUI, W. 2016. Proliferation, survival and metabolism: the role of PI3K/AKT/mTOR signalling in pluripotency and cell fate determination. *Development,* 143**,** 3050-60.

ZHANG, A., WANG, X., FAN, C. & MAO, X. 2021. The Role of Ki67 in Evaluating Neoadjuvant Endocrine Therapy of Hormone Receptor-Positive Breast Cancer. *Front Endocrinol (Lausanne),* 12**,** 687244.

ZHANG, K., WANG, F., HUANG, J., LOU, Y., XIE, J., LI, H., CAO, D. & HUANG, X. 2019. Insulin-like growth factor 2 promotes the adipogenesis of hemangioma-derived stem cells. *Exp Ther Med,* 17**,** 1663-1669.

ZHANG, W. & LIU, H. T. 2002. MAPK signal pathways in the regulation of cell proliferation in mammalian cells. *Cell Res,* 12**,** 9-18.

ZHU, D., MACKENZIE, N. C., MILLAN, J. L., FARQUHARSON, C. & MACRAE, V. E. 2014. Upregulation of IGF2 expression during vascular calcification. *J Mol Endocrinol,* 52**,** 77-85.

ZHU, Y., GUI, W., TAN, B., DU, Y., ZHOU, J., WU, F., LI, H. & LIN, X. 2021. IGF2 deficiency causes mitochondrial defects in skeletal muscle. *Clin Sci (Lond),* 135**,** 979-990.

III. Abbreviations

Table 8: List of Abbreviations

Abbreviation	Full Name
Adipq	Adiponectin
AKT	Protein kinase B
ASC-1	Alanine/serine/cysteine transporter-1
APC	Adipocyte progenitor cells
AT	Adipose tissue
BAT	Brown adipose tissue
CD	Chow diet
CT	Computed tomography
Dif. Adip/ Adipo	Differentiated Adipocytes
ECM	Extracellular matrix
ERK 1/2	Extracellular signal-regulated kinase-1/2
FABP4	Fatty acid binding protein 4
FBS	Fetal bovine serum
FFA	Free fatty acid
FIGIRKO	Adipose tissue specific double knockout of *InsR*/*Igf1r*
FIRKO	Adipose tissue specific double knockout of *InsR*
GO	Gene ontology
GWAS	Genome-wide association study
H&E	Hematoxylin & Eosin
HFD	High fat diet
IGF1	Insulin-like growth factor 1
IGF1R	Insulin-like growth factor 1 receptor
IGF2	Insulin-like growth factor 2
IGF2R	Insulin-like growth factor 2 receptor
IF	Immunofluorescence
Ins	Insulin
InsR	Insulin receptor
InsR-A	Insulin receptor isoform A
InsR-B	Insulin receptor isoform B
IP	Immunoprecipitation
MAPK	Mitogen-activated protein kinase
MH	Metabolically healthy
MHO	Metabolically healthy obesity
mRNA	Messenger ribonucleic acid
MS	Mouse serum
MUO	Metabolically unhealthy obesity
Neut Ab	Neutralizing antibody
OCR	Oxygen consumption rate
ORO	Oil red o
PET	Positron emission tomography
Pgc1α	Peroxisome proliferator-activated receptor gamma coactivator 1-alpha
PGF	Perigonadal fat

PI3K	Phosphatidylinositol-3-kinase
Pparγ	Peroxisome proliferator-activated receptor-γ
Pre/ Preadip	Preadipocytes
Rosi	Rosiglitazone
scRNA-seq	Single cell RNA sequencing
SCF	Subcutaneous fat
shRNA	Short hairpin RNA
Srr	Serine racemase
SVC	Stromal vascular cells
Tbp	TATA-box binding protein
Tfam	Mitochondrial transcription factor A
t-SNE	t-distribution stochastic neighbor embedding
T2D	Type 2 Diabetes
UCP	Uncoupling protein
vWAT	Visceral white adipose tissue
WAT	White adipose tissue
WB	Western blot
WHO	World health organization
wt	Wild-type

IV. List of Figures

V. List of Tables

VI. Appendix

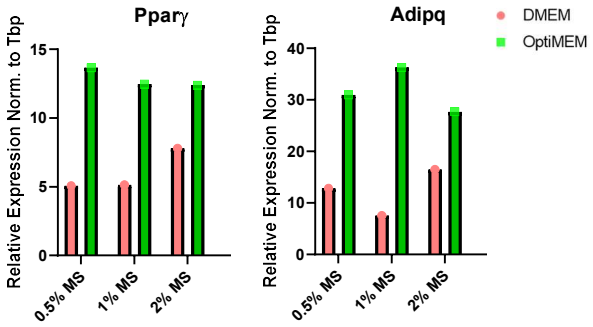

Figure 18: Differentiation trial using different media conditions. Immortalized subcutaneous preadipocytes were differentiated in the presence of different adult mouse serum (MS) concentrations (0.5, 1 and 2%) for 8 days using either DMEM+GlutaMAX or Opti-MEM. mRNA expression levels of *Pparγ* and *Adipq* (n=1).

VII. Acknowledgment

Coming to an end in my PhD journey, I would like to thank particularly to Dr. Siegfried Ussar for giving me the opportunity to work in his group. He thought me how to conduct good scientific practice and allowed me to extend my scientific knowledge. He trusted in my abilities any time and always supported me in my progress.

I also would like to thank my second supervisor Prof. Dr. Johannes Beckers and my mentor Dr. Matthias Meier for the fruitful discussions and support on my scientific progress.

Moreover, I would like to thank Dr. Lisa Suwandhi, Dr. Viktorian Miok and Dr. Tobias Wiedemann for their collaborative work.

In the past 4 years, I received countless support from the members of IDO, but I would particularly want to thank Dr. Theresa Bäcker, Dr. Qian Zhang (a.k.a. Tina), Dr. Ruth Karlina, Elena Lopez Gonzalez, Xiaocheng Yan and Dr. Yasuhiro Onogi for their scientific knowledge and extensive mental support. Furthermore, I appreciate that Dr. Ruth Karlina and Dr. Yasuhiro Onogi took the time to read my thesis and give constructive feedback.

I also would like to thank my best friend Stephanie Knizkov for her loving patience and just being there when I needed it.

Furthermore, I would like to thank my boyfriend Julian Kriesche, who encouraged, supported and showed me his caring heart and love all the time. Your presence made things easier. Thank you also for being a part of this journey and helping me polish my thesis with the formatting tips.

I am eternally grateful to my parents, especially to my mom for the unconditional love, faith and commitment for giving me a good education and letting me follow my dreams. I know you are proud of me no matter what, but I hope to see this pays off all the hard days you have been through.

Lastly, thank you all who passed through my life in these 4 years for just being there…